Geochemical Feasibility of Brine Exchange Between Arbuckle and Lansing-Kansas City Formations as a Produced Water Management Alternative

By:

Richard Barimah

Submitted to the Department of Civil, Environmental, and Architectural Engineering and the Faculty of the Graduate School of the University of Kansas in partial fulfillment of the requirements for the Degree of Master of Science in Environmental Engineering

Committee members:

_____

E. F. Peltier (Chair)

_____

S. J. Randtke (Co-Chair)

_____

R. Barati

Date Defended: July 9, 2019

Abstract

The State of Kansas is facing increasing demands on limited available drinking water sources. Reclaiming and reusing wastewaters for water applications able to utilize lower quality water sources could help to extend and conserve existing drinking water sources. Oil production in Kansas generates over one billion barrels of produced water each year, which must be properly managed in compliance with environmental regulations. Successful reclamation of this wastewater for industrial and other uses could reduce freshwater requirements in the oil industry and provide a new water source for other water needs of the state.

Produced waters from Kansas oil fields are usually very salty with a median total dissolved solids (TDS) concentration of 90,000 mg/l. However, there are a few oil formations in the Central Kansas Uplift area that have less salty water with a TDS of 40,000 mg/l or lower. Exchange of formation brine, where the highly salty brine from one formation is injected into the lower salinity formation, along with extraction of the lower salinity formation water to balance formation pressure, has been proposed as a way of managing produced water for potential reuse applications. This study was conducted to further investigate the feasibility of brine exchange as a produced water management practice from a geochemical and environmental standpoint. A geochemical software program (PHREEQC) was utilized, along with both the PHREEQC and Pitzer databases, to predict precipitation reactions that might occur during the brine exchange. These predictions were compared to laboratory results to determine the limits and degree of accuracy of the model. Adverse reactions such as precipitation of solids in the formation during the exchange could block the pore spaces and reduce the conductivity of the formation.

This study established that mixing Lansing Kanas City formation brine with Arbuckle formation brine (from the Wellington wellfield in Kansas) could potentially cause calcium carbonate scale

formation, and that cutting down the bicarbonate content is essential to prevent scaling. Also, using both the Pitzer and PHREEQC databases, PHREEQC accurately predicted the amount of carbonate scale formed at well oversaturated conditions, i.e., having a saturation index (SI) > 2, within the range of ionic strength investigated, i.e., 1 M to 3.65 M. However, the model is likely to overestimate the amount of scale formation at close to saturation conditions, for SIs between -0.5 and 2, for the mineral phases barite, celestite, gypsum, and anhydrite. For SIs in this range, both databases are likely to predict similar SIs for the sulfate minerals; but for the carbonate mineral phases, the predicted SIs from the Pitzer database are higher. This is due to the higher predicted activity for the carbonate ion, as the Pitzer database does not consider ion pairing or complexation, and more specifically the formation of $NaHCO_3^+$. pH predictions from both databases closely agree with the each other but failed to accurately predict measured pH values in lab experiments. This is most likely due to interference with pH measurement due to the high sodium ion concentration.

Acknowledgements

I would like to first and foremost express my gratitude to the chair and co-chair of my committee, Dr. E. Peltier and Dr. Randtke, for their immense support during the preparation, commencement and the final presentation of my research work. The valuable experience and knowledge I obtained under your leadership and guidance have indoctrinated in me scholastic skills that will be with me forever.

My heart-felt gratitude also go to my committee member Dr. Barati, for the helpful comments and critique that shaped my work into the scholarly piece it is today. I also want to express my gratitude to Dr. Barati's research group for providing me with the Indiana Limestone rock used for my experiment. In addition, I would like to Thank Dr. K. Peltier for her support and the valuable lab training she gave me during this research period. I also want to thank the National Science Foundation who partially funded my work through the EPSCoR collaboration award (OIA-1632892).

Finally, I cannot find words to express my deepest gratitude to my family for all the financial support, love and encouragement they provided me during this research work.

Table of Contents

List of Figures

List of Tables

Chapter 1 Introduction

Water is simultaneously produced and consumed by the oil and gas industry. Water is used in the oil and gas industries for drilling and hydraulic fracturing, processing at oil and gas refineries, and improved oil recovery, and as cooling water for power generation. Oil and gas bearing rocks contain water which is extracted during oil and gas production as "produced water". The amount and composition of water used, produced, reused or sent for disposal varies widely. It is generally dependent on the geological formation, time and length of production, regulations surrounding water use and disposal, and economic factors[1].

The volume of produced water generated in the state of Kansas in 2002 was about 1.2 billion barrels[1]. The predominant way of managing this colossal volume of water is to inject the produced water into the subsurface through regulated wells called class II injection wells. There are currently 5,000 disposal wells and 11,600 secondary/enhanced oil recovery wells in Kansas that make up the 16,600 permitted class II injection well in the state[2]. Deep well injection (disposal wells) has been associated with the incidence of earthquakes. Prior to 2010, only 30 earthquakes were recorded[3]. The increase in the number of disposal wells and volume of produced water injected are believed to have caused 127 earthquakes in 2014 alone[3]. As such, there is the need for reusing or recycling of produced water (PW) not only to reduce seismic activities, but also to augment freshwater supplies for use in the oil and gas industry or for other applications.

The State of Kansas is facing increasing demands on limited available drinking water sources. Reclaiming and reusing wastewaters for water applications that demand lower quality water supply could help to extend and conserve existing drinking water sources. Climate change,

population growth, urbanization and industrialization have all put immense pressure on the limited potable water resources available for use today. Current use of freshwater and ground water for fracking and other oil and gas production activities increased during the recent boom in oil prices, and freshwater use is expected to increase over the next decade[4]. Even though oil and gas activities consume freshwater resources, they also produce colossal amounts of wastewater (brine) with the potential for reuse to supplement existing water resources.

Produced waters from Kansas oil fields are usually very salty with an average total dissolved solids (TDS) concentration up to 100,000 mg/l. However, there are a few oil formations in the Central Kansas Uplift area that produce less salty brines with a TDS of 40,000 mg/l or lower. Exchange of formation brines, where the highly saline brine from one formation is exchanged with lower salinity brine of another formation, has been proposed as a way of managing produced water for potential reuse applications[5]. In previous work, Thompson[5] identified wells in the Arbuckle Production Group that produced significantly less salty brines than wells in the Lansing Kansas City Group. Both groups are in the Central Kansas Uplift Area and within realistic geographic distance to potentially make brine exchange economically and environmentally feasible. This study was conducted to further investigate the feasibility of brine exchange, as a produced water management practice, from a geochemical and environmental standpoint.

1.1 **Objectives**

The objectives of this work were to:

1. Predict, using a software model (PHREEQC), scale-forming minerals when Arbuckle and the Lansing-Kansas City (LKC) formation waters are mixed

2. Investigate the formation of scales using both experimental measurements and software analysis (PHREEQC) for high salinity brines

1.2 Scope

This study discusses the mineralogy of the study area, the chemical compatibility of the fluids that would be used in a hypothetical brine exchange, and how the fluids would interact with LKC formation rock. The study also assessed scale predictions form the PHREEQC software, using two distinct databases (Pitzer database and standard PHREEQC database) under varying conditions. The scope of this work does not consider the organic component of produced water (PW). It is limited to laboratory experiments with reagent-grade chemicals used to prepare solutions simulating the ionic composition of actual produced water samples.

Chapter 2 Literature Review

2.1 Introduction to literature review

This chapter reviews the use of freshwater in oil and gas production. The section also discusses produced water volume, composition, management as well as produced water treatment. A review of scale formation in the oil and gas industry is presented in this chapter together with a literature review on calcite (the main formation mineral for the Lansing Kansas City and Arbuckle formations). A literature on the mechanisms responsible for incremental oil recovery during low water salinity flooding in carbonate formation is discussed in this chapter. This chapter closes with a discussion on modeling of mineral chemistry in produced waters.

2.2 A closer look at water use in oil and gas production

Water use in the oil and gas sector is projected to increase worldwide[4]. The energy sector is the second largest consumer of available water, although it uses significantly less water than is consumed by irrigation practices. Figure 1 shows the distribution of water consumption amongst the various sectors that consumes significant proportions of water.

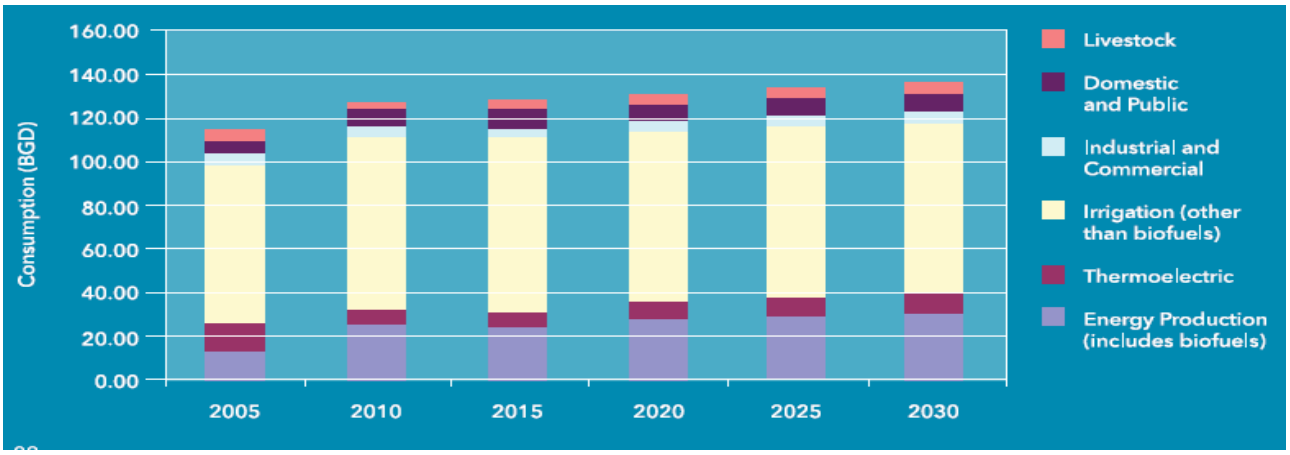

Figure 1: Global projected water consumption[4]

The estimated consumption by the energy sector encompasses water use in oil and natural gas exploration and production, and in energy production using coal, nuclear energy and biomass. Natural gas and nuclear energy use significantly less water per unit of energy production than biomass, oil refining, and oil exploration and production. Water use in crude oil production generally increases as you move from primary recovery to tertiary oil recovery. In the US, freshwater withdrawn for use as cooling water for thermoelectric power accounts for approximately 40% of total freshwater withdrawal[6,7]. Because the water withdrawn is not necessarily consumed in the cooling process, a lot of it is returned into nearby water resources, creating a significant difference between water consumption and withdrawal. Table 1 shows the water to energy production for the major primary energy production resources worldwide.

Table 1: Water use coefficients in primary energy production worldwide (from Xylem and incorporated into the 2015 report on water use in oil and gas production[4])

Energy Source		Water coefficient (m^3/TJ)	Source
Oil (1)			
Crude oil (OPEC)		78	Wu et al., 2009
Crude oil (Non-OPEC)			
	Primary recovery	6	Gleick, 1994
	Secondary recovery	600	Gleick, 1994
	EOR using steam	140	Gleick, 1994
	EOR using CO_2	640	Gleick, 1994
Bitumen			
	Mining	26	Wu et al., 2009
	In situ SAGD	8	Wu et al., 2009
	In situ CSS	14	Wu et al., 2009
	In situ multi-scheme	32	Wu et al., 2009
Heavy oil		14	Wu et al., 2009
Natural gas liquids		6	Gleick, 1994
Coal-to-liquids		53	Gleick, 1994
Natural Gas			
Conventional gas		negligible	Gleick, 1994
Unconventional gas			
	Coalbed methane	negligible	Elcock, 2008
	Shale gas	0.4	Elcock, 2008
	Tight gas	0.4	Elcock, 2008
Coal			
Surface mining		2	Gleick, 1994
Underground mining		12	Gleick, 1994
Upgrading (washing)		4	Gleick, 1994

2.2.1 Freshwater use in hydraulic fracturing

Freshwater users in the oil and gas industries compete with other water users such as industrial, agricultural and municipal water users. These competing demands cause water stress in areas that have relatively less available water. For example, fracking a typical non-conventional well in a shale formation in the Marcellus play requires 3 to 5 million gallons of water within a two to five day span[8]. This could create high water stress within the locality. Also, a large amount of flowback or produced water would have to be managed properly. This poses logistical problems to operators along with the high costs associated with acquisition of freshwater and disposal of the wastewater that follows. Factors influencing water economics for oil and gas operators include freshwater availability, water treatment, transportation cost to the well, transportation cost from the well to disposal site and cost of disposal (treatment to meet regulations or pumping cost associated with injection)[8]. High volume withdrawals can cause local water shortages, which can in turn lead to water quality degradation in locations with drier climates such as Texas, California, Kansas and Colorado[9]. Declining water quality creates a negative public awareness, threatening the energy production industry. Even in water abundant areas, seasonal variation in stream flow can lead to water shortages if withdrawals are high enough during the dry season[9].

2.3 Produced water

Subsurface geological formations are porous in nature and contain different fluids such as gas, oil and brine. Saline water is first trapped in rocks before its displacement by hydrocarbons with lower density. Over time, these fluids tend to coexist together in the formation. Brine could flow from above or below the hydrocarbon zone during production. It could also come from within the formation or from the injected fluids used for hydraulic fracturing or drilling[10]. Water that

comes out immediately after its application for fracking is known as the "flowback water". During the oil and gas extraction process, both the formation water and the flowback water are produced together with the hydrocarbons. The flowback and formation water combined are generally referred to as produced water. Produced water contains organic and inorganic substances in varying degrees that makes it difficult to treat and use for beneficial purposes. It often requires expensive treatment technologies or a "train" of treatment processes that makes it economically unappealing to most uphill energy producers. As a result of produced water's composition and associated environmental health concerns, there have been a lot of stringent regulations placed on discharges of produced water.

2.3.1 Produced water volumes

Several factors affect the volume of water produced during hydrocarbon extraction. Figure 2 shows the global produced water volumes estimated for onshore and offshore well fields. Reynolds and Kiker[11] summarized these effects as follows:

1. The location of the well field: In general, onshore wells generally produce more water than offshore wells. Also, the location of the well within a heterogeneous or homogeneous reservoir plays a major role. For example, in homogenous reservoirs, horizontal wells reduce the amount of water produced, while in heterogeneous formations, the specific area of the well in contact with the formation determines the volume of water produced.
2. The method of drilling: Vertical wells have a lower rate of water production than horizontal well with a similar drawdown.

3. The type of formation: Some formations contain more water than others, regardless of the drilling technology used.
4. Structural integrity of the wellbore: Compromising the wellbore integrity can allow more water into the well.
5. The age of the well: As the wellfield ages, there is a gradual decline of hydrocarbons and an increase in brine.

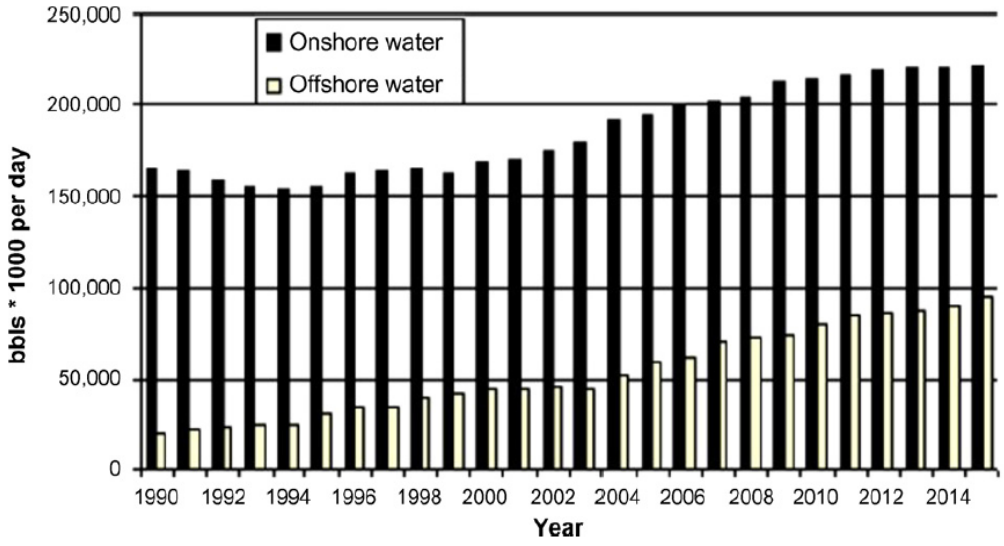

Figure 2: Global produced water volumes onshore vs off shore [12]

The volume ratio of produced water to oil averages about 10:1 in the U.S., but is higher or lower depending on the formation[13]. In the state of the Kansas this ratio is around 22:1[13]. The waste water volume accounts for between 80 to 95 % of liquid waste with the rest making up the organic component of the waste stream[14,15]. Figure 3 below illustrates the volume of produce water over the life of a wellfield.

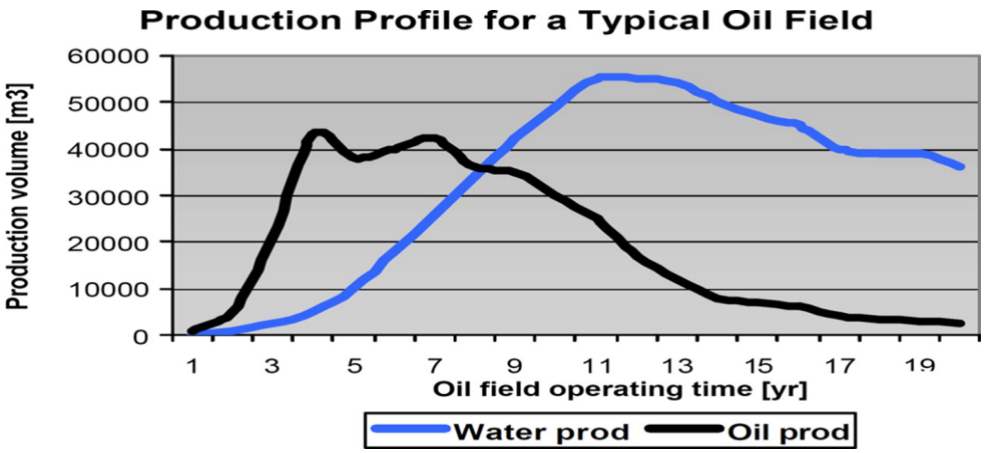

Figure 3: Typical produced water volume over the age of a well field[16]

2.3.2 Produced water composition

Produced water typically contains dissolved gases[17], dissolved minerals, dissolved and dispersed oil compounds, suspended solids (such as bacteria, formation minerals, and scale forming minerals), chemicals from injected fluids, and naturally occurring radioactive materials.

The total dissolved solids (TDS) concentrations in produced water vary widely, ranging from less than 1000 mg/l to over 300,000 mg/l[18,19]. The primary contributors to TDS in most produced waters are Cl^- and Na^+. Other ions such as K^+, Ca^{2+}, Mg^{2+}, Sr^{2+}, Fe^{2+}, Mn^{2+}, Ba^{2+}, SO_4^{2-}, and HCO_3^- are also found in produced water but typically at lower concentrations. However, these ions have significant impact on water chemistry parameters such as the buffering capacity and the scaling potential of the brine[17]. Heavy metals such as lead, copper, mercury, nickel, cadmium, silver, and zinc also occur in produced waters, mostly in trace quantities[17].

Naturally occurring radioactive materials (NORMs) have been found in some scales from produced water. ^{226}Radium and ^{228} radium are the most abundant NORMs in produced water[20].If present, they co-precipitate with barium sulfate precipitate[21]. Vegueria *et al*. found a strong correlation between barium and radium isotope concentrations[22].

Polar organic compounds such as benzene, toluene, ethylbenzene, and xylene (BTEX), as well as phenols, are naturally occurring organic compounds that are relatively soluble and commonly found in produced water[23]. Weak organic acids like propionic and formic acid are also found in produced water and are more soluble than BTEX. The salinity of produced water has little effect on the concentration of dissolved organics[24]. However, the pH and temperature do have an impact on the amount of dissolved organics present[10]. Toxic organic compounds like aromatic compounds are also present in produced water and are not well removed by water/oil separation techniques. There are usually higher BTEX concentrations in PWs from natural gas formations than from oil bearing formations[21]. Carboxylic acids, short-chain aliphatic hydrocarbons, and phenols are also soluble organic compounds found in produced water[21].

Synthetic and natural chemicals are added during production. These chemicals either prevent operational problems or increase the efficiency of the drilling or fracturing fluids. These chemicals include biocides, emulsion breakers, corrosion and scale inhibitors, foaming agents, clay stabilizers, buffering agents, acids, surfactants, polymers, oxidizers, enzymes and heavy metals (for example, titanium and zirconium)[25]. In 2014 Stringfellow *et al.*[25] reported 81 chemical additives that have been used in hydraulic fracturing fluids. Out of these, 70% were organic with 50% being biodegradable. There was no toxicology information found on 1/3 of the reported chemicals, with about 5 chemicals suspected to be carcinogens. About 21 chemicals were identified as making high to moderate contributions to the chemical oxygen demand (COD) of fracturing fluids[25].

2.3.3 Produced water management

Produced water is managed through one or more of the following ways: (1) treatment to meet surface water or offshore discharge regulations, (2) recycling for drilling or incremental

enhanced oil recovery, (3) treatment for beneficial reuse such as irrigation, wetlands protection, or watering livestock, (4) injection into deep wells, (5) evaporation, and (6) off-site commercial disposal[10,26,27, 28]. Veil[29] reported only four produced water management practices in the U.S. (the first four practices mentioned above) as of 2007, which increased to six management practices in 2012. Figure 4 illustrates the distribution of produced water management practices from among the options available in the U.S. Deep well injection for disposal and use of produced water for enhanced oil recovery are the most widely used management practices in the U.S. Deep well injection has been associated with earthquakes (as discussed later herein).

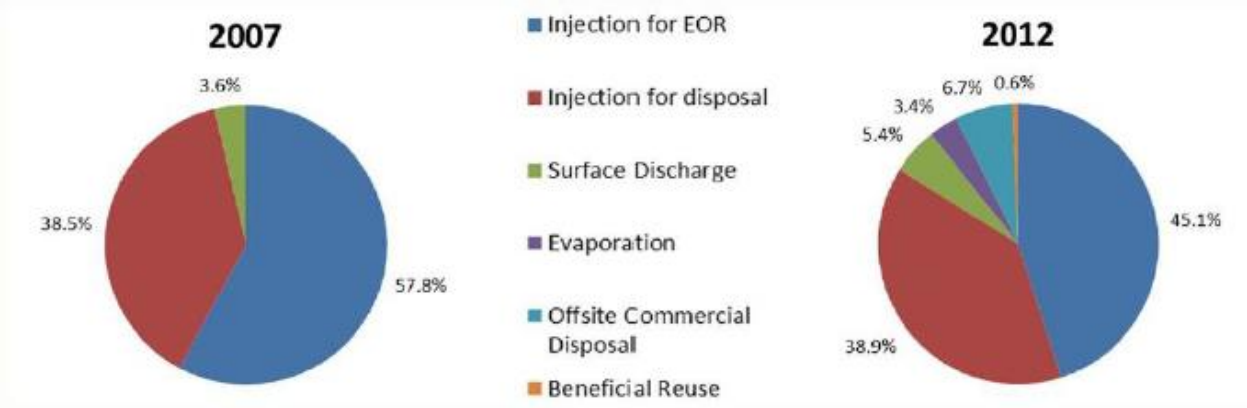

Figure 4: Distribution of produced water management practices in the US[29].

2.3.3.1 Produced water for enhanced oil recovery or use in preparing fracturing fluids

A boom in oil prices resulted in a 54 % annual growth rate of enhanced oil recovery (EOR) practices between 2007 to 2011 even though EOR accounts for only 2 % of oil production[4].The use of PW for EOR or injection for disposal are the most environmentally friendly and cheapest amongst the management options available. In 2007 about 96 % of total produced water was injected into the subsurface, but this declined to 84 % in 2012 as shown in Figure 4 [29]. There is a general reduction of reservoir pressure during extraction. Over time, the reservoir pressure drops below a threshold that cannot sustain anymore production. Therefore, water is reinjected into the

formation to either maintain or increase the reservoir pressure, thereby increasing oil recovery[30]. Use of produced water for EOR cuts freshwater use and its associated adverse impacts. The use of PW for EOR is also very advantageous if the volume, demand, and distance of the wellfields are within reasonable limits. Also, the final volume of PW requiring disposal shrinks significantly making the other options more economically feasible. However, high salinity PW presents challenges in EOR applications, and it is generally avoided for such applications.

2.3.3.2 Produced water for beneficial reuse

If the quality of PW is relatively good, it can potentially be used with minimal treatment for applications that require a higher quality water. Water demand for applications such as livestock watering, wildlife watering and habitat, dust control, wetland development, and vehicle and equipment washing can be met by either supplementing freshwater resources with produced water or by the use of produced water as a stand-alone source. Each of these applications have water quality requirements that must be met before the water is suitable for this use. Another factor to consider apart from quality requirement is the cost of using produced water for these applications. If using fresh water is cheaper than using PW, reuse of PW would be very low regardless of its quality. The logistics of storing, transporting, and treating PW play a major role in determining the cost of using it. In drier climates, reuse of PW is often given more attention than in areas where there is an abundance of fresh water[29]. PW from coal bed methane formations is known to be of higher quality (relatively lower in salinity), such that is can generally be more readily treated and used, depending the quality requirements of the application in question[29].

2.3.3.3 Produced water reuse for irrigation

There is a gradual push towards reuse of PW for agriculture irrigation and livestock watering. The suitability of PW for irrigation purposes should be assessed based on the chemical, physical and microbiological quality of the water. The high salinity of PW is a major limiting factor in use for irrigation. Sodium, boron and chloride are the major chemicals in produced water associated with plant toxicity[31,32]. The cationic composition of most PWs is dominated by sodium, and the direct use of PW for irrigation without adequate treatment would excessively increase the amount of sodium ion in the soil, increasing its sodicity to unacceptable levels. A low calcium to sodium ratio affects ion selectivity in root membranes and will result in the selection and accumulation of sodium in plants. Boron toxicity causes leaf burn, anthocyanin, leaf cupping, chlorosis, premature leaf drops anthocyanin, branch dieback, rosette spotting, and reduced growth[31-33].

In addition to the ions discussed above, trace levels of metals and organic compounds, as well as inorganic compounds and other parameters such as temperature and pH, can also affect the use of PW water for irrigation. Toxic and nutritional effects of trace elements in irrigation water, and recommended maximum concentrations, are listed in Table 2.

Table 2: Recommended maximum concentrations of trace elements in irrigation waters[31,33]

Element	Recommended maximum concentration, mg/L	Remarks
Al (aluminum)	5.0	Can cause nonproductivity in acid solids (pH < 5.5) but in more alkaline soils (pH > 5.5) will precipitate, eliminating any toxicity.
As (arsenic)	0.10	Toxic level for plants varies widely, ranging from 12 mg/L for Sudan grass to <0.05 mg/L for rice.
Be (beryllium)	0.10	Toxic level for plants varies widely, ranging from 5 mg/L for kale to 0.5 mg/L for bush beans.

Cd (cadmium)	0.010	Toxic to beans beets and turnips at concentrations as low as 0.1 mg/L in nutrient solutions. Conservative limits are recommended because of the potential for cadmium to accumulate in plants and soils to concentrations that may be harmful to humans and animals.
Co (cobalt)	0.050	Toxic to tomato plants at 0.1 mg/L in nutrient solution. Tends to be inactivated by neutral and alkaline soils.
Cr (chromium)	0.10	Not generally recognized as an essential growth element. Conservative limits recommended because of lack of knowledge of toxicity to plants.
Cu (copper)	0.20	Toxic to a number of plants at 0.1 to 1.0 mg/L in nutrient solutions.
F (fluoride)	1.0	Inactivated by neutral and alkaline soils.
Fe (iron)	5.0	Not toxic to plants in aerated soils but can contribute to soil acidification and to reduced availability of essential phosphorous and molybdenum. Overhead sprinkling may result in unsightly deposits on plants equipment and buildings.
Li (lithium)	2.5	Toxic at levels >0.075 mg/L
Mn (manganese)	0.20	Toxic to a number of crops at a few tenths to a few mg/L but usually only in acid soils.
Mo (molybdenum)	0.010	Not toxic to plants at normal concentrations in soil and water. Can be toxic to livestock if forage is grown in soils with high levels of available molybdenum.
Ni (nickel)	0.20	Toxic to a number of plants at 0.5 to 1.0 mg/L; reduced toxicity at neutral or alkaline pH
Pb (lead)	5.0	Can inhibit plant cell growth at very high concentrations.
Se (selenium)	0.020	Toxic to plants at concentrations as low as 0.025 mg/L and toxic to livestock if forage is grown in soils with relatively high levels of added selenium. An essential element for animals but in very low concentrations.
Sn (tin)	—	Effectively excluded by plants; specific tolerance unknown.
Ti (titanium)	—	(See remark for tin)
W (tungsten)	—	(See remark for tin)
V (vanadium)	0.10	Toxic to many plants at relatively low concentrations.
Zn (zinc)	2.0	Toxic to many plants at widely varying concentrations; reduced toxicity at pH> 6.0 and in fine-textured or organic soil

2.3.3.4 Produced water disposal into the subsurface

One of the most common practices for managing waste streams from the oil and gas industries is injecting them into class II injection wells. Oil and gas producers often haul their waste streams to an offsite location where they can find the closest class II well. This style of management does not consider the waste stream as an unconventional resource where it could be treated and reused for a different purpose. This management practice can be relatively cheap or can substantially add to the final disposal cost. The distance to the injection site and the volume of waste stream determines the cost of disposal to producers. The cost increases as the volume of the waste and distance to the disposal site increases. On top of this potentially high cost, deep well injection has been linked to seismic activities and has been found to cause earthquakes in areas where there has been a high amount of waste injected along fault lines[3]. These liquids can cause the fault lines to slip, with the magnitude of the slippage determining the magnitude of the induced seismicity. In Kansas, the Arbuckle formation area contains many class II injection wells[3]. Data from the Kansas Geological Survey indicate that high volumes of waste disposed into areas of seismic concern caused a high incidence of observed earthquakes. Figure 5 shows the area of seismic concern in the Arbuckle region.

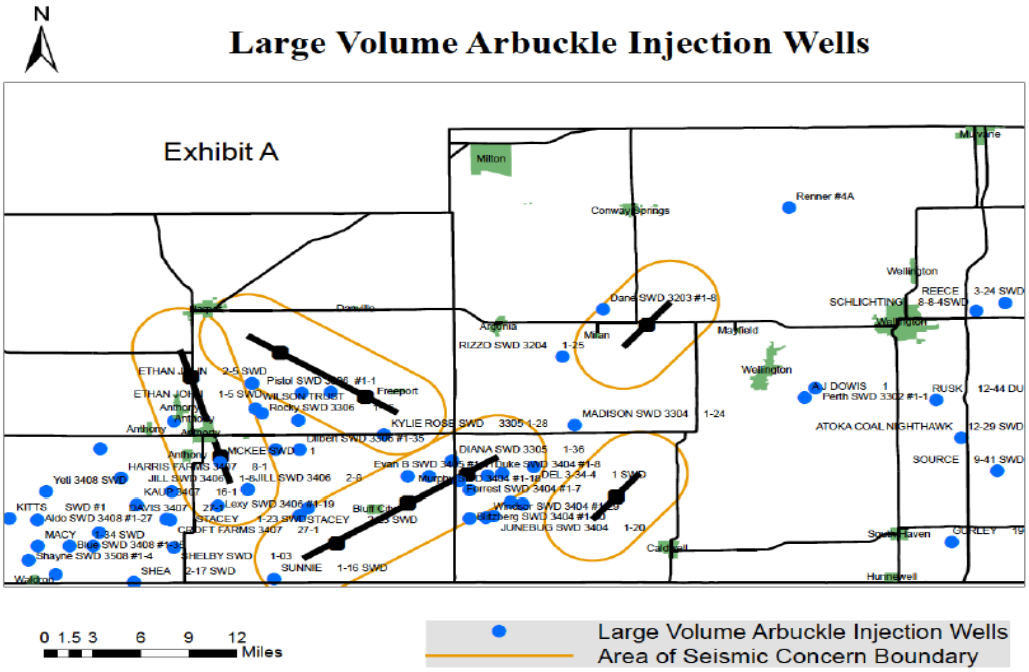

Figure 5: Areas of seismic concern in the Arbuckle formation area[3]

The number of injection wells being used within the boundary was highest from January to June of 2015. This period experienced the highest frequency of earthquakes between January 2013 to January 2018[3]. As the number of class II injection wells in operation decreased from 439 to 99 over the years within the boundary, so did the frequency and magnitude of earthquakes, as shown in Figure 6. Because of the strong connection between deep well injection of PW and earthquakes in areas of seismic concern, there would be additional advantages in these areas to shift from deep well injection to reuse of the PW.

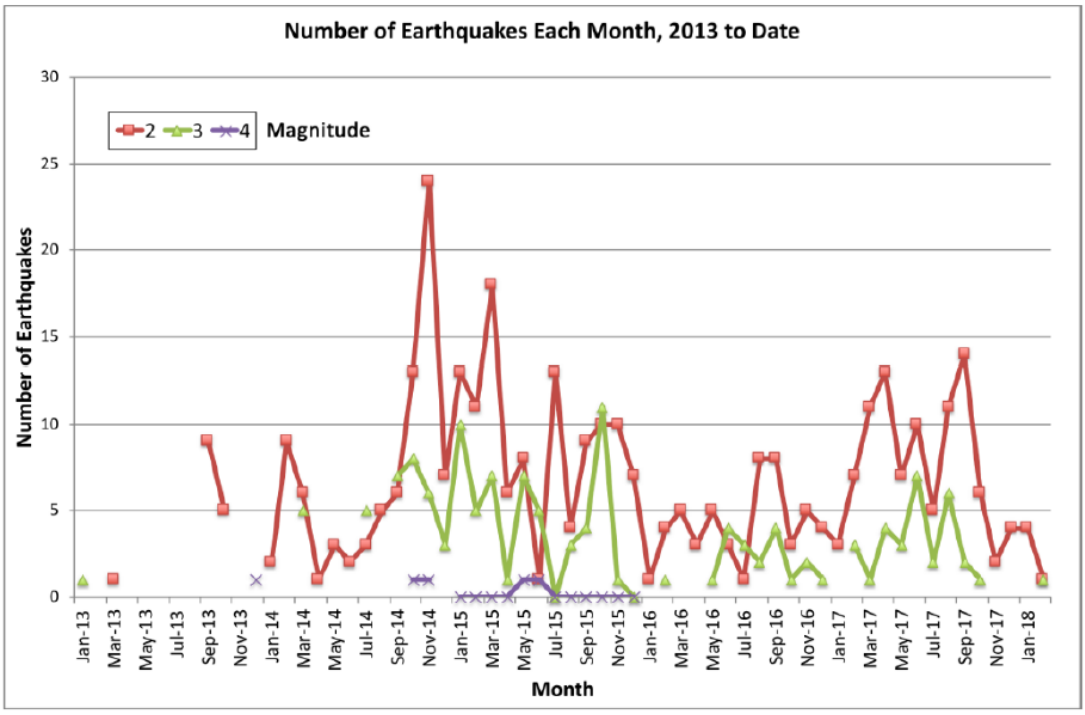

Figure 6: Number and magnitude of earthquakes as the number of class II injection wells in use decreased from 439 to 99 in Harper and Sumner Counties[3]

2.4 Produced water treatment

The level of produced water treatment needed depends on the disposal or reuse option chosen, and the composition of the PW itself. Treatments include de-oiling, removal of heavy metals and NORMs, softening, degassing, removal of organic compounds, removal of sodium and chloride ions (the main contributors to ionic strength), and disinfection. Depending on the disposal or reuse option, a combination of these treatments may be required. These treatment options can be categorized into physical, chemical, biological, and membrane treatment. Although membrane treatment is a physical process, it is discussed separately, below. Treatment of PW using biological processes is rarely used and therefore excluded in the discussion.

2.4.1 Chemical treatment

Chemical precipitation processes, often accompanied by coagulation, flocculation and sedimentation, can be effective in removing some of scale forming cations found in PWs, such as calcium, magnesium, barium and radium. Lime softening and modified hot lime softening have been used to reduce the hardness of some produced waters[10]. Chemical oxidation can be used to aid in the removal of dissolved ions such as Fe^{+2} that can be oxidized to a form that can be precipitated. Chemical treatment processes are usually part of a more integral complex treatment train, with each process targeting specific components of the PW.

2.4.2 Physical treatment

Physical treatment of produced water can involve the use of adsorbents, clarifiers, oil-water separators, coagulants, flocculators, sand filters, cyclones, evaporation ponds, air strippers, gas flotation devices, electrocoagulation, and electrodialysis processes. Adsorption of organic compounds found in produced water have been achieved by the use of resins, activated carbon, zeolite, organoclay products, and copolymers. Copolymers have been found to remove 85 % of the organic content found in produced water[17,34–36]. Sand filters have been demonstrated to have a high efficiency rate (about 90 %) for removing iron from produced water[37]; but for this to be achieved, the system should be pH adjusted or aerated with oxygen to initiate the iron oxidation reaction. Cyclones are used to separate oil, gas, water and solid particles from produced water. They are manufactured from plastic, ceramic or metals with a conical base and a cylindrical top[16]. Evaporation ponds are artificial ponds designed to hold produced water on or offsite so natural solar energy can cause the water to evaporate leaving the salts and chemicals behind[38]. They are mostly used in areas where the cost of land is relatively cheap, and the climate is warmer and dryer. They often require a liner to prevent the seepage of the water into the ground

beneath[39]. Also, they must be covered with a net to prevent animals that are drawn to the water from getting poisoned. When reuse is not a goal, this style of management is often chosen. Gas flotation systems are designed to bring suspended solids, which otherwise would not settle in sedimentation tanks, to rise to the top of the water so they can skimmed off as froth[40]. Gas flotation systems involve fine bubbles, created by the pressurized injection of gas into the produced water, that allow suspended particles and insoluble hydrocarbon to be brought to the surface for removal. This technology can remove grease and oil, volatile organics, natural organic matter, and suspended solids from produced water[40,41]. Electrodialysis is the process of attracting dissolved ions to an electrode with an opposite charge. There are membranes that are put in between two electrodes that select for anions or cations. This method of treatment is adequate for PWs with low TDS[42]. Electrochemical charge driven systems include electrodialysis (ED), electrodialysis reversal (EDR), capacitive deionization (CDI) and electrodeionization (EDI) that are all possible options for the removal of dissolved ions in PW[43].

2.4.3 Membrane filtration

Membranes are used in removing particulate matter, pathogens, organic matter, and dissolved ions from produced water. Some of the most widely membrane processes include microfiltration (MF), ultrafiltration (UF), nanofiltration (NF) and reverse osmosis (RO). MF and UF are mostly used to remove suspended particles from produced water. They often serve as a pretreatment step for NF or RO to decrease membrane fouling and increase the longevity of the NF and RO membranes. At times, UF with relatively smaller openings than MF can be used to separate oil and larger organic molecules from the produced water. Lia and coworkers have shown 98 %, 90 %, and about 99 % removal of TOC, COD and residual oil using UF membranes modified with nano-aluminum particles[44]. UF membranes have also been found to meet regulatory

requirements for total hydrocarbons (THC), suspended solids, and dissolved constituents when used for the treatment of the PW from the North Sea oilfield[45]. NF membranes remove dissolved ions with an average molecular weight of 300 to 1000, as well as divalent ions, organics and microorganisms in the waste stream[31]. NF has a higher water recovery and operates at a lower pressure than RO. RO membranes are used for desalting produced water. They can effectively remove nearly all dissolved ions and cut down the TDS to close to freshwater quality standards (the typical exception being the secondary drinking water standard for chloride) but operate with a relatively lower recovery and high pressure than NF membranes. The drawbacks of RO and NF are limited water recovery, requirement for extensive pretreatment, and large waste stream (concentrate). The efficiency of the membranes, as well as their useful life, depends on the TDS concentration in the PW. A higher TDS increases the fouling propensity and decreases the life span of the membrane. The recommended maximum TDS is around 40,000 mg/l[43].

2.5 Scale formation in oil and gas production

One of the fundamental problems that have attracted much attention in recent years is the formation of scales on pipelines and equipment, above and below ground, and in producing formations. Oilfield scaling problems resulting from oil-field water flooding have been reported in oil fields in Indonesia, Algeria, Saudi Arabia, and Russia[46,47]. Scales are normally formed if two incompatible fluids are mixed to form a supersaturated solution with respect to a given mineral. They can also form as a result of changing temperature and pressure. The solubility of all mineral scales decreases when the pressure decreases, at a constant temperature. This effect is more pronounced for divalent scale forming cations[48]. The key in successfully predicting scale formation and corrosion in the oil and gas industry is accurately determining the pH, brine chemistry and scaling tendencies of a production system[48]. Scales such as barite, celestite,

calcium sulfates and halite are not pH sensitive. On the other hand, dolomite, calcite, siderite and sulfide scales are strongly pH dependent[48].

2.5.1 Barite

The mineral formed by the reaction between barium and sulfate ($BaSO_4$) is referred to as barite. Barite can be formed as a consequence of supersaturation resulting from the mixing of a sulfate containing water (e.g., seawater) with a water that contains barium. The thermodynamic solubility constant of barite is 1.1×10^{-10} which is relatively less soluble than calcium carbonate. It can also be formed from the mixing of waters from two zones if one contains sulfate and the other contains barium. If the saturation state of the mineral is very high, no amount of scale inhibitor can stop its formation. The scale may not form immediately upon mixing[49]. Logs of barium vs sulfate for a large number of wells suggest that barite scale forms under downhole conditions[50]. Either Ba^{2+} or SO_4^{2-} is usually the limiting reagent, thus high concentrations of the two ions are never present simultaneously. Barium and sulfate concentrations below 1 and 15 mg/l, respectively, are difficult to measure[48]. During water flooding, the conditions around the injection well and the production well can change drastically[51]. The potential for barite scale formation is highest in these regions.

The temperature of the formation affects the critical saturation index (SI) at which barite precipitates. The critical SIs for temperatures of 25 and 120 °C are shown in Figure 7. The rapid formation of barite from produced water usually incorporates strontium ions into its structure when present. It has been found that for every seven barium ions, up to one strontium ion is incorporated into the barite mineral structure[20] . Barite is also one of the biggest sources of NORMs as $^{226}Ra^{2+}$ is also able to substitute into the crystal lattice[20].

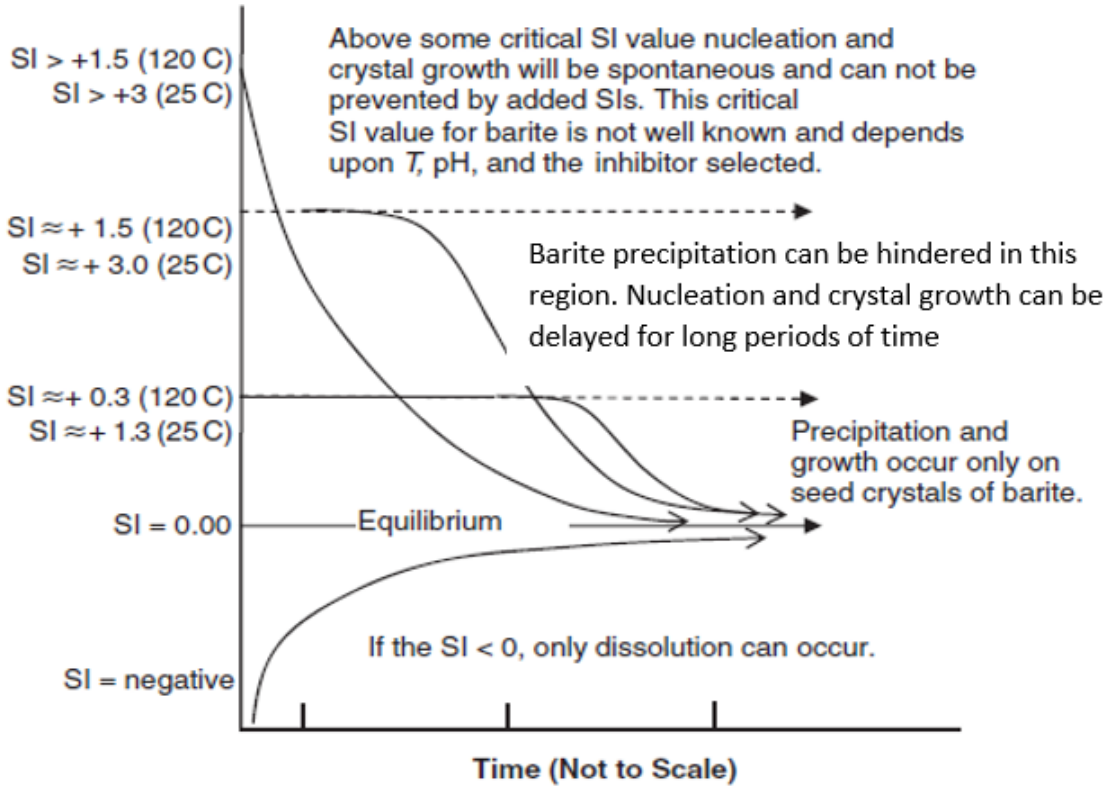

Figure 7: Critical SI values for barite precipitation at different temperatures (modified from Kan and Tomson[48])

2.5.2 Calcium sulfates

Gypsum ($CaSO_4 \cdot 2H_2O$) and anhydrite ($CaSO_4$) are the commonly reported phases of calcium sulfate. Gypsum has been °reported to form between 40 to 90 ^oC while anhydrite forms above 90 ^oC[48]. Gypsum has also been reported to be stable below 38 ^oC while anhydrite is the only stable phase above 58 ^oC and at a pressure of about 100kPa[52]. In high ionic strength solutions, where the activity of water is low, a third phase called hemihydrate or bassenite ($CaSO_4 \cdot 1/2H_2O$) usually forms at intermediate temperatures[48,53]. From Figure 8 gypsum is the stable phase at low temperature and pressure while anhydrite is more stable at a temperature of about 60 ^oC. Lu *et al.*[54] and Kan and Tomson[55] found the formation of anhydrite to occur at lower temperatures when hydration inhibitors like methanol and monoethylene glycol (MEG) lowered the activity of

water. Calcium sulfate precipitates can form when produced water that contains calcium and sulfate near saturation experiences a pressure drop or increase in temperature. They can also form due to the mixing of incompatible fluids during water flooding[54–56].

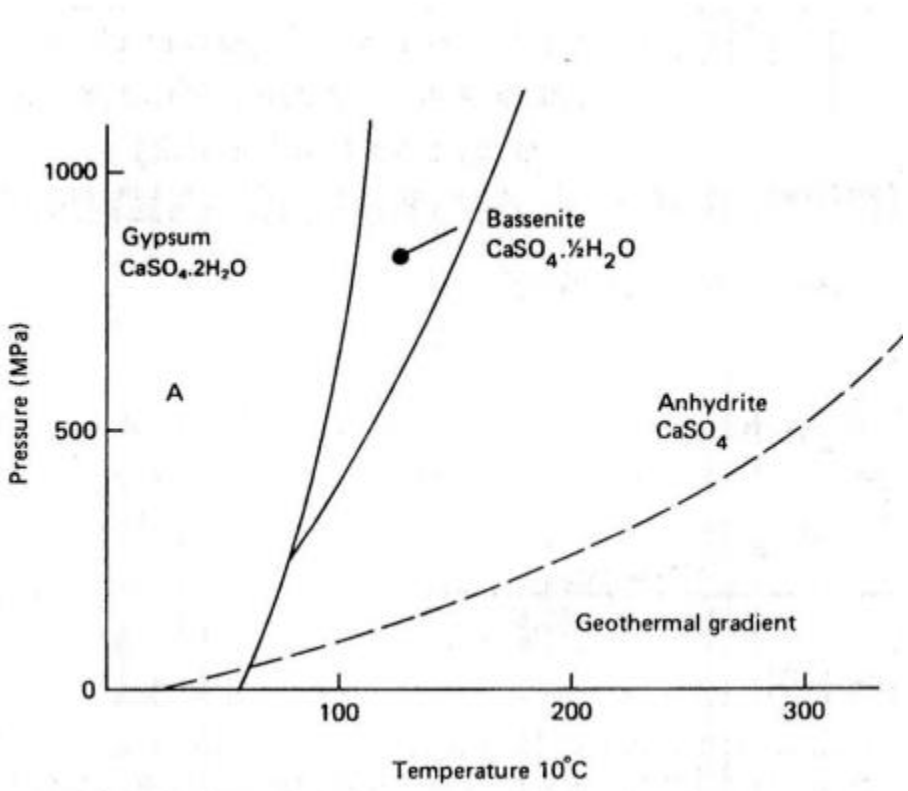

Figure 8: Gypsum and anhydrite phase stability with respect to pressure and temperature[53].

2.5.3 Silica

Ordinary "low" quartz is the stable form of silica between temperatures of 0 to 200 ^{0}C while amorphous silica is metastable within this range[57]. Silica usually does not form under production conditions because it polymerizes very slowly at lower temperature[48]. Silicates polymerizes to form large polymers with time, with slower kinetics at lower temperature and faster kinetics at high temperatures[48]. The extent of nucleation is predicated on the degree of supersaturation and

the interaction of silanol groups to form polymers or aggregates[58]. At pH 8 or greater, silica precipitates quickly turn into aggregates[58].

2.5.4 Dolomite

Dolomite precipitates do not form under abiotic laboratory conditions at room temperature and pressure despite multiple attempts to do so[48,59]. Inducing dolomite precipitation has been achieved in the lab in the presence of both aerobic and anaerobic microorganisms, or under special conditions such as high pressure, temperature and pH[60,61]. Vasconceolos *et al.*[62] performed an experiment to precipitate dolomite in the presence of sulfate reducing bacteria (SRB) from the Desulfovibrio group. They proposed that the direct involvement of these anaerobes can help overcome the kinetic barrier to dolomite nucleation, by increasing the pH and alkalinity of the solution, and also reducing the inhibition effect of sulfate on dolomite formation[63]. Other researchers like Sanchez-Roman *et al.* [64] conducted an experiment at 25 ^{o}C and 35 ^{o}C with SO_4^{2-} concentrations of 0 to 56 mg/l in an attempt to induce dolomite precipitation. They used aerobic microorgansims (V.marismortui and H. meridiana) that are known to cause the formation of Ca–Mg carbonate precipitates with an initial Mg/Ca ratio of 7.5. From the study, it was inferred that sulfate had no inhibitory effect on dolomite formation as claimed by other researchers.

2.5.5 Halite

The mineral formed by sodium chloride precipitation is called halite. Halite precipitate has been found at wellheads of gas reservoirs. The declining pressure head coupled with the increase in the solubility of water in methane is responsible for this phenomenon[65]. Pitzer *et al.* [66] estimated the solubility of halite to be 6.275 M at 50 ^{o}C. When the formation brine is saturated with respect to halite, a slight decrease in temperature can cause halite precipitation[48].

2.5.6 Sulfides

Sulfide scale control is still a subject that is not well understood. Precipitation of metal sulfides is caused mainly by a decrease in temperature and an increase in the concentration of heavy metals in solution in the absence of other anions that are capable of reacting with these heavy metals[67]. The solubility of sulfides generally increases with temperature, as such it is more likely to form near wellheads where there is considerable drop in temperature[67]. These scales include PbS, CaS, ZnS, FeS_2, FeS and are not limited to these examples. Hot gas fields contain about 25 % or more by volume of H_2S gas[48]. As such, sulfide scale is more predominant in gas formations that contain heavy metals.

2.5.7 Calcium carbonate

The crystallization of calcium carbonate ($CaCO_3$) mostly occurs in three abundant polyforms: calcite, aragonite and vaterite. Of these three polyforms, calcite is the most thermodynamically stable form in pure water at ambient conditions followed by aragonite and vaterite[68,69]. The other polyforms of calcite include monohydrocalcite, ikaite and amorphous calcium carbonate (ACC)[70]. The thermodynamic conditions determine which form is crystalized and the less stable forms of calcium carbonate could transform into another stable polyform if the right thermodynamic conditions are met, with vaterite (the metastable form of calcium carbonate) being a precursor of aragonite and calcite[71]. ACC is the most unstable polyform of calcium carbonate which quickly transforms to the other stable polyforms of calcium carbonate in solutions at ambient temperature[72]. The structure with the lowest Gibbs free energy at a particular temperature and pressure determines the most stable crystal[68]. Calcite is the most common type of scale found in major industrial settings. In an oil field setting, Kan and Tomson[48] have argued that pressure drop is the main cause of calcite scale in saline waters[48].

They stated that if the bottom hole pressure drops by a factor of 5 to 10, there is a likelihood of calcite scale forming at the wellhead[48].

2.6 Low salinity water flooding (LSWF) in carbonate formations

Water flooding has been in existence since 1865[36]. It is the most commonly used oil recovery technique. Waterflooding is the process of injecting relatively high salinity water (more saline than freshwater) to increase reservoir pressure to enhance or improve oil production. Water flooding has been modified by adding specific ions to aid in the wettability alteration of rock surfaces from an oil-wet to a water-wet condition. This technique has seen an extensive application in sandstone and carbonate reservoirs. Laboratory experiments conducted by researchers have pointed to one conclusion: LSWF enhances oil recovery in both secondary and tertiary oil recovery scenarios[73–87]. In sandstone, wettability alteration is related to the properties of the associated clay. For carbonates however, the actual mechanism responsible for wettability alteration is still under contention, with a lot of research speculating about the possible causes of improved oil recovery.

2.6.1 Wettability alteration during LSWF of carbonate formations

Production efficiency in oil bearing petroleum reservoirs is determined by the wettability of the rock surface. Overall, water-wet formations favor oil production over oil-wet rock surfaces[88]. Yousef *et al.*[89] used seawater and its dilutions with TDS concentrations ranging from 57,670 down to 600 ppm to perform a series of core flooding experiments. Contact angle and interfacial tension (IFT) measurements were conducted at reservoir conditions to investigate the effect of low salinity on oil recovery from carbonate rocks. The result showed an 18 % incremental oil recovery after flooding the core in succession with seawater and a stepwise dilution of seawater. The results from Figure 9 illustrated that IFT had little to do with the incremental oil recovery.

In Figure 10, the change in contact angle on the rock surface was observed from an intermediate water-wet zone to a water wet-zone after coreflooding, illustrating wettability alteration. After performing a nuclear magnetic resonance test, they surmised that wettability alteration occurred due to dissolution of the rock and the resulting change in the surface charge of the rock. They also concluded that the wettability alteration, and not the change in interfacial tension, was the cause for the observed incremental oil recovery.

Aladasani *et al.*[90] simulated published results of the core-flooding data from Yousef *et al.*[89]. They concluded that the incremental oil recovery during LSWF is caused by alteration of the wettability from oil wet to intermediate wet. They also observed that the capillary pressure became less negative, increasing the end point relative oil permeability and hence the observed incremental increase in oil recovery in Yousef *et al.*'s[89] work.

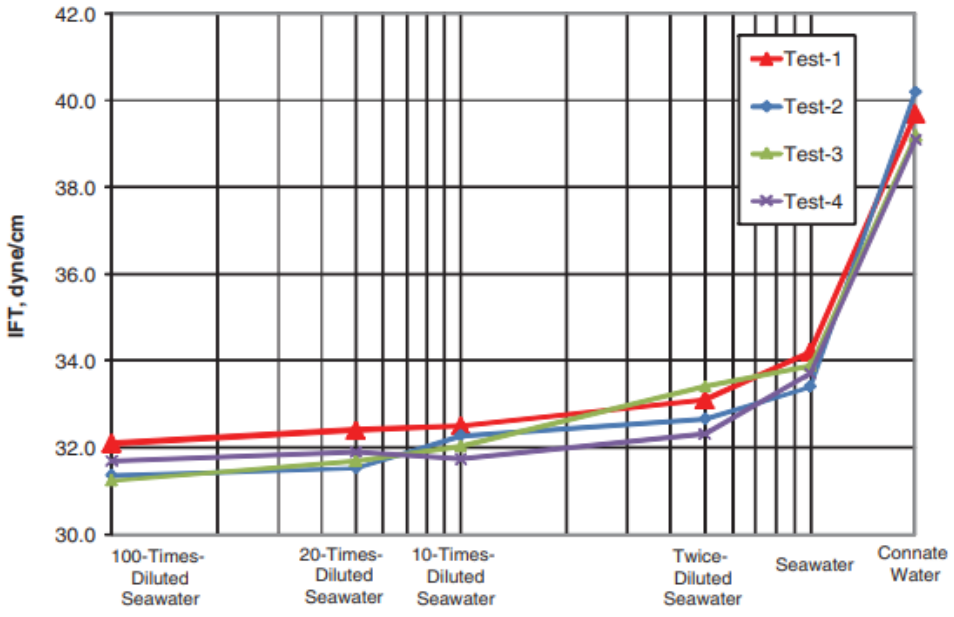

Figure 9: IFT measurement after coreflooding with seawater and its dilutions[89]

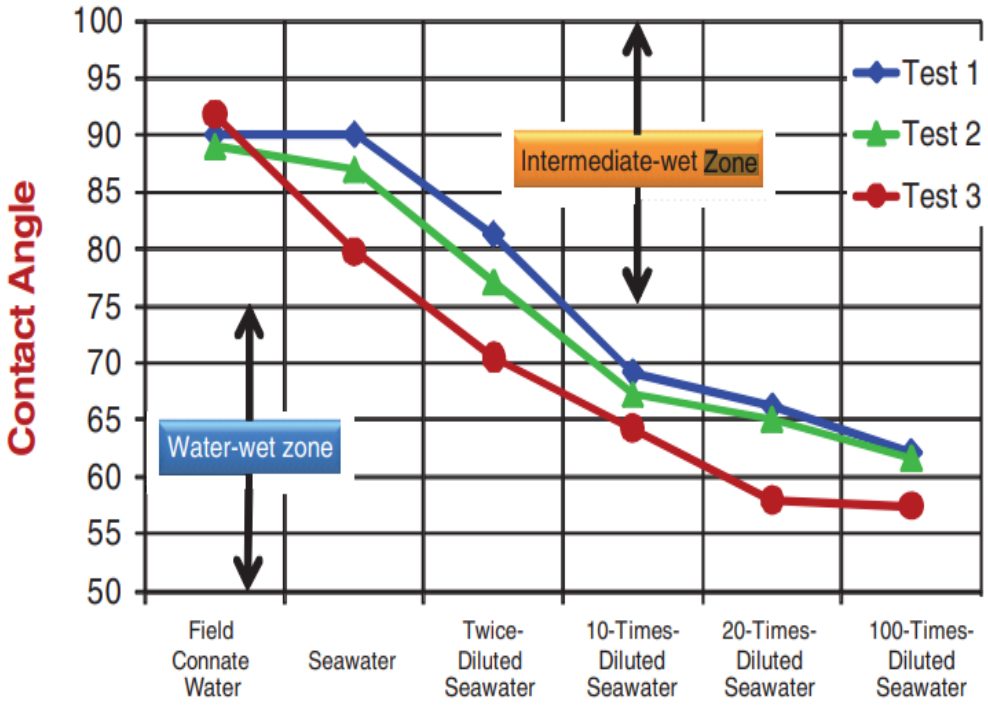

Figure 10: Contact angle measurement after coreflooding with seawater and its dilutions[89]

2.6.2 Wettability alteration due to ion exchange

Some researchers have attributed wettability alteration of rock surfaces to be due to the presence of Ca^{2+}, Mg^{2+} and SO_4^{2-} ions[76,80–87]. The rock surfaces of carbonate formations have been found to have a positive charge, below a pH of about 8 to 9.5[91], which interacts with the carboxylic acid functional groups of oil constituents to form bonds[92], thereby making the rock surface oil-wet and retarding oil flow. These bonds can be disrupted by the reaction between the free electropositive ions (especially divalent cations such as magnesium and calcium) and the carboxylic acid groups of the oil at the rock surface. Brady et. al[92] explained that this type of reaction forms complexes with a net positive charge, such as R-COO-Ca+. The net positive charge on the rock surface repels the net positive charge on the carboxylic acid complex, inhibiting bonding of the oil to the rock surface. In addition, Strand *et al.*[93] studied the effect of sulfate on wettability alteration by performing spontaneous imbibition studies on calcite,

magnesite, and dolomite. They discovered that the influence of sulfate on the imbibition of these rocks was more pronounced at high temperatures. At high temperatures, sulfate is able to react with the positively charged surface of the rock, giving the surface a net negative charge and causing a break in the electrostatic force between the rock surface and the carboxylic ions of the oil[94]. Figure 11 shows the contact angle measurements taken during the experiment.

Hognesen and his co-workers[95] performed an imbibition experiment on limestone and chalk core at 90-130 ^{o}C using seawater with a modified (increased) sulfate concentration and found sulfate to be a good catalyst for wettability alteration in the presence of surfactant. They used a sulfate concentration of 2.31 g/l, higher than the 1.7 g/l used in Strand *et al.*'s[93] work.

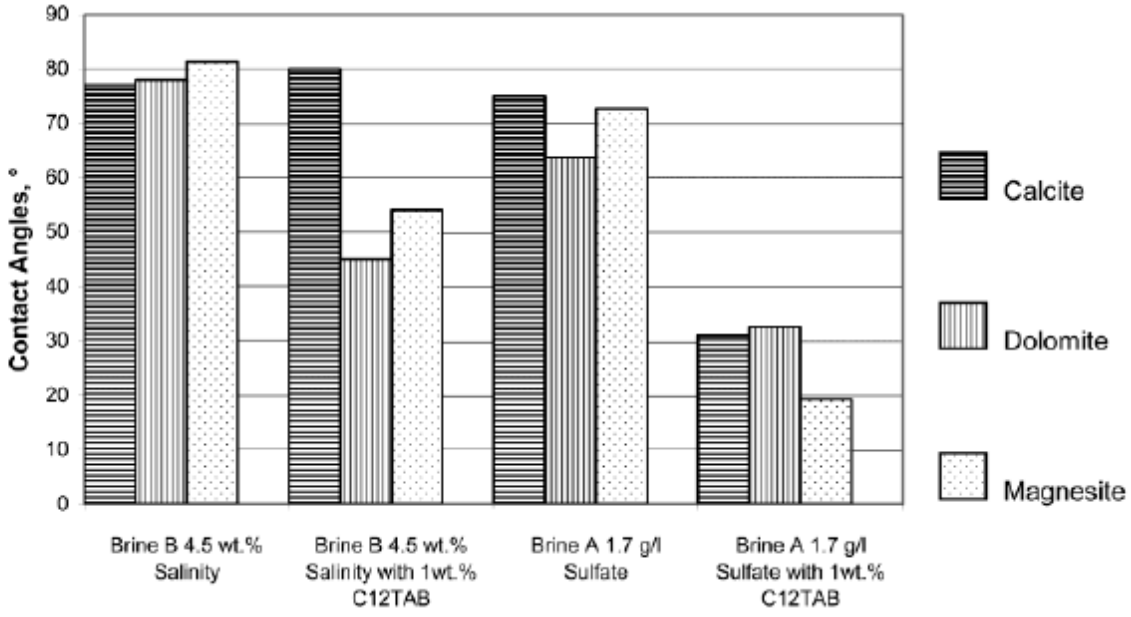

Figure 11: Contact angle measurements of brines with calcite, dolomite and magnesite under various conditions[97](C12TAB is the applied surfactant.)

Zhang et al.[85] also explained that, at high temperatures, Ca^{2+} and SO_4^{2-} as well as Mg^{2+} and SO_4^{2-} react at the surface of chalk to cause a displacement of the carboxylic acid groups of the oil,

reducing the electrostatic forces between the oil and the rock. This mechanism is depicted in Figure 12.

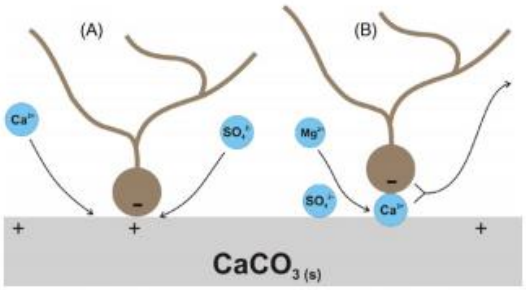

Figure 12: Suggested wettability alteration in chalk (from Zhang *et al.*[83,85])

Alameri *et al.*[74] also conducted an experiment to look into the observed incremental oil recovered in a carbonate formation during low salinity water flooding. After measuring the contact angle, interfacial tension (IFT) and the changes in the concentrations of $Ca^{2+,}$ Mg^{2+}, Cl^{-} and SO_4^{2-} ions, the decrease in the concentrations of these ions lead them to believe is was possible that multi-ion exchange on the surface of the rock caused the observed wettability alteration.

2.6.3 Calcite dissolution

Al-shalabi *et al.*[96], in their attempt to understand the cause of wettability alteration, performed an extensive investigation by matching model predictions with previously published data[89,96]. In their research, UTCHEM software was used to match the results of a published coreflooding experiment that used seawater and its dilutions. After modeling the process, they performed an optimization and sensitivity analysis of the published result. They concluded that carbonate mineral dissolution and changes in the surface charge of the rock were the reasons behind wettability alteration in carbonate formations[96]. Al-shalabi *et al.*[97] argued that the change in pH due to dissolution changes the wettability if the pH exceeds the point of zero charge. This

expands the electric double layer and also changes the rock's surface charge. Figure 13 illustrates the change of the rock surface from an oil-wet to a water-wet surface[36].

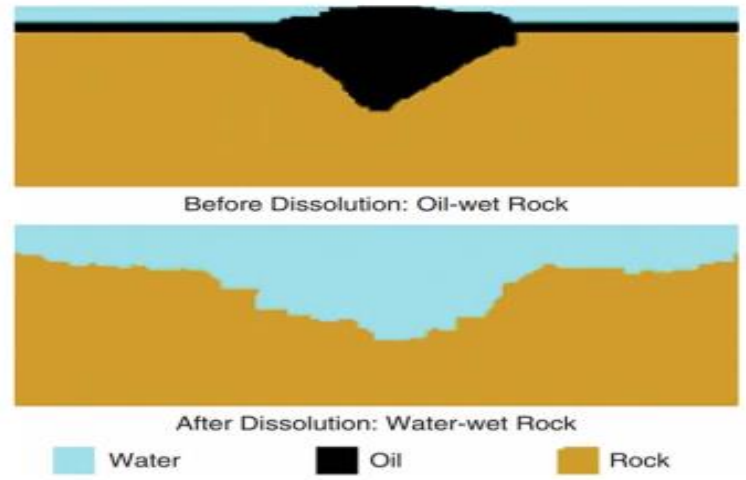

Figure 13: Wettability alteration due to mineral dissolution[98]

Austad *et al.*[73] drew a parallel between the low salinity effect of the work of Zhang *et al.*[83] and carbonates containing anhydrite. Instead of adding sulfate to the injected brine, dissolution of the rock provided the required sulfate to serve as the catalyst for wettability alteration, as explained by Zhang *et al.* [83]

In contrast to the above findings, Mahani *et al.*[99], after measuring the zeta potential and contact angle in the solution and on the surfaces of dolomite and limestone rocks, reported an increase in in the oil recovery during low-salinity water flooding without any observed mineral dissolution. A summary of the proposed mechanisms for wettability alteration is shown in Figure 14.

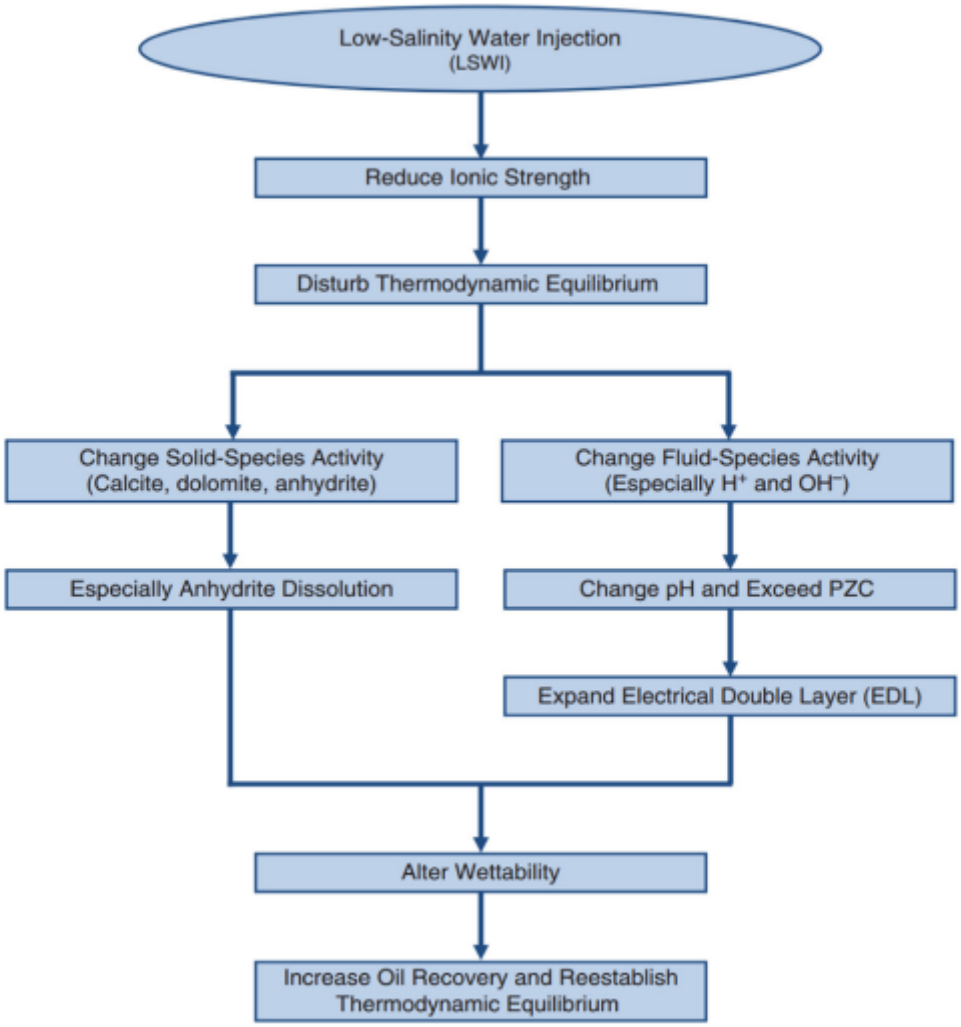

Figure 14: Flow chart for the proposed mechanisms of wettability alteration in carbonate formations[36]

2.7 Theory of calcite dissolution

The previous section underscores the importance of calcite dissolution in understanding the geological and environmental setup in formations contain hydrocarbons (oil and gas formations). The kinetics of calcite dissolution and precipitation at varying temperatures have been investigated in a number of studies[100–108].

2.7.1 Kinetics

There has been a large variance in the reported rate constants for calcite dissolution and precipitation kinetics. These discrepancies can be attributed to experimental techniques and their associated reaction conditions such as the solution saturation stage, CO_2 partial pressure, the solution ionic composition, pH, seed surface properties, calcite dissolution or precipitation inhibitors, and the hydrodynamics of the solution[108].

Plummer *et al.*[100] considered calcite dissolution in a CO_2 -H_2O solution using free-drift methods and pH stat at ambient surface conditions. The ranges of temperature, pH and P_{CO2} were 5 to 60 ^oC, 2 to 7, and 0.0003 to 0.97 atm, respectively. From the study they suggested that calcite dissolution is governed by the following equilibrium reactions:

$$CaCO_{3(s)} + H^+_{(aq)} \rightleftharpoons Ca^{2+} + HCO_3^- \quad (1)$$

$$CaCO_{3(s)} + H_2CO_{3(aq)} \rightleftharpoons Ca^{2+} + 2\,HCO_3^- \quad (2)$$

$$CaCO_{3(s)} + H_2O \rightleftharpoons Ca^{2+} + HCO_3^-{}_{(aq)} + OH^- \quad (3)$$

The rate of dissolution (R_f) was given by the following equation:

$$R_f = k_1\{H^+\} + k_2\{H_2CO_3\} + k_3\{H_2O\} \quad (4)$$

where k_1, k_2, and k_3 are dissolution rate constant(molescm^{-2}s^{-1}) and {α} are the activities of the species present. The values of the dissolution constant depend on the temperature and are related by the following equation:

$$\text{Log } k_1 = 0.198 - 444/T - 3 \quad (5)$$

$$\text{Log } k_2 = 2.84 - 2177/T - 3 \quad (6)$$

$$\text{Log } k_3 = -1.10 - 1737/T - 3 \quad (7)$$

Appelo and Postma[109], citing Plummer *et al.*[102], described k_3 to be related to temperature by the following equation:

$$\text{Log } k_3 = -5.86 - 317/T \text{ for } T \leq 298 \qquad (8)$$

$$\text{Log } k_3 = -1.10 - 1737/T - 3 \text{ for } T \geq 298 \qquad (9)$$

The overall rate (dissolution and precipitation) equation from the study was given by:

$$R = k_1\{H^+\} + k_2\{H_2CO_3\} + k_3\{H_2O\} - k_4(\{Ca^{2+}\}\{HCO_3^-\}) \qquad (10)$$

$$\text{where the rate of precipitation, } R_b = k_4(\{Ca^{2+}\}\{HCO_3^-\}) \qquad (11)$$

In the study by Plummer *et al.*[100], experiments were not run to observe the rate of calcite precipitation. Reddy *et al.*[106] measured the rate of calcite precipitation at 25 ^oC and fixed partial pressure of CO_2 between 0.03 and 0.3 atm to validate the equation put forward by Plummer *et al.*[100] Talman *et al.*[110] tested this same model at 100, 150, and 210 °C and found the Plummer *et al.*[100] model to be applicable at these temperatures.

Chou *et al.*[111] used a continuous fluidized bed reactor at 25 °C to investigate the dissolution of various carbonate minerals. Their observation was similar to that of Plummer *et al.*[100]. The following overall rate equation was put forward as a result of their study:

$$R = k_1\{H^+\} + k_2\{H_2CO_3\} + k_3\{H_2O\} - k_{-4}(\{Ca^{2+}\}\{CO_3^{2-}\}) \qquad (12)$$

where $k_{-4} = k_{3/} K_{sp,}$ and K_{sp} is the thermodynamic solubility. Kanel and Morse[112] also described the rate of calcite dissolution (R_f) as follows:

$$R_f = k_f(1-\Omega)^n \qquad (13)$$

where Ω is the ratio IAP/K_{sp}, IAP is the ion activity product, K_{sp} is the thermodynamic solubility product constant, and k_f is the dissolution rate constant.

Morse in his later work with Arvidson[113] gave the following equation for the overall rate:

$$R = (\frac{A}{V})K\,(1-\frac{IAP}{Ksp})^{n} \qquad (14)$$

where A is the surface area of the calcite mineral, v is the volume of solution, K is the rate constant, and n is the overall order of the reaction.

2.7.2 The reaction order (n)

There is a wide variance in both the rate constants and reaction orders determined from laboratory experiments. Walter and Morse[114] together with Keir[115] ascribed a high reaction order to the rate of calcite dissolution in seawater (n = 3 and 4.5, respectively). Others have argued for a linear dependence on the saturation state of calcite in seawater (thus, n = 1)[115]. However, perturbation due to aquatic organisms may affect the in-situ rate and hence the reaction order. The reaction orders reported by Nancollas and Reddy[116] and Davies and Jones[117] were 1 and 2, respectively.

2.7.3 Rate controlling mechanisms

There are generally two rate limiting steps in calcite (limestone) dissolution in water: (1) dissolution at the surface of the mineral, which is dependent on the ionic composition at the liquid-rock boundary; and (2) diffusion of the dissolved ions (Ca^{2+}, HCO_3^-, and CO_3^{2-}) from the boundary to the bulk solution, which also depends on physical factors such as the V/A (volume to surface area) ratio of the mineral, flow conditions (e.g., turbulent or laminar flow) and carbon dioxide partial pressure in equilibrium with the solution[118].

Morse and Arvidson[113] broke down the rate controlling mechanism for dissolution into seven steps. These physical and chemical processes are listed as follows:

1. Diffusion of the reactants from the bulk solution to the mineral surface
2. Diffusion of the product form the mineral surface to the bulk solution
3. Adsorption of the reactant unto the mineral surface
4. Transport of the reactant from the solid surface to active energy site
5. Transport of the product away from the reaction site
6. Chemical reaction between the solid surface and adsorbed reactants, which may include intermediate steps such as hydration, bond formation, etc.
7. Desorption of the product from the mineral surface into solution

In general, the slowest of these steps becomes the rate limiting step. The rate is said to be diffusion controlled when steps 1 and 2 are the slowest. Also, a combination of the surface-controlled mechanisms in steps 3 through 6 can become the rate limiting step. Most soluble minerals have the diffusion control mechanism as their rate limiting step while insoluble minerals are usually surface controlled[119]. Carbonate minerals belong to the latter group. The saturation state varies linearly with the rate at which the reaction proceeds if the rate is diffusion controlled. On the contrary, the saturation state varies non-linearly if the rate is surface controlled[113]. Diffusion controlled kinetics prevail under extreme undersaturation. If the saturation state approaches equilibrium, the rate limiting step gradually transitions from a diffusion-controlled to a surface-controlled reaction[113].

Multiple researchers have found dissolution rates to be slower in the field compared to laboratory experiments because the physical and chemical conditions play a pivotal role in dissolution and precipitation of calcite[120–124]. Hydrodynamic conditions with respect to the mineral surface

(stagnant, turbulent or laminar flow) affect the transport of reactants or products to and from the diffusive boundary layer (DBL) formed around the rock[113]. In flowing conditions, molecular diffusion is substantially slower than advective transport. When molecular diffusion through the boundary is slower than the surface controlling mechanism, it becomes the rate limiting step. The thickness of the boundary around the mineral also shrinks considerably in turbulent flow condition which can also control the rate of reaction [113]. The concentration gradient of the dissolved mineral between the DBL and bulk solution is responsible for the movement of flux of solute across the water-sediment interface [125]. With suspended mineral sediment present, transport of the product and reactant from the surface as well as the individual reaction that forms or dissolve the mineral in the diffusive boundary layer is actually faster and affects the rate constant because of the reduction in size of the DBL. Also, exposing all the mineral surface to resuspension of the sediments reduces the DBL around each grain, increasing the rate constant[125].

2.7.4 Effect of pH

Calcite dissolution has been found to occur under different rate controlling mechanisms in three pH regimes: low, transitional and high[126]. Sjöberg and Rickard[126] discovered that in the low pH regime (pH< 4), the dissolution rate is diffusion controlled and it is directly proportional to the H^+ concentration. Equation 18 below describes the relationship between the rate of dissolution and the H^+ ions. In this regime, movement of H^+ through the DBL from the bulk solution, and diffusion of the reactant from and to the surface of the mineral through the DBL become the rate limiting steps[127,128].

$$R_f = k'_f\{H^+\}^{0.9} \qquad (18)$$

where k is the rate constant and $\{H^+\}$ is the activity of the hydrogen ion. Between pH 4 and 5.5, the dependence of the rate constant on the H^+ ions in the solution varies. This regime is normally referred to as the transition zone. The hydrodynamic conditions, nature of the mineral surface and composition of the bulk solution determines the pH at which the transition zone occurs. Calcite dissolution in this regime is controlled by both surface-reaction and diffusion through the DBL[102,107,127].

The rate is no longer dependent on pH above a pH of 5.5[100]. This is usually referred to as the high pH regime or H+ independent regime as shown in Figure 15. The reaction rate is directly proportional to the square root of the product of the calcium and carbonate concentration.

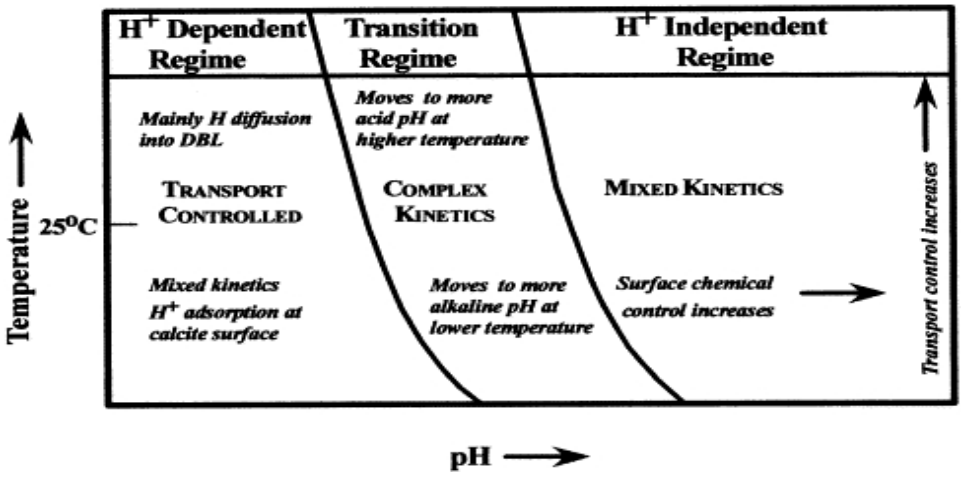

Figure 15: The dependence of calcite dissolution kinetics on pH and temperature[129]

2.7.5 Effect of calcium concentration

The influence of Ca^{2+} goes beyond the saturation state of the mineral itself. Sjöberg[130], in a study on calcite dissolution kinetics, found a 17 % increase in the rate constant when the concentration of calcite in the initial solution increased from 0 to 10 mM. Gutjahr *et al.*[131] found an approximately 40 % increase in the rate constant when the concentration of calcium in the solution was increased from 0.16 to 4.090 mM. Even though there is a wide discrepancy between

the reported values from these works, the underlying premise that increasing calcium concentration increases the rate constant was found to be true in both studies. Gledhill and Morse[132] conducted an experiment with high ionic strength solutions and they also found that an increase in the calcium ion concentration caused an increase in the rate constant.

2.7.6 Effect of magnesium concentration

Sjöberg[133] and Buhmann and Dreybrodt[134] found a strong inhibitory effect of magnesium on the dissolution rate of calcite. Sjöberg[133], after expressing the inhibitory effect of magnesium as a Langmuir-type adsorption, concluded that the rate of calcite dissolution becomes independent of the inhibitory effect of magnesium after a threshold concentration is exceeded[133]. The concentration of magnesium used in his work was less than 50 mM. Other researchers such as Campton and Brown [135] found the inhibitory effect of magnesium to be strong at neutral to alkaline pH (8-9) while Alkattan *et al.*[136] found the effect of magnesium at acidic conditions (pH 1-3) to be negligible[136]. Campton and Brown[135] conducted their experiment in an alkaline environment which enhanced the inhibitory effect of magnesium[135]. Van Cappellen *et al.*[137] and Pokrovsky and Schott[138] have reported a lower inhibition effect of cations below the point of zero-surface charge of pH 8.2[137,138]. Gledhill and Morse[132], after varying the concentration of magnesium between 0.02 and 0.12 M, discovered only a moderate inhibition effect on the rate of calcium dissolution. They alluded to the work of Sjöberg[133] as a basis for their observation that increasing the concentration of magnesium beyond a certain threshold concentration does not affect the rate constant any further.

2.7.7 Effect of sulfate

Sjöberg[130] found that sulfate reduces the dissolution rate by 40 % if the concentration in the solution is equal to the concentration of sulfate found in seawater[133]. In the presence of

increasing magnesium and calcium concentration, Sjöberg[130] observed an increase in the inhibitory effect of sulfate on the mineral dissolution of calcite[133]. Gledhill and Morse[132] also found that at lower sulfate concentrations (<<less than seawater) the effect of sulfate can be analogous to that caused in seawater if the total dissolved solids (TDS) is greater than 200,000 mg/l. It should be noted that this is true only if the $pCO_2 > 0.1$ and pH< 6.5. They also found an increased inhibitory effect similar to what Sjöberg[130] observed when the concentrations of calcium and magnesium in the solution were increased[133].

2.7.8 Effect of pCO_2

The carbonate system's speciation, i.e., the relative concentrations of carbonic acid (H_2CO_3), bicarbonate (HCO_3^-) and carbonate (CO_3^{2-}), depends very heavily on pH. In general, carbonic acid dominates the species at acidic pH (pH<6.3), bicarbonate dominates at neutral pH, and CO_3^{2-} dominates in the basic region (pH>10.3)[139]. When dissolved in water, carbon dioxide reacts with water to form carbonic acid. At high pCO_2, therefore, solutions tend to be relatively acidic. Aqueous CO_2 reacts with water to form carbonic acid H_2CO_3. Carbonic acid diffuses into the DBL and reacts with the calcite surface to increase dissolution of calcite in the DBL. The concentration gradient caused by the rapid dissolution of calcite facilitates the transport of Ca^{2+} and CO_3^{2-} from the DBL into the bulk solution. The acidic pH allows the carbonate ion to quickly react with water to convert to bicarbonate. Hence, high pCO_2 pressure increase both the amount and the rate of dissolution.

2.7.9 Effect of ionic strength

Ionic strength has been reported by Morse and Gledhill[132] to inhibit the rate of calcite dissolution as shown in Figure 16. In their experiment, they varied the ionic strength from 1 M to 4 M while keeping the pCO_2 at 0.5atm and temperature at 25 ^0C[132]. The solution contained 6,480 mg/l of

calcium, 1,625 mg/l of magnesium, and no sulfate They cited Sjöberg[130] as an explanation for their observation[133]. Sjöberg[130] alluded to the fact that the activity of water at high ionic strength decreases hydration of metal ions. A decrease in the number of water molecules surrounding calcium ions could retard the rate of calcite dissolution because the hydration energy might be less able to overcome the attractive forces within the mineral lattice. Also, Morse and Gledhill[132] suggested that stronger interparticle attraction in high ionic stength solutions increases the rate of precipitate formation and seed growth in a manner similar to colloid flocculation. Finneran and Morse[140] investigated the effect of ionic strength on the dissolution of calcite in a solution containing KCl and NaCl without phosphate and magnesium ions, and found the rate to be faster in KCl than NaCl. They also observed that the rates generally decreased with an increase in ionic strength. They contended that for calcite dissolution to proceed, a minimum of 45-55 % mole fraction of free solvent is required in undersaturated conditions at temperature and pCO_2 ranges of 25-55 ^{o}C and 0.1-1 atm, respectively[140]. A study by Zuddas and Mucci[141] on the effect of ionic strength on calcite precipitation from seawater showed that an increase in the ionic strength increased both the partial reaction order of the carbonate ion and the forward reaction rate constant. Conversely, Pokrosky and coworkers[142] found that, far from equilibrium, the calcite dissolution rate did not change with ionic strength in a pure NaCl solution up to 1M.

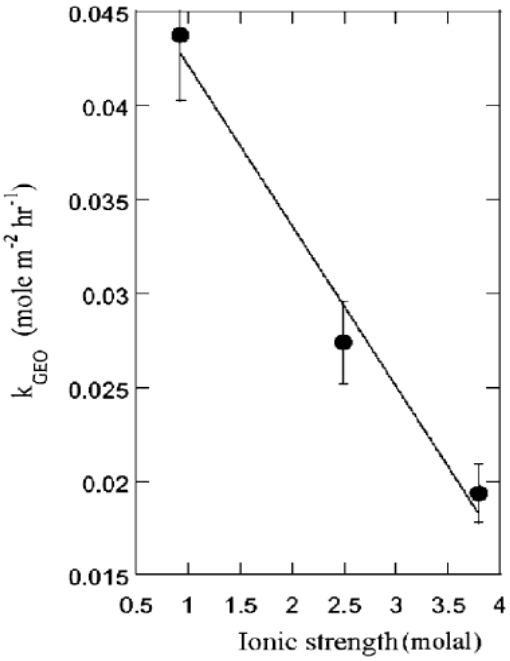

Figure 16: Change in the dissolution rate of calcite as ionic strength increases[132]

2.8 Modeling mineral chemistry in PW

The primary causes of formation damage are influenced by physiochemical, chemical, hydrodynamic, mechanical and biochemical factors[143]. Understanding these factors through modeling, field and laboratory experiments is imperative to combat against reservoir damage in EOR applications involving water flooding.

Civan[143] cited Bishop's[144] summary of the mechanism controlling formation damage as follows: fluid-fluid incompatibilities, rock-fluid incompatibilities, solids invasion, phase trapping or blocking (entrapping of water-based fluids), chemical adsorption or wettability alteration, fines migration, and biological activities during drilling. Among the mechanisms listed above, rock-fluid incompatibility and fluid-fluid incompatibility are two of the major causes of scale formation in petroleum reservoirs. For predicting the equilibrium of dissolved salts, the mean ion activity and the solubility product must be known. The solubility products of many salts can be

found from thermodynamic data. However, the activity of free ions governs the solubility of minerals or salt, especially in higher ionic strength solutions, as discussed below.

2.8.1 Activity corrections and coefficients

The interactions of ions with other ions in solution with low background ion concentrations are oftentimes ignored. However, in high ionic strength solutions, the behavior of specific minerals or chemicals becomes non ideal, making the concentration of ions available ions for reaction (free ions) lower than the analytically measured concentration. The background ions partially shield the interactions between specific ions as well as the charges of these ions. Ions can also come close enough in a way that allows them to form new species, or complexes. Activity coefficients are used to correct concentrations of specific ions in high ionic strength solutions. The effective free ion concentration of ions in a mixture available for chemical reaction is the "activity" of the ion. In very dilute solutions, activity and the concentration are generally considered equal. Failure to accurately predict activity coefficients in high ionic strength solutions can lead to large errors when estimating the solubility of inorganic minerals or species. The Debye-Hückel theory and model for estimating activity corrections are essentially based on two fundamental laws: (1) coulomb's law of electrostatic attraction and repulsion between particles with opposite or similar charges, and (2) the Boltzmann distribution law, which describes the effect of temperature on the attraction and repulsion forces that exist between charged particles[139]. The Debye-Hückel equation, which assumes ions behave as point-charges, has the form:

$$\ln\ \gamma_i = -\frac{Z_i^2 e^2 k}{2DkT} \qquad 20$$

where γ is the activity of the ith ion; e is the unit charge on the electron; k (in the denominator) is the Boltzmann's constant; D is the dielectric constant; k (in the numerator) is the reciprocal of the thickness of the electrical double layer surrounding the ion (also known as the Debye radius), which depends on the ionic strength of the solution; Z the integer value of the charge of the ion; and T is the temperature in kelvin. This equation assumes an infinitely dilute solution and, as the concentration of dissolved ions increases, the shielding of ions by other ions is not properly accounted for. This leads to an overestimation of the Coulomb forces, producing activity-coefficients that are too small. This error becomes significantly worse as the ionic strength (I) increases above 0.005 M[139]. Another parameter was introduced to mitigate the error encountered using the Debye-Hückel equation at high ionic strength, leading to the extended form of their equation. They called it the "ion size parameter," represented by **a** in the equation below:

$$\log\ \gamma_i = -\frac{Z_i^2 A\sqrt{I}}{1+Ba_i\sqrt{I}} \qquad (21)$$

where A and B are constants, with A = 1.8248 x 10^6 $(DT)^{-3/2}$ and B = 50.29 x10^8 x $(DT)^{-1/2}$; T is temperature in degrees Celsius and I is the ionic strength of the solution. The constant **a** represent the mean distance between the ion of interest and the other surrounding ions. The extended Debye-Hückel equation is generally assumed to model ion activity well up to I ~ 0.1 but fails to account for specific ion interactions that occur in higher ionic strength solutions. The Davies equation was then introduced to account for the specific effect of ion interactions at I > 0.1. The Davies equation becomes less accurate when the I become greater than ~ 0.5. There is a gradual decline in the activity of ions as I approach 0.5. Above this threshold, the activity begins to increase as the ionic strength increases as shown in Figure 17.

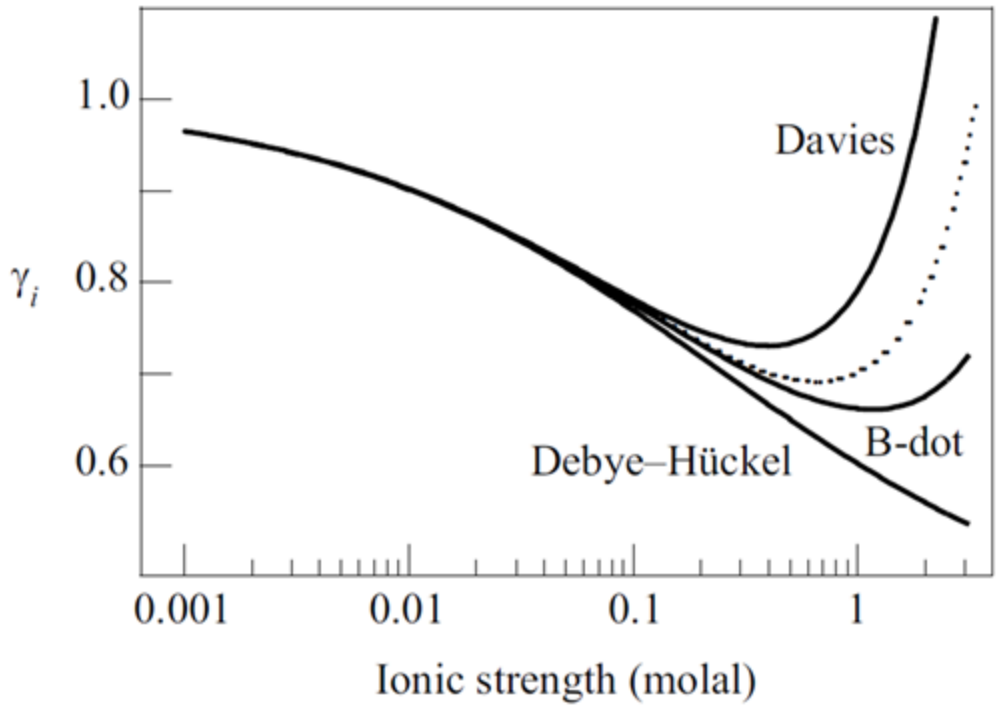

Figure 17: Variation in activity as ionic strength increases. The dashed line represents the extended Debye-Hückel equation[145].

Pitzer and his co-workers[147] in 1970 developed an ionic interaction model that extended the Debye-Hückel equation by introducing short range non-electrostatic ionic interactions not accounted for by the Debye-Hückel theory. The solvent, the concentration of the solute, temperature and pressure were incorporated into a virial expansion together with the Debye-Hückel term to form the Pitzer ion interaction equation. With increasing dilution, the Pitzer equation gradually approaches the Debye-Hückel limit[146]. The Pitzer model has widely been accepted as appropriate for predicting ion interactions at high ionic strength, up to ~ 4 M[48]. The coefficients for the Pitzer model were derived in binary, tertiary and quaternary systems such as NaCl-H_2O, NaCl-Na_2SO_4-H_2O and Na-Ca-Cl-SO_4-H_2O respectively. The Pitzer model accounts for both the short-range interactions of ions in concentrated solutions and the long-range interactions described by the Debye-Hückel equation[147]. The electrostatic repulsion or attraction

(long-range interactions) that exists between ions is a derivative of Coulomb's law of attraction describing the forces that that exist between charged species. The simplest form of the Pitzer equation is shown below.

$$\log\ \gamma_i = -\frac{Z_i^2 A\sqrt{I}}{1+Ba_i\sqrt{I}} + \sum B_{ij} m_j \qquad (22)$$

The first term represents the extended Debye-Hückel equation (long-range ionic interactions) and the last term accounts for specific ion interactions (short-range interactions). The Bij constant varies linearly with ionic strength. The virial expansion series of the binary and ternary interactions are used in deriving the Gibbs free energy as shown below[48]:

$$G_{Pitzer}^{Excess} = RT[w_w f^{\gamma} + w_w^{-1}\sum\lambda_{ij}(I)n_i n_j + w_w^{-2}\sum\mu_{ijk}n_i n_j n_k] \quad (23)$$

where w_w is weight of water in kg, I is the ionic strength in molality, n is moles, μ_{ij} and λ_{ij} are ternary and binary constant respectively, and

$$f^{\gamma} = A_{\phi}\left[\frac{\sqrt{I}}{1+1.2\cdot\sqrt{I}} + \frac{2}{1.2}\ln(1+1.2\cdot\sqrt{I})\right] \qquad (24)$$

where A_{ϕ}= 0.3915 at 1atm and 25 ^{o}C. The activity coefficient can be rewritten as:

$$\ln\gamma_i = \left(\frac{\delta G_{Pitzer}^{Excess}/RT}{\delta n_i}\right) \qquad (25)$$

The coefficients in the Pitzer model depend on the pressure, temperature, ionic strength and the composition of the solution. The constants and coefficients were derived in binary and ternary system such as NaCl-H_2O and NaCl-$NaSO_4$-H_2O, respectively. There are about 36 constants included in the original derivation of the Pitzer model, however many parameters for other mineral species have not yet been established.

Chapter 3 Materials and Methods

3.1 Brine exchange

The idea of exchanging formation brines of different salinity was proposed as a way of cutting down on the colossal amounts of produced water disposed into deep injection wells. The incentive for an effective produced water management scheme is not only environmental, in fact water management is the largest contributor to the operating cost of producing wells. Thompson[5] suggested closing the wastewater loop by exchanging formation water in a way that would enable the treatment of the less salty brine and reusing it for activities that require relatively low-quality water. With this scheme, little treatment is required to separate the oil from the brine before applying it in well fields for fracturing or incremental oil recovery. Figure 18 demonstrates the theory of brine exchange. Oil fields were identified by Thompson[5] from the Arbuckle and LKC strata that are good candidates for practicing this proposed water management systems. They include the Trapp, Hall-Gurney, Fairport, Kraft-Prusa, and Gorham fields.

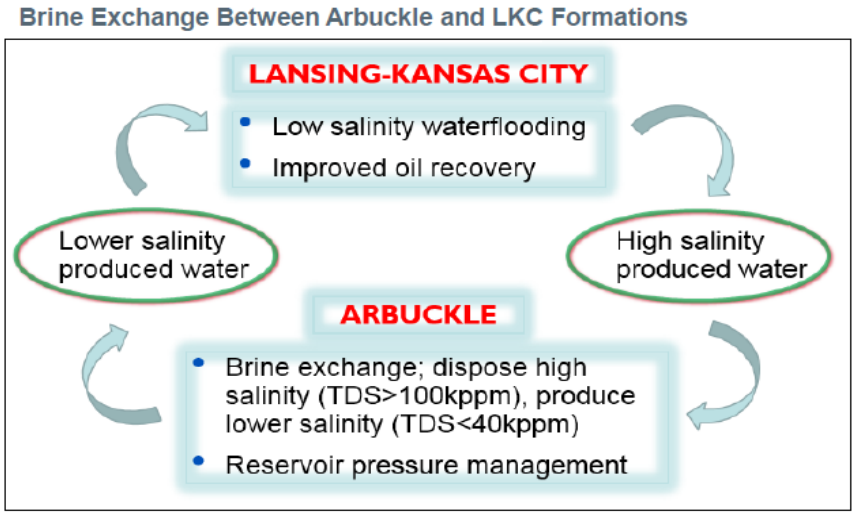

Figure 18: Potential brine exchange between the Arbuckle and LKC production Groups[5]

3.2 Study formations

The northwest and southeast Central Kansas Uplift (CKU) is known to contain two main hydrocarbon reservoirs: the Lansing-Kansas City (LKC) Group and the Arbuckle Group. While the LKC reservoir produced water is associated with high total dissolved solids, the Arbuckle Group is characterized by relatively low salinity produced water[148]. Both the LKC and Arbuckle are carbonate reservoirs made of interbedded shales and silts deposited in shallow to deep marine settings. Porosity is characterized by carbonate dissolution and precipitation[149]. The Arbuckle and LKC Group are prolific formations producing 36 % and 19 %, respectively, of Kansas oil from 1889-2002. The Arbuckle, being the most prolific oil producing formation has strong water drives that provide the required energy for production[150].The characteristics of these two hydrocarbon reservoirs are ideal for the purpose of this investigation. Figure 19 represents oil production by stratigraphic unit in Kansas.

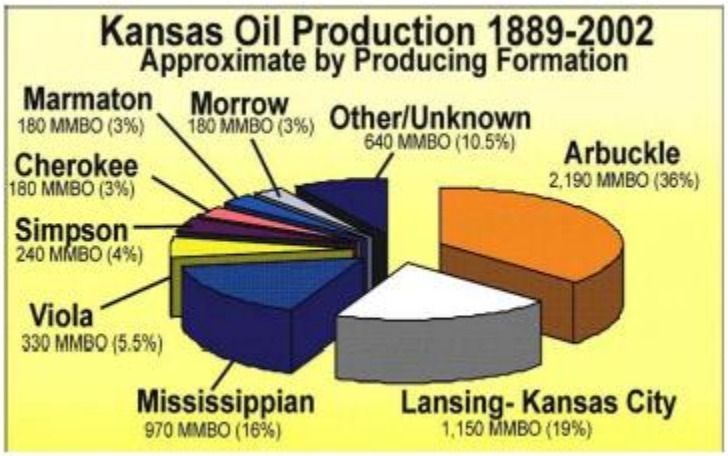

Figure 19: Oil production by stratigraphic unit in Kansas[148]

3.2.1 The Arbuckle Group in Kansas

The Arbuckle Group in Kansas emanates from the Cambrian-Ordovician craton in North America [151]. The Arbuckle consists of dolomized carbonate rock with regional unconformity[151]. The north to the southern section of the Arbuckle is rich in cherty dolomite, dolomitic limestone and dolomite deposits[152]. The limestone and dolomite regions of the Arbuckle in Kansas over the years have been known for their abundant oil production and are said to be the most prolific of the Arbuckle Group [150]. The Arbuckle reservoirs in Kansas account for 2.19 billion barrels of oil out of a total of 6.1 billion barrels of oil produced through 2002. They also account for about 69 % (1.269 million barrels) of oil produced in the Central Kansas Uplift area as shown in Figure 20. The Arbuckle Group has a high water cut. A large portion of its porosity is primary in nature, developing from the original sedimentation process[153].

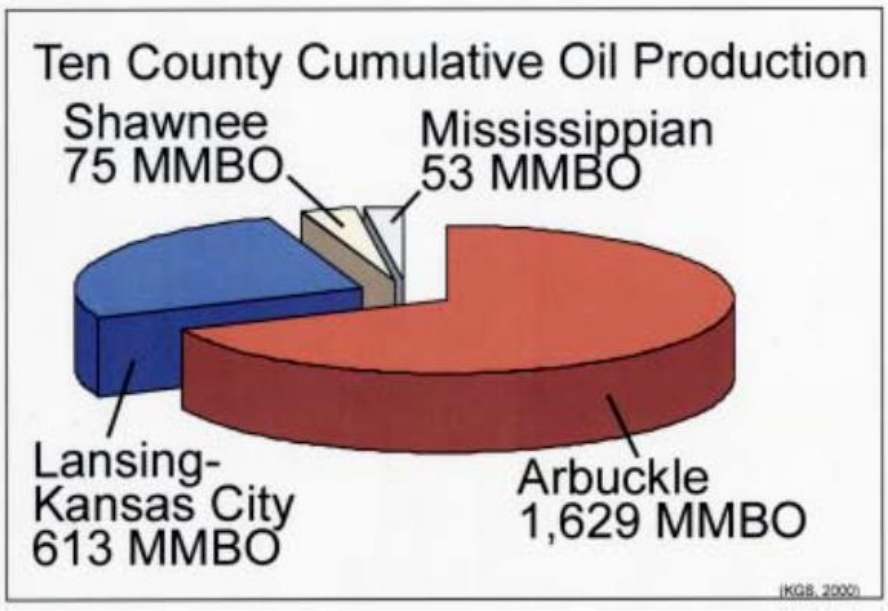

Figure 20: Ten county cumulative oil production in the Kansa Uplift Area. [153]

3.2.2 The LKC Group

The LKC Group are part of the Pennsylvanian series rocks. They were formed in geological times by the continuous cycle of covering and retreating of seawater in the region. The LKC Group is characterized by limestone rocks, shales and coal. Over the Central Kansas Uplift (CKU), the thickness of the LKC Group ranges from 200-400 ft. Carbonate facies in northwestern Kansas are highly variable[154]. The LKC Group is the second largest producer of hydrocarbon in Kansas with majority of the production coming from the CKU. The most prolific portions of the LKC Group located around the CKU are found 1500-2000 ft. below sea level[155]. Figure 21 shows total oil production from the LKC Group.

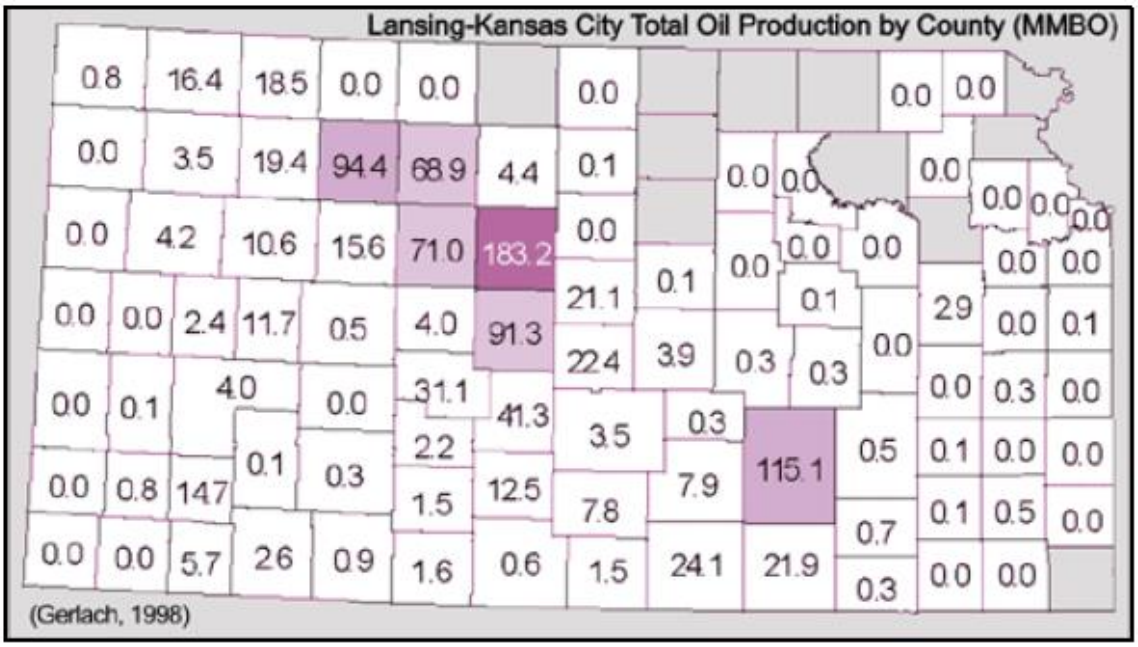

Figure 21: Lansing-Kansas City oil production by county[153]

3.2.3 Lansing-Kansas City and Arbuckle mineralogy

The mineralogy of LKC and Arbuckle is comprised of calcite, dolomite, quartz, chlorite, illite, feldspar, and albite. Illite and quartz are the dominant minerals, and illite is interpreted to be

associated with burial diagenesis of the shale intervals. Calcite is also abundant, while dolomite is present mostly in small amounts[156].

Major elements identified in the intervals include calcium, magnesium, aluminum, silicon, phosphorous, potassium, and iron. Calcium is the most abundant element while silicon is the second most abundant element. Magnesium averages 3 % by weight and is found in increased concentrations where dolomites are present[156].

3.3 Brines

Synthetic brines were prepared using laboratory grade reagents from Fisher Scientific (Pittsburgh, Pennsylvania) to investigate the geochemistry behind calcite dissolution kinetics as well as scale prediction using PHREEQC. The recipe and chemicals used for preparing the brines used in this study are listed in Table 4 in the Appendix. The various brines prepared were based on the composition of typical produced waters from the LKC and Arbuckle Groups, as well as synthetic analogues of two waters, used previously in our research groups' treatment studies, obtained from oil production wells in Reno County and Douglas County, Kansas. The compostion of the synthetic Arbuckle brine used in this study, which has a TDS higher than 40,000 mg/l, was based on analysis of a produced water sample collected from Wellington, KS, which is outside the area identified by Thompson[5] as presenting the most abundant opportunities for brine exchange.

Table 3: Compositions of brines used in this study

Parameters	LKC[a]	5X diluted LKC[a]	82X diluted LKC[a]	Arbuckle Group[b]	Douglas County	Reno County
Ca^{2+}(mg/l)	11000	2200	134	2100	730	9200
Mg^{2+}(mg/l))	2800	560	34	750	310	2500
Ba^{2+}(mg/l)	0	0	0	0	470	3.8
Sr^{2+}(mg/l)	0	0	0	0	90	1900
Na^{+} (mg/l)	48000	9600	585	22740	9800	36000
K^{+}(mg/l)	400	100	6	210	128	400
Cl^{-}(mg/l)	101774	20383	1243	39951	17245	80866
SO_4^{2-}(mg/l)	260	52	3	459	0	100
HCO_3^{-}(mg/l)	0	0	0	1400	852	84.5
IS, mol/L	3.3	0.65	0.04	1.25	0.53	2.59
TDS, ppm	164318	32895	2006	67711	31416	131054
pH	6.6	6.3	6.23	6.87	7.01	6.85
Temperature	40	40	40	22	22	22

[a]The compositions of the synthetic LKC brine and its dilutions were similar those of the brines used by Tetteh *et al.*[77,79] and Tetteh and Barati[78].

[b]The composition of the synthetic Arbuckle brine was based on the composition of a produced water samples obtained from a wellfield in Wellington, KS.

3.4 Preparation of powdered calcite

Powdered Indiana Limestone was used to determine the rate and amount of calcite dissolution in a closed system. Pure calcite is often used in laboratory experiments to understand its behavior under various conditions. Diluted and undiluted samples of synthetic LKC brine were put in contact with the powdered limestone at reservoir conditions (40 ^{o}C). Before this, the rock was crushed with a jaw crusher, a disc mill and a ball mill in that order to create finely powdered particles. This was repeated several times and the powder was sieved through a 106 µm screen. The composition of the Indiana Limestone rock was determined using scanning electron microscopy (SEM) and X-ray diffraction (XRD). The rock was found to be 99 % calcite, with trace amounts of dolomite and quartz.

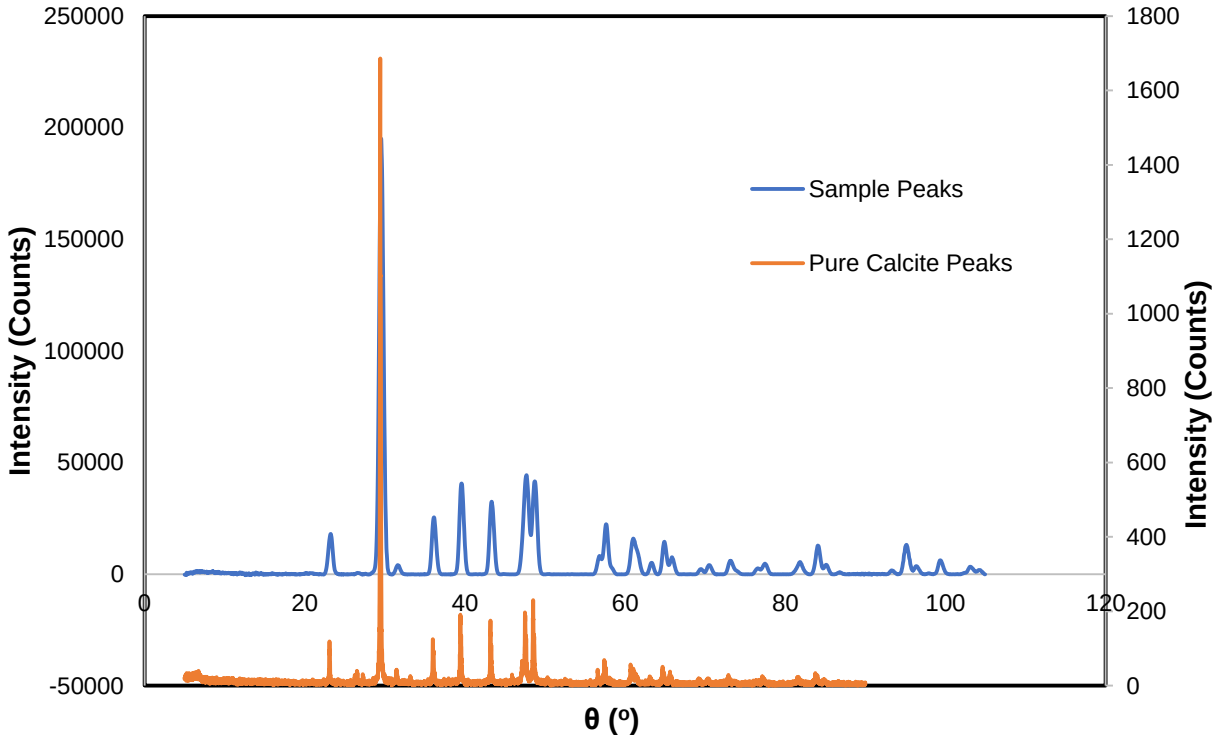

Figure *22* below illustrates the XRD image of the Indiana Limestone used in this study.

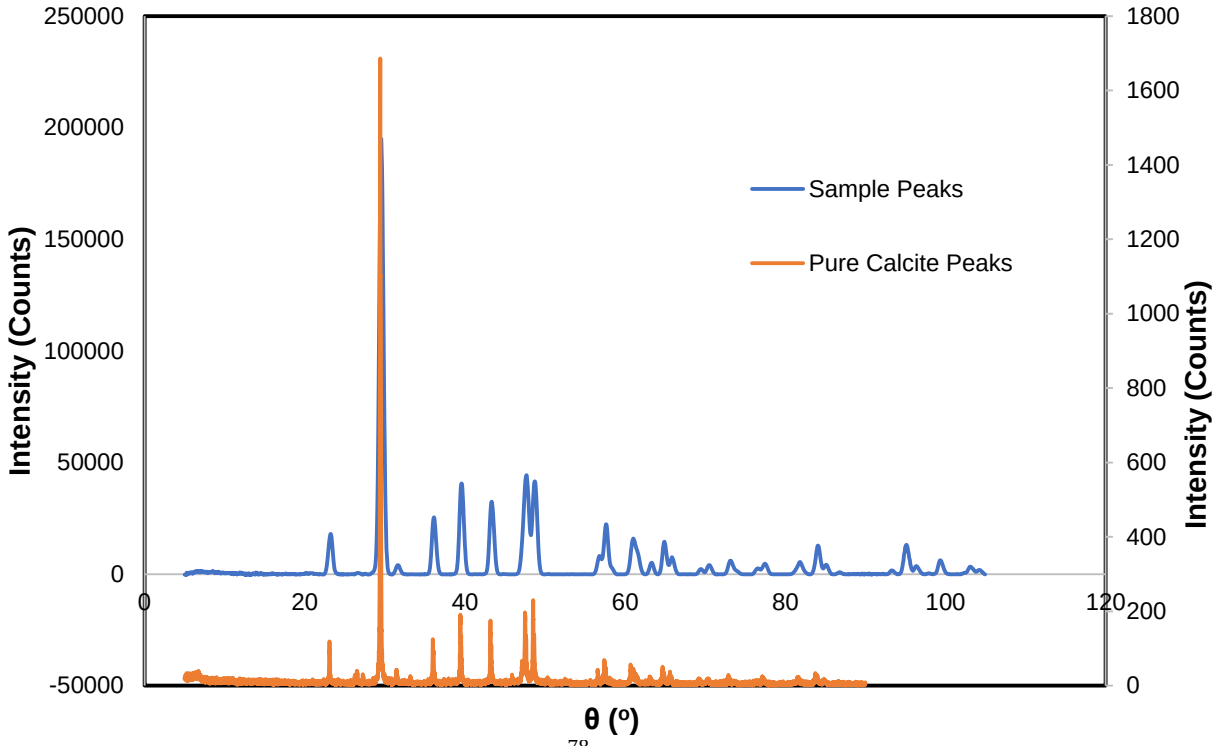

Figure 22: XRD image of Indiana Limestone[78].

3.5 Calcite dissolution experiment

The dissolution experiment was conducted by adding 0.3 g of Indiana Limestone powder to a series of 15 ml conical polypropylene centrifuge tubes with flat polyethylene caps (ThermoFisher Scientific), each containing 15 ml of preheated brine (using LKC, 5X diluted LKC and 82X diluted LKC brines), which were then placed on a shaker. All 15 ml test tubes were horizontally placed in the shaker to facilitate mixing and stored in a constant temperature cabinet (at 40 ^{o}C). At each time step (0, 5, 10, 20, 25, 30, and 50 min; 1, 2, 3, 5, 8, and 24 h; and 2, 3, 5, and 10 days), a 15 ml sample was sacrificed for analysis. After each time period, a sample was removed from the cabinet and about 3 ml of the sample were filtered through a 0.45-micron filter, from which 1000 times dilutions were prepared in triplicate using deionized water, which were then analyzed for calcium and magnesium concentrations using inductively coupled plasma - atomic emission spectroscopy (ICP−AES). The pH of the solution was immediately

checked using the remaining 12 ml solution left in the centrifuge tube. During the ICP−AES analysis, the ICP−AES equipment was calibrated with QC standard 23 (from RICCA Chemical Company) to measure concentrations from 1 mg/l to 10 mg/l. The difference between initial and final ion concentrations was used to determine the amount of dissolution or precipitation of the calcite mineral. The experiment was repeated two more times.

3.6 pH measurement

An Accumet pH meter (model number AB 150 from Fisher Scientific) with an electrode (part number 13-620-223A) was used for pH measurement throughout this study. The pH electrode was calibrated with a pH buffer group which included pH 4, 7 and 10 buffers. pH measurement was performed immediately after each experiment by sticking the pH electrode into the solution using a manual temperature compensation of 25 ^{o}C. For all pH measurements, the effects of ionic strength and sodium ion concentration were not corrected for. This was because all samples prepared in the lab had a mixture of multivalent ions in the background solution that reduced the influence of sodium on the pH measurement. However, an experiment was performed to assess the effect of ionic strength on pH by adding sodium chloride in a stepwise manner to increase the TDS from 10,000 mg/l to 200,000 mg/l in 5 ml samples containing pH 7 or 10 buffer. The correlation obtained from fitting the data points was used in an attempt to replicate the pH measurements made using the Accumet pH meter. The correlations were tested on the synthetic Douglas County (DC) and Reno County (RC) brines, and various mixtures of the two.

3.7 Effect of background sodium chloride ions on ICP analysis

To neutralize the effect of ionic strength on the ICP measurement, both the starting and final concentrations of the various divalent ions were measured and recorded at the same time. Thus,

any effect of ionic strength on the measurements would apply equally if both were diluted to the same degree. This procedure was followed to reduce the effect of the background matrix on measured results. Cation precipitation was then estimated based on the difference between the initial and final concentrations of the samples. For the mixtures of DC and RC brines, the initial concentration was not measured but estimated from the brine compositions prior to mixing, thereby introducing a potential source of error. To address this issue, the effect of the background ions concentrations on measurement of the final concentrations in the samples was investigated.

The effect of the background sodium chloride ions on ICP analysis was investigated by preparing NaCl solutions to produce a background chloride concentration of 6000, 26,000 and 53,000 mg/l. These target concentrations were derived from the chloride concentrations found by mixing the DC and RC brines in ratios of 80:20, 50:50 and 80:20, respectively. A standard cation solution was prepared in these NaCl solutions to contain 1000 mg/l of calcium, magnesium, barium and strontium in 2 % nitric acid solution. (The full composition of this brine is shown Table 5 in the appendix.) The prepared cation solutions were then diluted to make 1, 2, 5, 7.5 and 10 mg/l standards that were used to calibrate the ICP equipment. The calibration curves were compared to the calibration curve derived from QC standard 23 (from RICCA Chemical Company), shown in Figures 23 to 26 and referred to as the base solution. The measured ICP intensities (in counts) at each concentration were recorded and the slope of each curve calculated. The slopes for each cation are shown in Table 6 in the appendix.

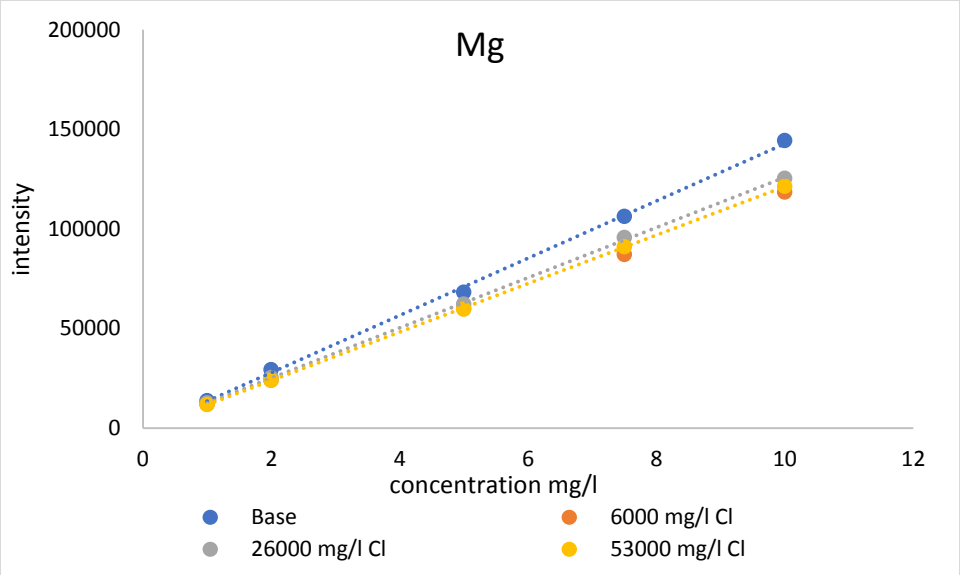

Figure 23: Effect of background chloride ions on Mg measurement

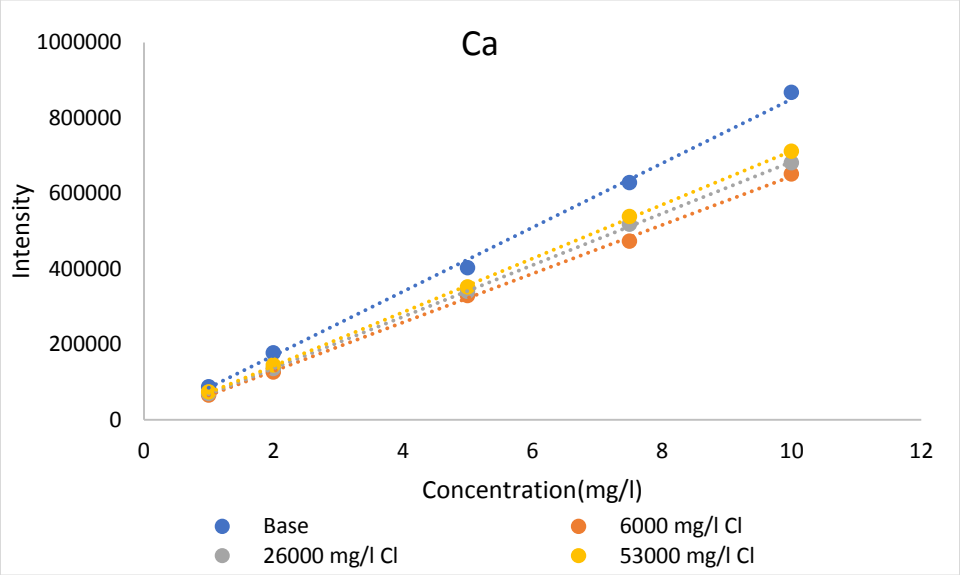

Figure 24: Effect of background chloride ions on Ca measurement

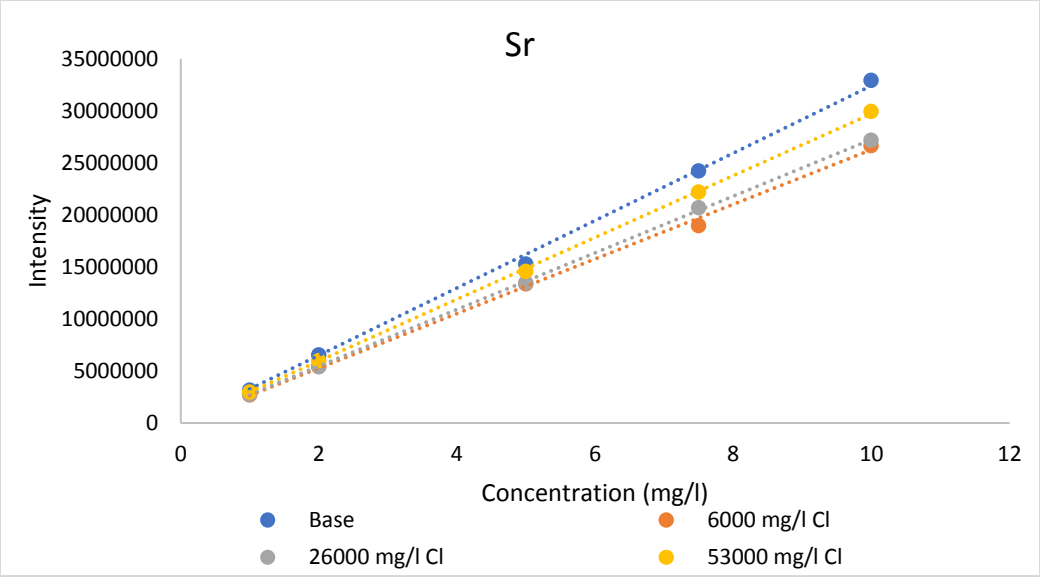

Figure 25: Effect of background chloride ions on Sr measurement

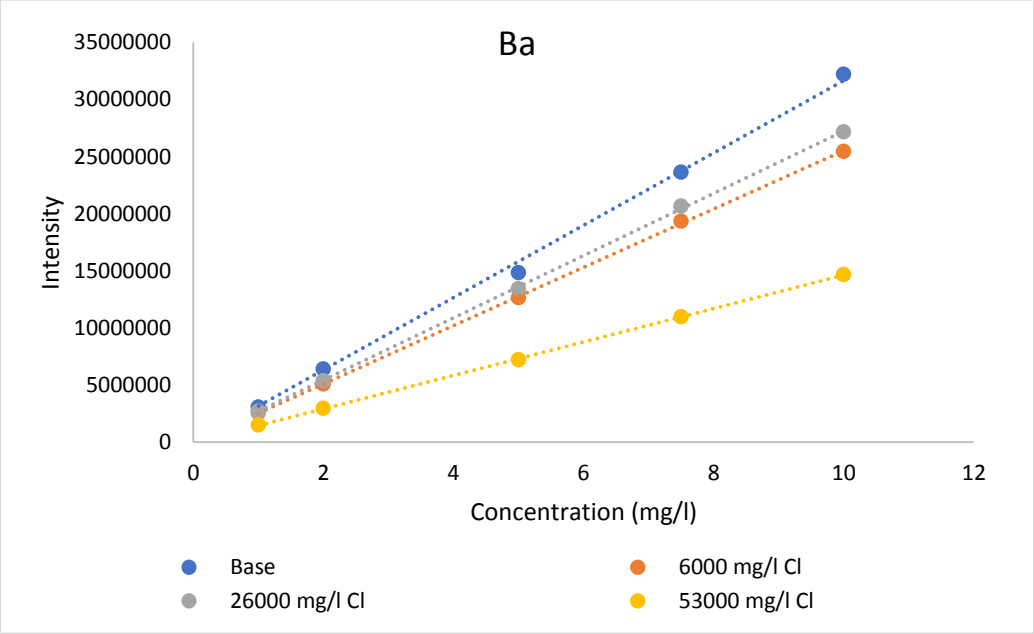

Figure 26: Effect of background chloride ions on Ba measurement

The results indicate that background ions concentrations at the levels used in our experiments would cause the instrument to under-report the dissolved ion concentration for all four elements. This would in turn result in over-estimation of the amount of precipitation, since the difference

between the calculated initial sample concentration and the final measured sample concentration is used to determine the amount precipitated.

From Figures 23 to 26 above, the background sodium chloride ions caused an underestimation of the measured concentration of 12 to 17 % for magnesium, 16 to 23 % for calcium, 8 to 16 % for strontium 17 to 20 % for barium. The 53,000 mg/l chloride solution for barium was not considered in the analysis because the data point seems to be an outlier. For mixtures of DC and RC brines, percent removal values that fall within the ranges shown above for the respective ions can be considered to be zero.

3.8 Precipitation experiment

To investigate PHREEQC's accuracy in predicting formation of scales that occur in oil and gas operations, three ranges of SI values were explored, and the resulting precipitate formation was observed:

- SI values far below saturation (SI<−2)
- SI values close to saturation (−0.5<SI<2)
- SI values far above saturation (SI>−2)

These predictions were compared with experimental results to further understand the limitations and accuracy of the software using both the standard PHREEQC and Pitzer databases.

3.8.1 SI values far below saturation (SI<−2)

For SI values far below saturation, the LKC brine was allowed to equilibrate with CO_2. This experiment was performed in two ways:

(1) At room temperature (22 ± 1 ^{o}C) the LKC brine was allowed to equilibrate with atmospheric CO_2 in an uncontrolled environment by pouring 100 ml into a beaker and allowing it to sit in the lab for three days; when the pH became constant samples were prepared for ICP−AES analysis. The sample volume lost due to evaporation was noted and accounted for in PHREEQC.

(2) To avoid potential experimental errors introduced by evaporation and salinity changes, pure CO_2 gas from a CO_2 tank was bubbled through 50 mL of brine. The CO_2 was humidified by bubbling it through DI water in a glass washing bottle with a fritted disk. To ensure equilibrium, the humidified CO_2 gas was left to bubble through the solution until the pH dropped from 6.21 to 3.5. The samples were allowed to sit for 3 days in a closed centrifuge tube, after which the magnesium and calcium concentration were measured. A negligible change was observed when the measured concentrations were compared to the initial concentrations in the samples after the 3 days analysis. The samples were then adjusted to a pH of 5.52 (equilibrium pH predicted by the model when CO2 and LKC brine are in equilibrium) by adding 80 microliters (µl) of a 1 M NaOH solution. This would cause the total carbonate, which exists predominantly as H_2CO_3 at pH 3.5, to be partially converted to bicarbonate, with a negligible change in the carbonate ion concentration. The samples were allowed to sit for 3 days and analyzed again for change in magnesium and calcium concentrations. The whole experiment was then repeated three more times.

3.8.2 SI values close to saturation (−0.5<SI<2)

SI values near saturation were explored by mixing synthetic Douglas County (DC) and Reno County (RC) brines in ratios of 20:80, 50:50 and 80:20. For the mixing ratio 20:80, 2 ml of the DC brine and 8 ml of the RC brine were added to a test tube. The test tube was swirled

repeatedly to ensure adequate mixing. After three days, samples were taken for ICP–AES analysis to determine the change in the concentrations of Ca^{2+}, Mg^{2+}, Ba^{2+}, and Sr^{2+} ions in the solution. The amount of precipitation or dissolution of each cation was determined by the difference between the initial and final cation concentrations. This process was repeated for the mixing ratios 80:20 and 50:50. But this time 8 ml of the DC and 2 ml of the RC Brine, and 5 ml each of the two brines were mixed the prepare the 80:20 and 50:50 ratios, respectively.

3.8.3 SI values far above saturation (SI>2)

Barium, calcium, magnesium and strontium precipitation were induced by creating solutions where SI values were far beyond saturation (SI> 2). Barium precipitate was induced by adding 0.5 M sodium sulfate to the DC synthetic brine at 22 ^{o}C; 3.55 g of sodium sulfate were weighed out using an electronic balance (A&D, GF-2000) and added to 50 ml of the DC brine, which was then stirred and allowed to sit for three days before preparing samples for ICP−AES analysis. The initial and final pH values, as well as cation concentrations of the mixture, were measured and recorded at the beginning and at the end of the experiment. The experiment was conducted three times to assess its reproducibility (precision).

Also, a 1 M dosage of sodium carbonate was added to the Reno County brine to precipitate calcium, magnesium and strontium carbonate out of solution. A volume of 50 ml of the RC brine was poured into a 50 ml centrifuge tube and 5.23 g of sodium carbonate were weighed out and added to the sample. After three days, triplicate samples were collected for cation analysis by ICP−AES. The experiment was repeated three more times.

3.9 PHREEQC

PHREEQC, a computer program used for aqueous geochemical simulations, was employed to simulate the mixing scenarios of Arbuckle and LKC brines at varying pressures. PHREEQC evolved from the Fortran program PHREEQ, originally an acronym for pH-REdox-EQuilibrium[157]. PHREEQC was developed by the United States Geological Survey and has been widely used for speciation and chemical equilibrium calculations. It can also perform batch-reaction calculations, transport modeling, surface complexation and ion exchange calculations[157]. PHREEQC version 3.4.0 was used for all the modeling work in this study.

The precipitate function was used to predict how much of a given supersaturated phase would need to be precipitated to reach equilibrium. Two databases were used for this investigation: the Pitzer database (pitzer.dat) and the standard PHREEQC database (phreeqc.dat). Pitzer.dat is based on Pitzer's[158] interaction model designed for high ionic strength solutions (up to 6M)[159]. Phreeqc.dat was developed for chemical equilibrium calculations in groundwater[160]. The two databases are different in terms of the number of ion pairs and complexes considered, the included mineral phases, and how they account for the effects of ionic strength (Pitzer vs Debye-Hückel theory) as described in section 2.8.1.

The two databases were compared with each other in terms of their ability to predict pH, precipitation, and the SIs of potential scale-forming minerals pertinent to brine exchange. The effects of ionic strength on the predictions from the two databases were also assessed.

The synthetic brine compositions shown in

Table *3* were modeled using both databases with the PHREEQC software program. The results for modeled solutions were then compared to those obtained in laboratory experiments. The models were allowed to form precipitates by specifying 1M of the mineral to be in contact with the solution. All mineral phases that were predicted by both databases to be saturated were allowed to precipitate by using the precipitate keyword function and stating 1M of the mineral to be in contact with the solution. This was performed for all simulations run using both databases.

The results were then compared as follows:

- The SI and pH predictions from both databases were compared to each other.
- The pH predictions from both databases were compared to the experiment pH results.
- The amounts of solid phases dissolved or precipitated were compared between both databases and the experimental work.

Chapter 4 Results and Discussion

4.1 Modeling the Arbuckle and the LKC brines in the PHREEQC model

The Arbuckle and LKC brines were modeled in PHREEQC to determine their scale forming tendencies. The results from the model showed that the LKC brine was undersaturated with respect to all minerals using both the standard PHREEQC and Pitzer databases.

The Arbuckle brine was predicted to be saturated with respect to calcite, aragonite and dolomite Using both databases. Using the Pitzer database and allowing the model to precipitate the mineral phases with respect to their saturation state predicted just a 12.4 % reduction in the concentration of calcium ion in the solution, which was associated entirely with calcite precipitation. The model (using the Pitzer database) predicted that the magnesium ion concentration would remain unchanged; and calcite, dolomite and aragonite had SI indices of **+1.46, +2.81, and +1.18**, respectively. On the other hand, using the PHREEQC database, the SI indices for the minerals above were **+1.26, +2.50 and +1.12**, respectively, and allowing precipitate formation gave an 8.98 % reduction in the calcium concentration. Dolomite contributed 2.50 % to the overall loss in calcium concentration while calcite contributed 6.48 % to the loss in calcium. The loss in magnesium from dolomite precipitation was 4 %.

Dolomite and calcite contributed to precipitate formation when using the PHREEQC database. In contrast, only calcite contributed to calcium removal when the Pitzer database was used. The corresponding SIs for dolomite and calcite were higher for the Pitzer database, yet only calcite was formed in contrast to the PHREEQC database. One reason for this observation might be the preference for calcite precipitation over dolomite if they both reach supersaturation. At atmospheric temperature and pressure, calcite would preferentially precipitate out of solution. This effect is more pronounced when using the Pitzer database than the PHREEQC database.

4.2 Mixing the Arbuckle and LKC brines in the PHREEQC model at different pressures

Mixing of Arbuckle and LKC brines was modeled with different mixing ratios and varying reaction pressure within the range used in Thompson's work[5]. As the percentage of Arbuckle water increases in the mixture, both models predict an increase in precipitate formation. When the reaction pressure was varied between 14.7 psi (1atm) and 2000 psi, the effect on SI was almost negligible, for both databases, for calcite, dolomite, aragonite, gypsum and anhydrite, as shown in Figure 28 (which is a representative of all other mixing ratios). However, at high reaction pressures, there is a slight increase in the solubility of the scale forming minerals. Anhydrite and gypsum remained undersaturated regardless of the reaction pressure or Arbuckle volume in the mixture in both databases.

When the PHREEQC model was used, the point of saturation for calcite, dolomite and anhydrite occurred when the mixture contained 40 % by volume of the Arbuckle brine. On the other hand, using the Pitzer database, precipitate formation was predicted for these minerals with only 5 % Arbuckle brine, by volume, in the mixture. The SI values associated with these minerals indicate a supersaturation state (SI>1), making the two waters incompatible according to the Pitzer database. As shown in Figure 27, the Pitzer database predicted higher SI for the carbonate minerals compared to the PHREEQC database across all mixing ratios at 1 atm. Based on these results, it could be inferred that the Pitzer database is likely to predict a higher saturation state for these minerals at most conditions.

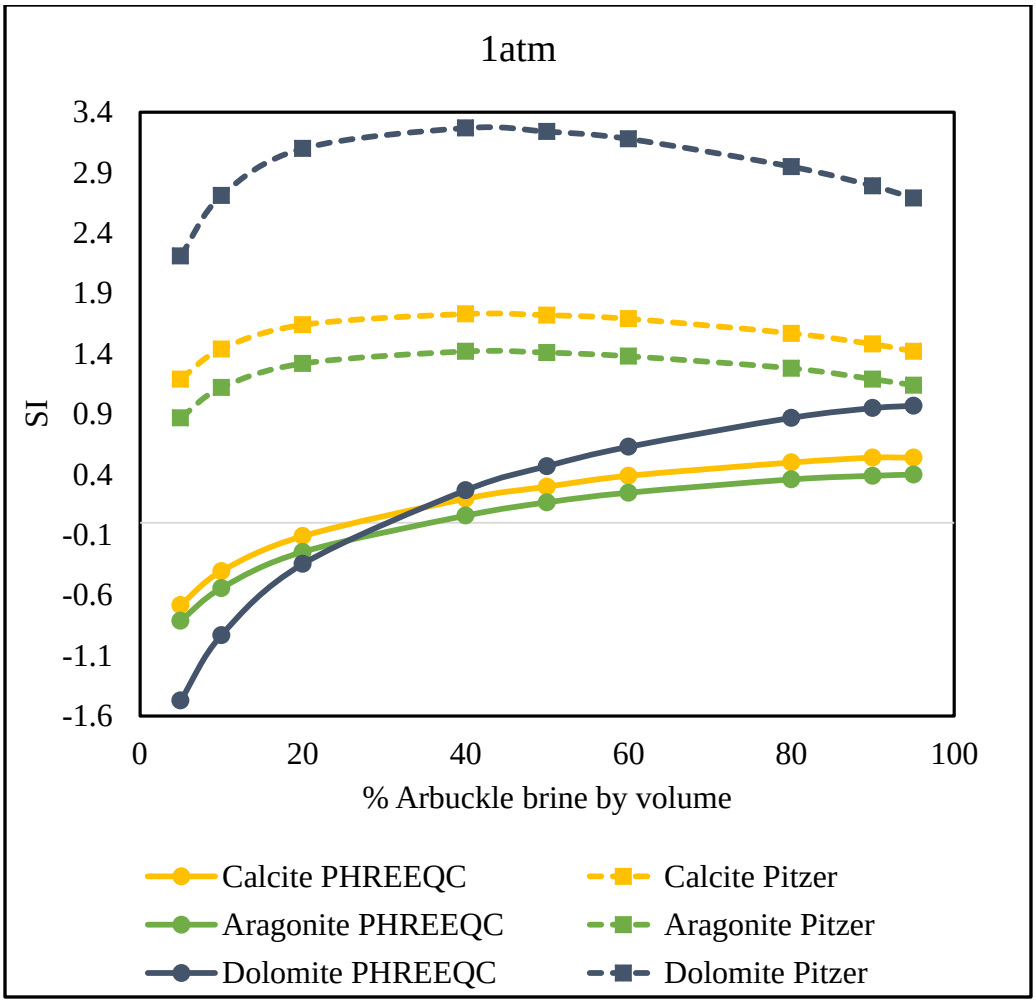

Figure 27: SI at 1 atm for selected carbonate minerals as the percentage of Arbuckle water increases in mixtures of LKC and Arbuckle produced waters

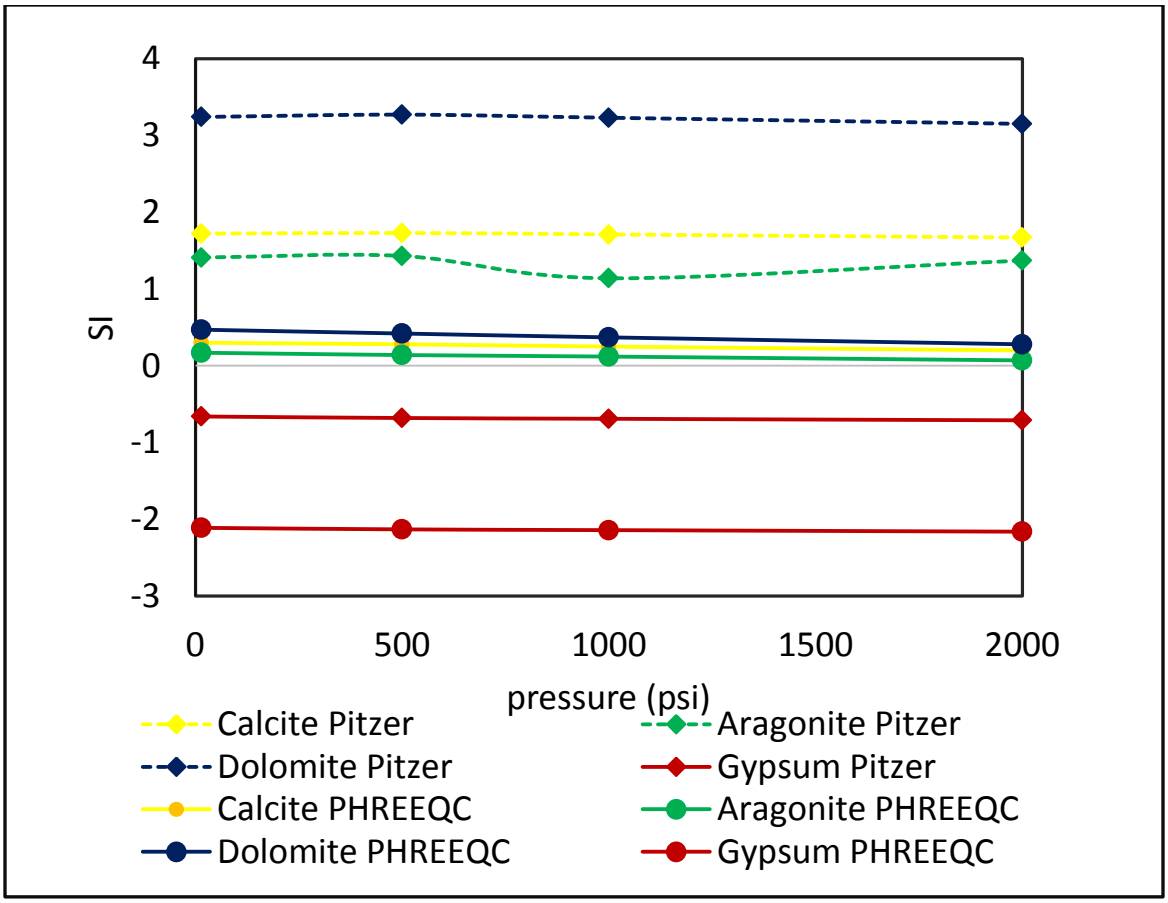

Figure 28: Effect of pressure on the SI of potential scale forming minerals for a 50:50 mixture of LKC and Arbuckle brines

4.3 Effect of ionic strength on the saturation state of selected minerals

In simulations using PHREEQC, the Reno County brine was modified by adding varying amount of sodium chloride to produce solutions with an overall ionic strength from 1 to 5 M. Simulations were conducted at standard atmospheric pressure and temperature. Figure 29 demonstrates the difference in SI (ΔSI) between the two databases (SI value predicted using the PHREEQC database minus the value predicted using the Pitzer database) as the ionic strength is varied. A value of zero indicates that the two databases yielded the same SI for the given mineral. A positive ΔSI indicate the PHREEQC database predicts a higher SI than the Pitzer

database for the mineral in question. A negative value of the ΔSI signifies that the Pitzer database predicts a higher SI than the standard PHREEQC database.

For barite and celestite the difference between the predictions from the two databases is negligible up to an ionic strength of about 3 M.

As seen in Figures 30, 31, and 32, the saturation state of the carbonate minerals becomes more positive as the ionic strength increases. The Pitzer database SI predictions have a steeper response to the increase in ionic strength than the standard PHREEQC database for the carbonate minerals.

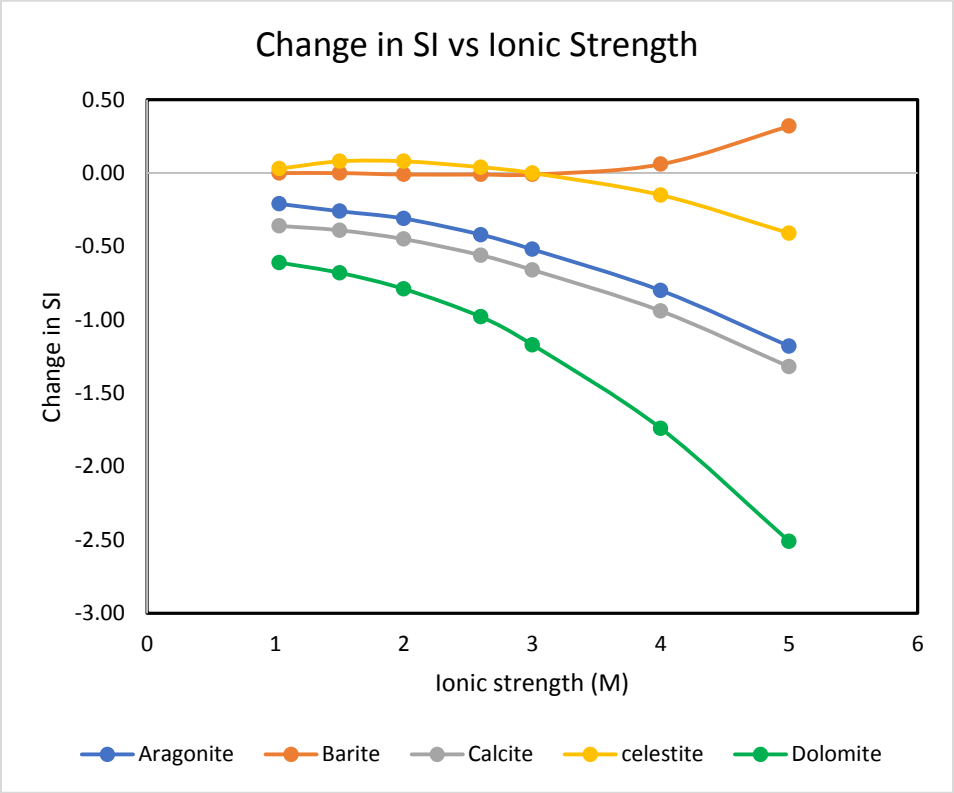

Figure 29: Effect of the choice in database on the solubility of aragonite, calcite, barite, celestite, and dolomite as ionic strength increases; SI value predicted using the PHREEQC database minus the value predicted using the Pitzer database.

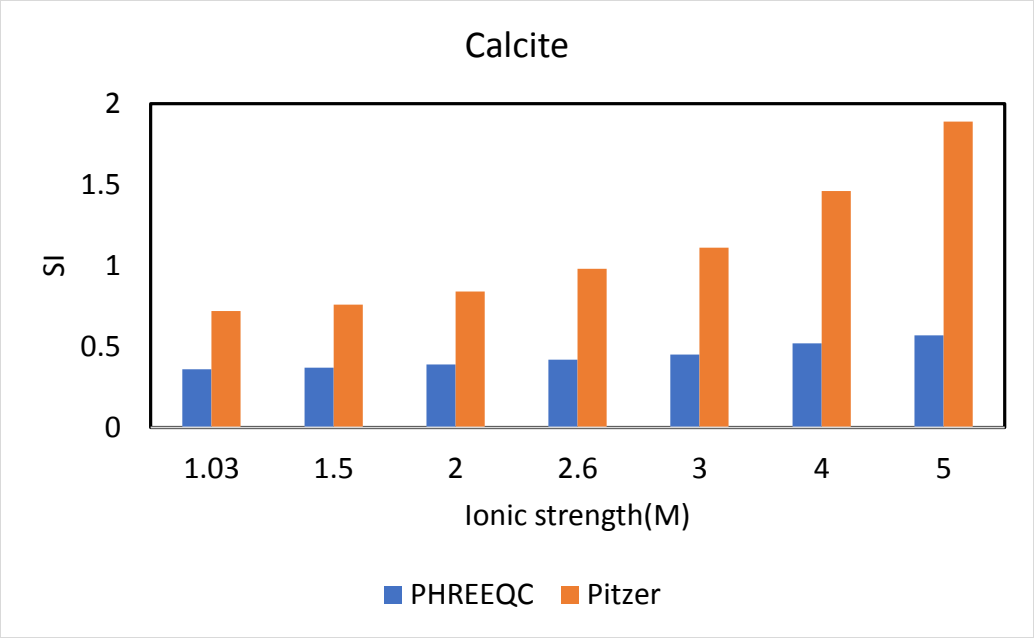

Figure 30: SI of calcite when the RC brine was modified by changing the sodium chloride concentration to increase the ionic strength and modeled using both the PHREEQC and Pitzer databases

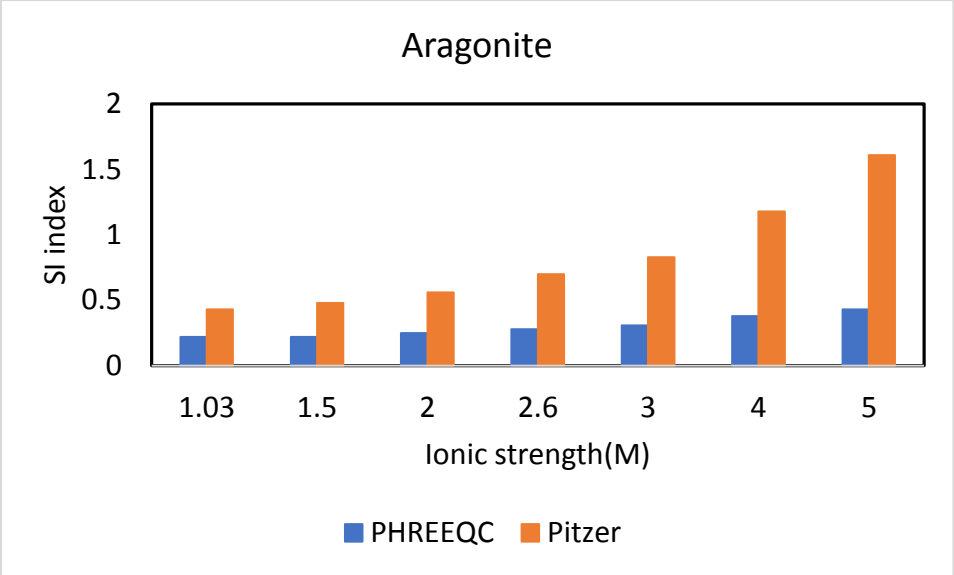

Figure 31: SI of aragonite when the RC brine was modified by changing the sodium chloride concentration to increase the ionic strength and modeled using both the PHREEQC and Pitzer databases

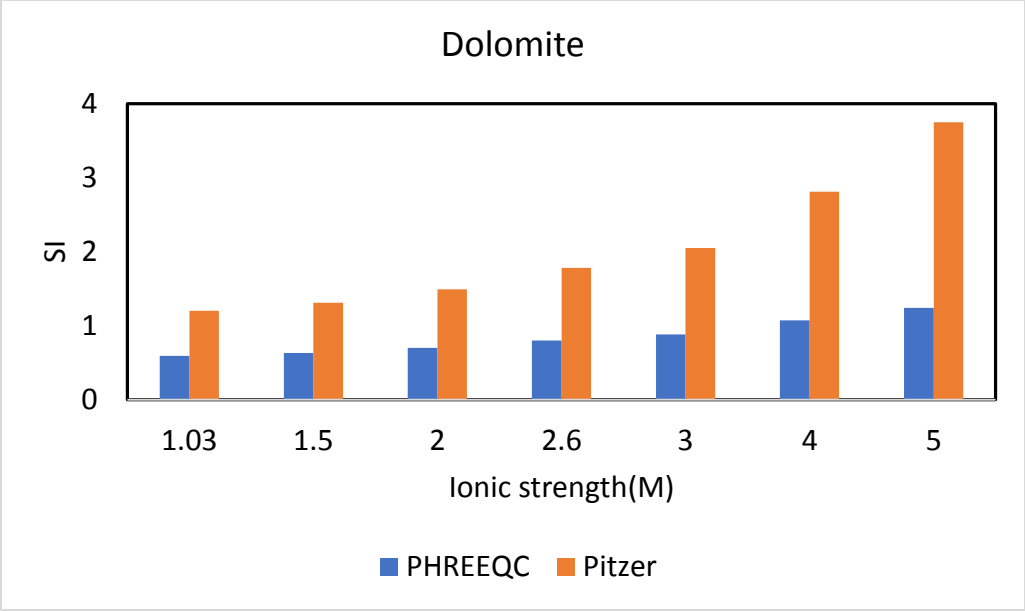

Figure 32: SI of dolomite when the RC brine was modified by changing the sodium chloride concentration to increase the ionic strength and modeled using both the PHREEQC and Pitzer databases

4.3.1 The carbonate minerals

The SI predictions for the carbonate minerals (dolomite, calcite, and aragonite) using the Pitzer database were significantly higher than those predicted using the PHREEQC database. For all three minerals, the Pitzer database predicts SI values in an increasing order as ionic strength increase. When the PHREEQC database is used, the saturation index remains fairly constant with increasing ionic strength albeit noticeable changes occur at very high ionic strength solution as shown in FiguresFigure *31* to Figure *33* above in section 4.3. On average the Pitzer database predicts an SI about 2.5 times the value of the SI predicted using the standard PHREEQC database. This factor is around 2 when the ionic strength is close to 1 M and increases to more than 3 at ionic strength of 4 M and above. The carbonate minerals studied here essentially comprise of calcium, magnesium and the carbonate ion as well as bicarbonate. The pH of the

mixture is 6.85, making the bicarbonate ion the dominant aqueous species in the carbonate system. The PHREEQC database includes calcium complexes while the Pitzer database does not. Even though this is the case, including complexes had little influence on the concentration of free Ca^{2+} ion estimated using the PHREEQC database, i.e., the free ion was 99.62 and 99.71 percent of total dissolved calcium at 1 M and 3 M ionic strength, respectively, with activity coefficients of 0.248 and 0.45, respectively.

The main factor underlying the observed differences in SI has to do with the Davies equation and Pitzer equation used for activity correction in the PHREEQC model and the Pitzer model, respectively. As shown in Figure 33, activity coefficients associated with the Pitzer database are generally higher than those predicted using the PHREEQC database. Above ionic strength of 3 M, the activities of magnesium and calcium become greater than the free ion concentration with this effect being more pronounced using the Pitzer database. For example, at an ionic strength of 5M, the activities of calcium are 1.4 and 5 times the concentration of the free ion in the PHREEQC and Pitzer databases, respectively. Likewise, the magnesium ion activities at the same ionic strengths are 3 and 8 times more than the free ion concentrations when using the PHREEQC and Pitzer databases, respectively. This phenomenon makes the dolomite SI more susceptible to the choice of database because ionic strength has a strong influence on the magnesium ion activity correction in the Pitzer database.

Also, the carbonate ion activity has an effect on the observed difference in SIs estimated using the two databases. The carbonate ion activity coefficient from the PHREEQC database is higher than that from the PITZER database shown in in Figure 34 A. However, paying close attention to the actual concentrations at each ionic strength, the actual concentrations available for the reaction after activity corrections are higher in the Pitzer database than the PHREEQC database,

as shown Figure 34 B. One reason for this is the number of total carbonate complexes formed in each database. The PHREEQC database includes 14 complexes while the Pitzer database has only one complex ($MgCO_3^0$). The difference in complex formation causes the Pitzer database to have a higher concentration of available carbonate ion for dolomite, calcite and aragonite mineral formation.

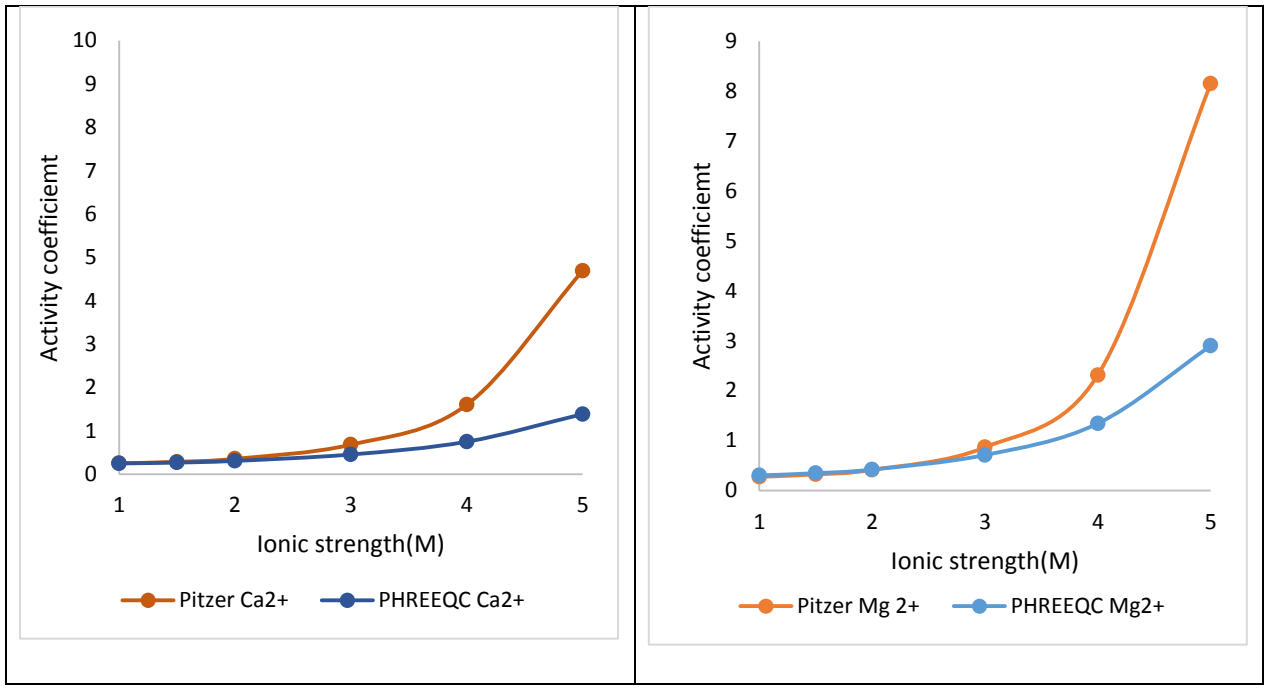

Figure 33 A) Activity coefficient for Ca^{2+} as ionic strength increases. B) Mg^{2+} activity coefficient as ionic strength increase

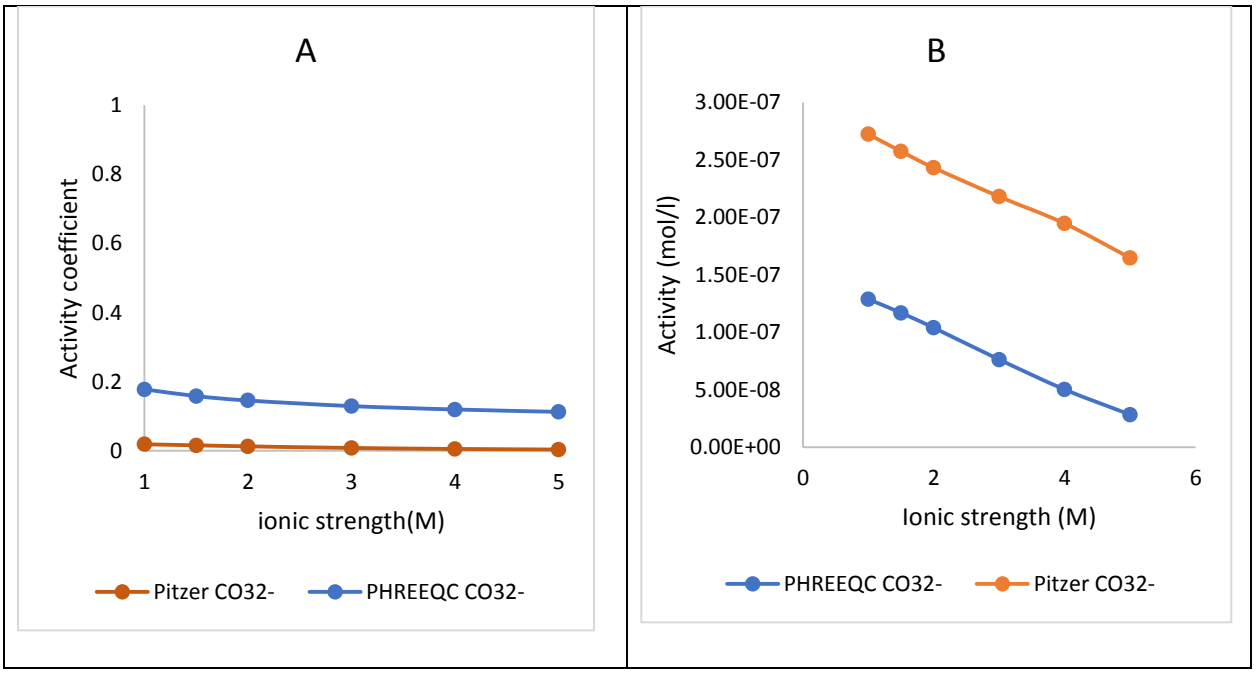

Figure 34: A) Activity coefficient of the carbonate ion as ionic strength increases. B) Activity of the carbonate ion as ionic strength increases

4.3.2 The sulfate minerals

Barite SIs predicted using the PHREEQC and Pitzer databases are very comparable to each other at ionic strengths up to about 3 M. The disparity between the two databases becomes more and more obvious as the ionic strength becomes ≥ 4.0 M. At this point, the SI predictions from the PHREEQC database become greater than those from the Pitzer database, with a complete fall off at 5M as shown in Figure 35. Barium has no complexes in the Pitzer database and the activity coefficient gradually approaches 1 as shown in Table 11 in the appendix. On the other hand, barium has complexes in the PHREEQC database, but they have no effect on the SI predictions. The complexes are generally less than 0.5 % of the total barium concentration in the solution. The noticeable sulfate complexes when the PHREEQC database is used for modeling are shown in Table 9 in the appendix.

At an ionic strength of 3 M or less, the predicted SIs from both databases are very similar although the databases use different pathways to arrive at a similar result. The sulfate ion activities from the PHREEQC database are higher than sulfate activities from the Pitzer database, as shown in Figure 36 B. On the contrary, the barium activities are higher in the Pitzer database than in the PHREEQC database. As a result of these differences, the combined effect of the of the activities of barium and sulfate from the two databases result in ion activity products which are very comparable, yielding similar SIs. It is difficult to deduce which database pathway arriving at the IAP is closer to the truth, since the individual activities of sulfate and barium in solution were not measured.

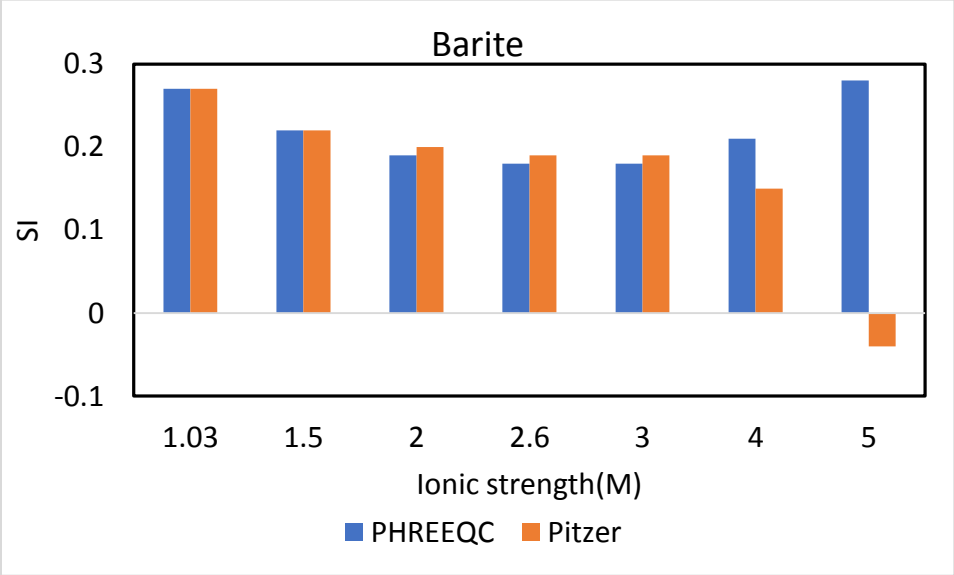

Figure 35: SI of barite when the RC brine was modified by changing the sodium chloride concentration to increase the ionic strength and modeled using both the PHREEQC and Pitzer databases.

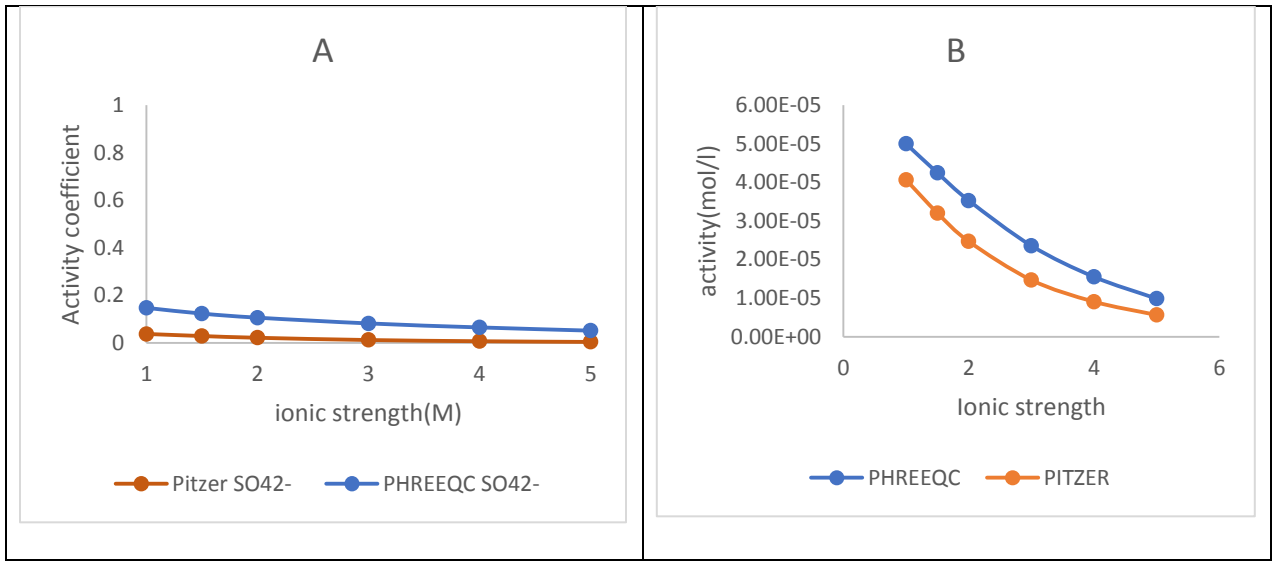

Figure 36: Activity coefficient as ionic strength increases for sulfate ion. B) Activity as ionic strength increases for sulfate ion

The predicted SI values for celestite using both the Pitzer and PHREEQC databases generally decreased as ionic strength increased up to about 3 M. The decrease occurs more sharply when using the Pitzer database than for the PHREEQC database. The activity of the strontium ions increases sharply in the Pitzer model as the ionic strength increases while the sulfate ion activity decreases with an increase in ionic strength. Even though the sulfate activity is higher in the PHREEQC database, it is not high enough to fully compensate for the sharp increase in strontium activity predicted using the Pitzer database. Thus, the difference in strontium activity is the main driver for the observed differences in SI between the two databases shown in Figure 37.

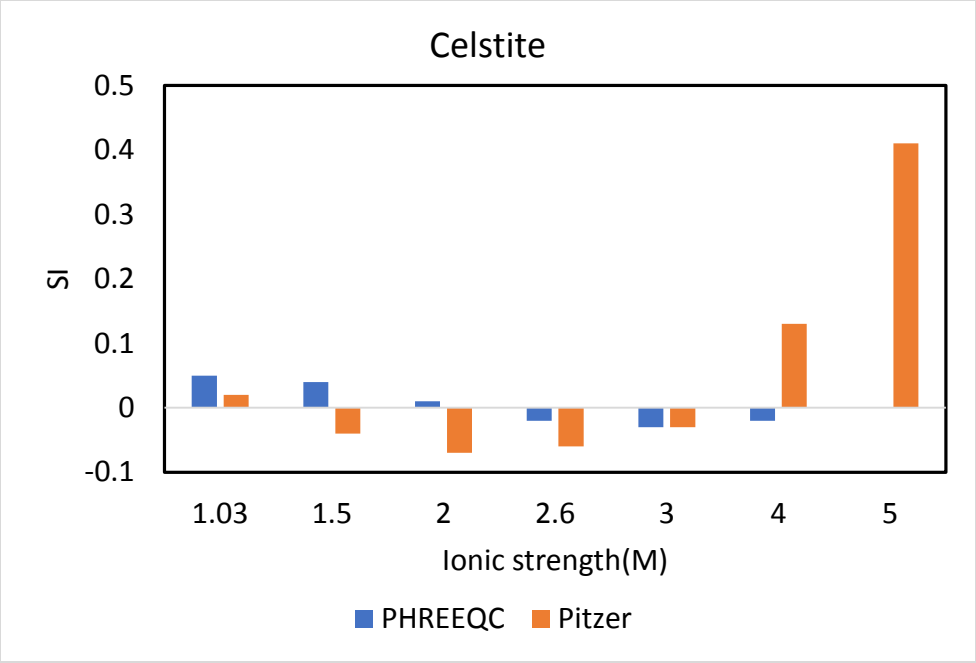

Figure 37: SI of celestite when the RC brine was modified by changing the sodium chloride concentration to increase the ionic strength and modeled using both the PHREEQC and Pitzer databases.

4.4 Equilibrating Arbuckle and LKC brine mixtures with calcite

The LKC and Arbuckle brines were mixed together at different ratios after which the mixtures were equilibrated with powdered Indiana Limestone (primarily composed of calcite, the main mineral in the LKC formation). At calcite equilibrium, the amount of calcium precipitation increased as the volume of the Arbuckle brine increased regardless of the database used. The Pitzer database predicted this trend beginning at about 5 % Arbuckle water by volume, while the PHREEQC database did same at about 20 % Arbuckle water by volume. The LKC brine had zero carbonate content and mixing that with Arbuckle brine caused the bicarbonate concentration in the mixture to increase. Hence, as the Arbuckle brine increases in volume in the mixture, so does the amount of carbonate in the mixtue, which in turn leads to calcite precipitation with increasing Arbuckle volume in the mixture. The Pitzer database predicted a much higher amount

of precipitation at every mixing ratio. One reason for this observation is that minerals are relatively less soluble in the aqueous phase when the Pitzer database is used as seen in Figure 30 to 32. Figure 38 illustrates the amount of dissolution or precipitation of Ca^{2+} as the percent Arbuckle water by volume increases. A positive value on the ordinate of the chart represents precipitation while a negative value connotes dissolution. The presence of organic compounds as well as solids from the formation may affect the size and morphology of crystals, precipitation kinetics and the equilibrum of the reaction[161]. It should however be noted that the possible effects of organic compounds were not accounted for in this investigation since there was no organic component added to the synthetic brines. Organics such as antiscalants, e.g., polyphosphonates, if present, can inhibit precipitation while organics such as methanol could aid in precipitation[162,163]. Adsorption of organic matter on active crystal site could impede precipitation[164]. It is therefore very important to also assess what kinds of organic compounds are in the PW before assessing what effects they might have on scale formation.

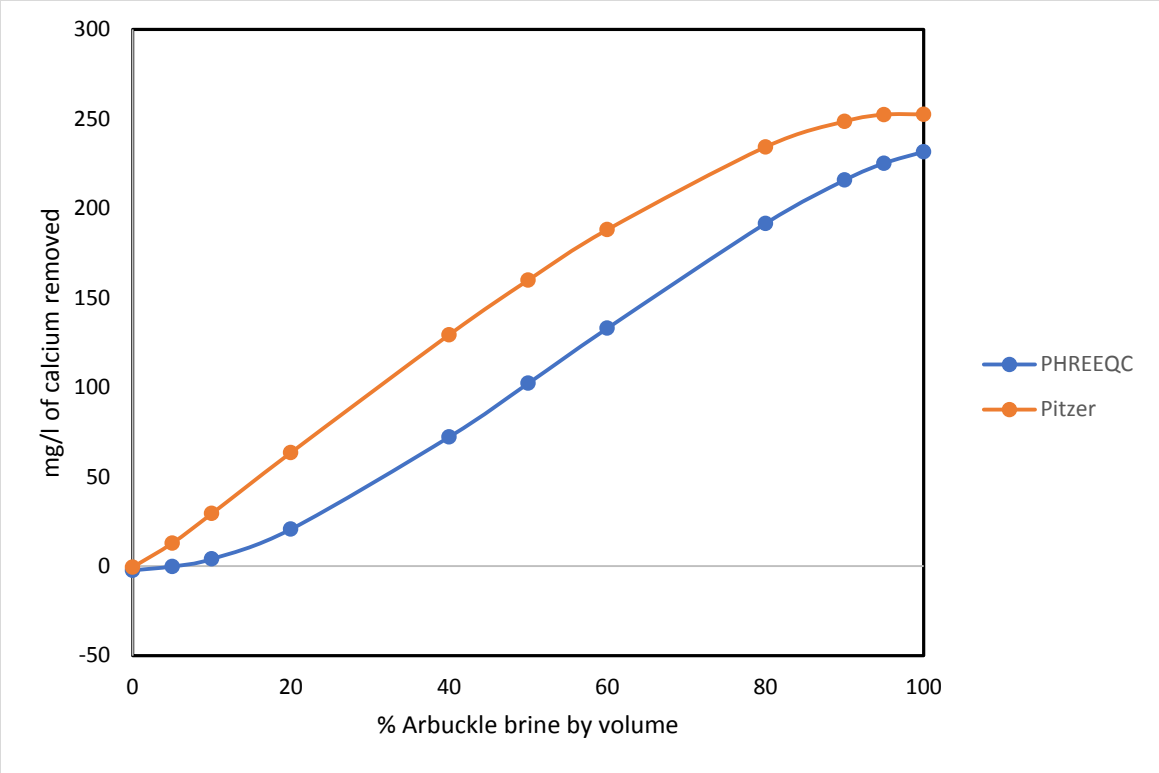

Figure 38: Change in the precipitated calcium concentration as the percentage of Arbuckle brine in the mixture increases

Also, changes in the solution pH as a result of calcite equilibration support the observation of more precipitate formation when the Pitzer database is used. When calcite is removed from solution, the solution pH drops lower, for a given buffer capacity, if more calcite is formed. Thus, the difference in pH for a given solution is a direct result of how much precipitation occurred. However, as the percentage of Arbuckle water approaches 100 %, the predicted solution pH values from both databases converge, even though the amounts of calcite precipitated are different. A difference of 31 mg/l calcium precipitation between the two databases did not correspond to a significant difference in solution pH, as shown in Figure 39. The fundamental reason for this discrepancy, as already mentioned above in other contexts, is the difference in computation of the activity corrections for the Ca^{2+} and carbonate ions by the two databases.

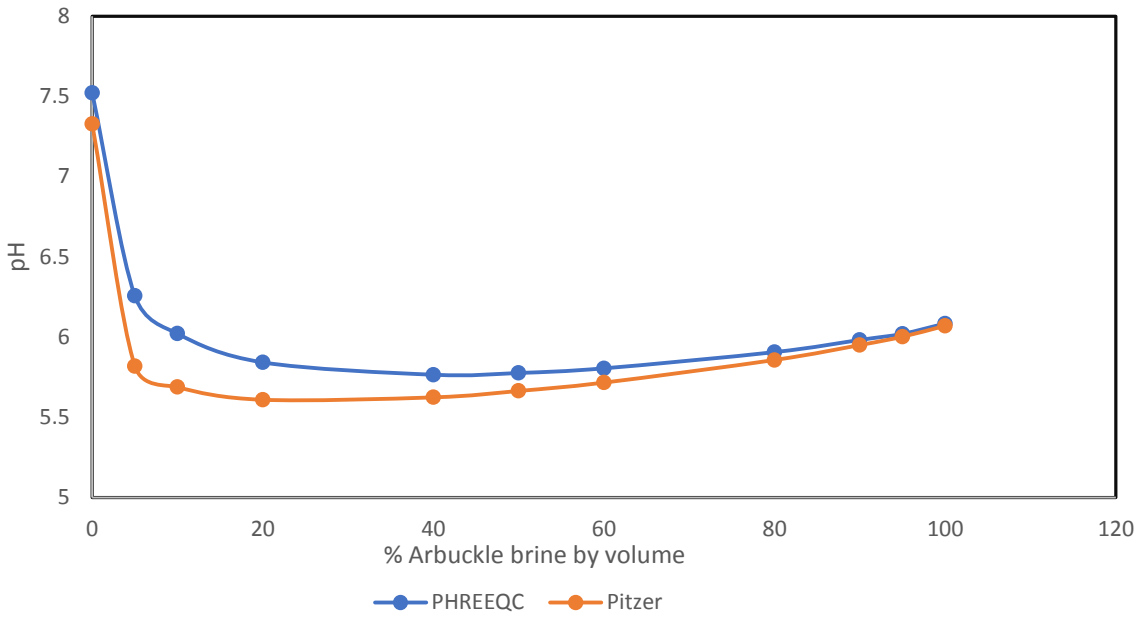

Figure 39: Effect of increasing percent Arbuckle water on the pH of the mixture

4.5 Calcite dissolution experiment

The LKC and 5 times diluted LKC brines took about 10 min. to approach equilibrium with powdered calcite (Indiana Limestone) based on monitoring the amount of calcium dissolution over time as shown in Figure 40. The 82 times diluted LKC brine took about 30 min. to approach equilibrium. The amount of calcite dissolution decreased in the following order: LKC, 5 times diluted LKC, and 82 times diluted LKC. It is very important to note that the rate of calcite dissolution from the calcite-brine mixture was very fast at the onset (<10 min.) in all three brines, as shown in Figure 40. Similar observations have been made by other researchers[165],[166]. Close to equilibrium, it took longer to detect any significant changes in both the concentration of the calcium ion (Figure 40) and the pH of the solution (Figure 41). In Figure 41, the changes in pH within the first 10 min. of the experiment demonstrate the effects of dissolution, i.e., all of the

solutions were initially undersaturated with respect to $CaCO_3$(s), as expected, since the starting carbonate concentration was zero for all three brines.

The volatile nature of the changes in the concentrations of the calcium ions in all three suspensions makes it difficult to accurately determine the equilibration time from Figure 40 below; but it appears that all three suspensions were close to equilibrium in about 10 minutes and there appears to be little or no net change in calcium ion concentrations after 30 min. However, using the pH change as the reaction proceeds indicates that there are slow but noticeable changes in pH over extended time periods. This raises questions as to whether the equilibration time put forward is accurate. The centrifuge tubes used were sealed but the manufacturer did not specify if the tubes were airtight or not. It is possible for the samples to have been in contact with atmospheric CO_2 despite being sealed, which could be the reason for the drift in pH observed as the time proceeded

To better understand the complex nature of the calcite dissolution experiment conducted using powdered Indiana Limestone, an experiment was conducted using reagent-grade $CaCO_3$. The pure reagent-grade powdered CaCO3 was added to LKC, 5 times diluted LKC, and 82 times diluted LKC brines. The experimental procedure followed was similar to that for the limestone powder dissolution experiment. The concentration of the Ca^{2+} ion was monitored after 24 h and 30 days. For the 24-hour measurements, the experiment was repeated 3 times, and for the 30-day measurements, the experiment was repeated 6 times. Dilutions were prepared in triplicate for ICP analysis.

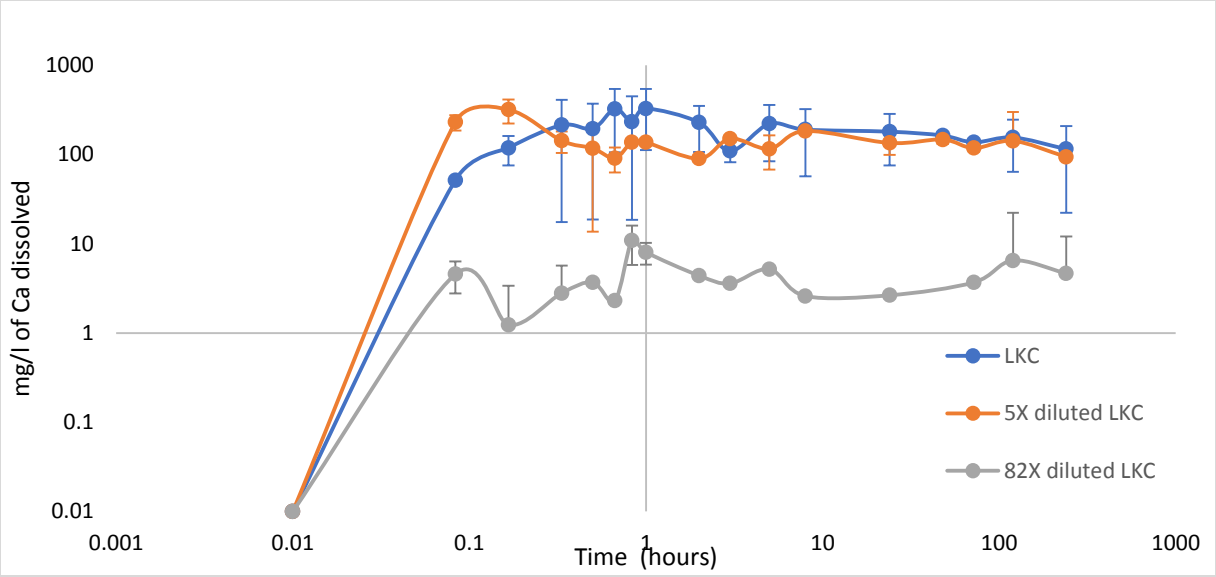

Figure 40: Amount of calcite dissolution with respect to time in the LKC brine and its dilutions

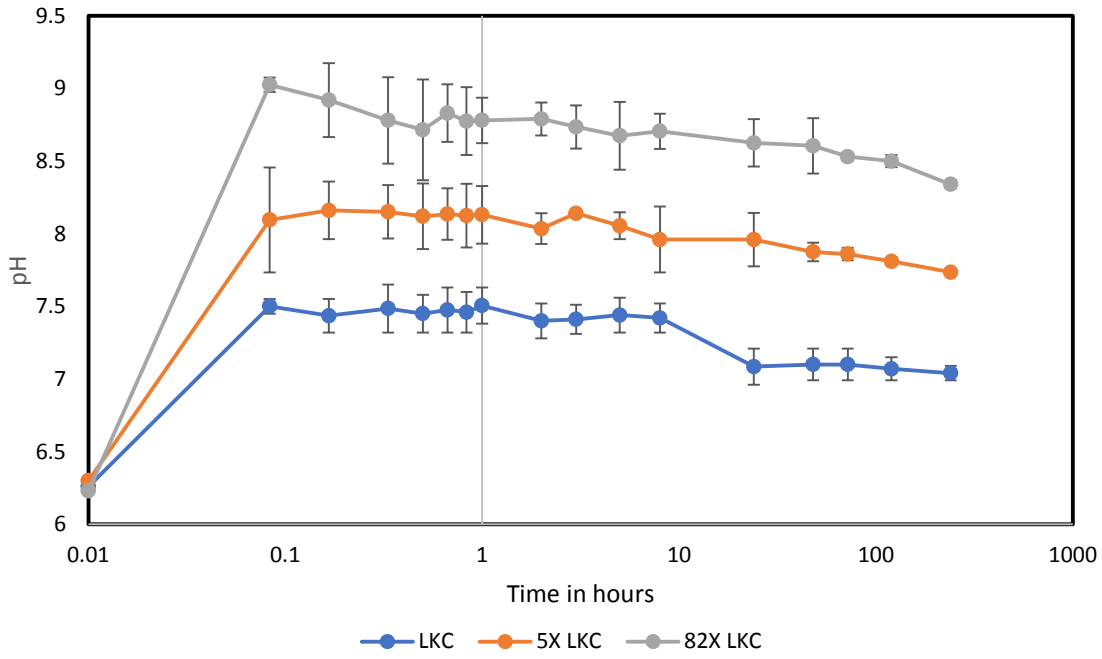

Figure 41: Temporal change in pH of suspensions of powdered Indiana Limestone in diluted and undiluted LKC brines

The pH values after 24 h and 30 days in the suspension of reagent-grade $CaCO_3$ were very comparable to those found in the limestone experiment, as shown in Figure 41; however, the

dissolution behavior was very different, as shown in Figure 43. The calcium ion concentrations indicated that dissolution occurred only in the 82 times diluted LKC brine at both 24 h and 30 days. For the LKC brine and the 5 times diluted LKC brine, the changes in calcium ion concentration indicated a loss of calcium ions from the solution, contrary to what was observed when the powdered limestone rock was used, even though similar pH values were observed in both cases for all three brine samples.

The dissolution of calcium carbonate (calcite) should have been similar for both powdered Indiana Limestone and reagent grade $CaCO_3$, especially since the measured pH values were similar. The carbonate system controls the pH of the solution. Dissolved carbonate ions react with H^+ to form bicarbonate, and the pH of the solution increases as the H^+ ions are consumed. The initial dissolution of calcium carbonate in the suspension of powdered Indiana Limestone, and the reaction of carbonate to form bicarbonate, occurred quickly, within the first 10 min. of the reaction, as shown in Figure 41 above. From the results using the reagent-grade calcium carbonate, it can be inferred that calcium ions in the solutions of the 5 times diluted LKC and 82 times diluted LKC brines were adsorbed onto the surface of the calcium carbonate particles, since the calcium concentrations decreased as shown in Figure 43. On the other hand, the limestone rock experienced only desorption which might be due: 1) a smaller number of adsorption site on the limestone surface, or 2) that the difference in surface area between the powdered limestone and the regent grade $CaCO_3$. It should be noted that the surface area of the powdered limestone and the reagent grade $CaCO_3$ were not measured, and surface area is mentioned as a possible reason for the discrepancy observed.

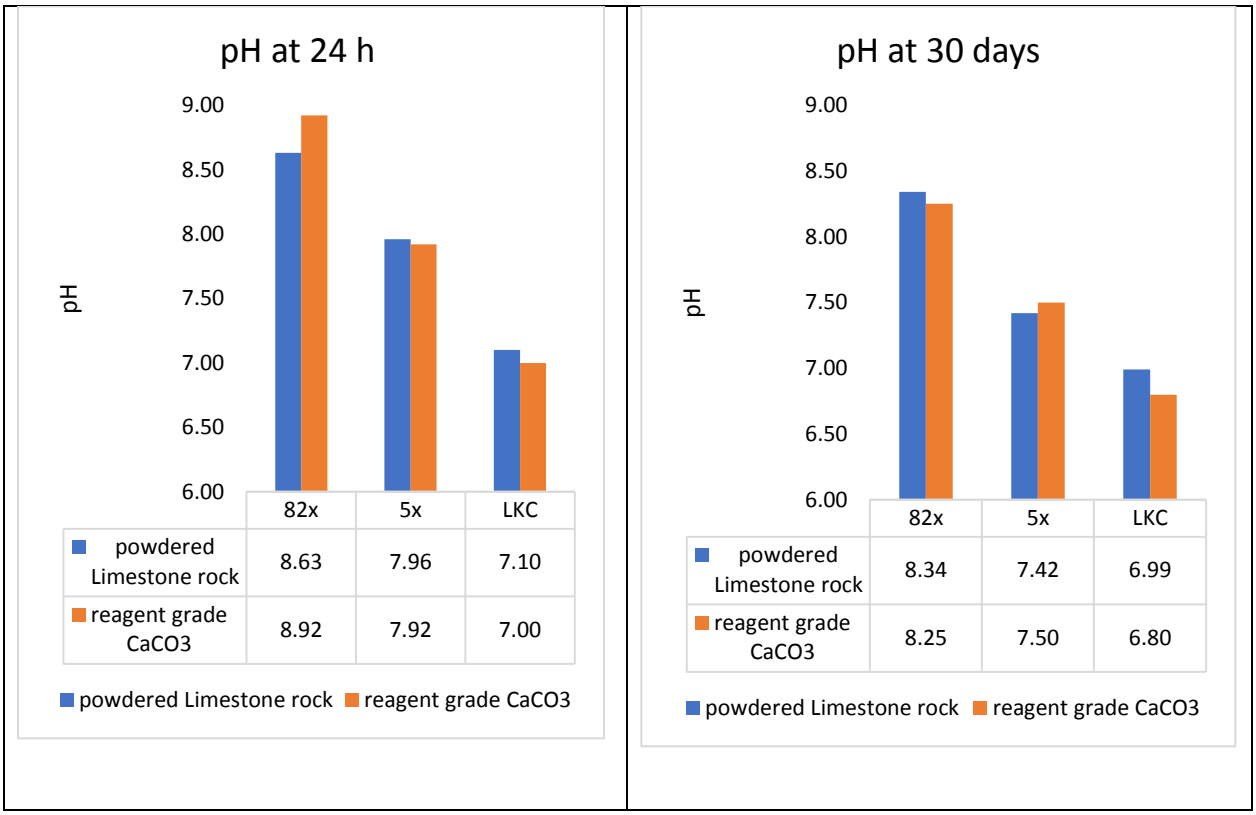

Figure 42: pH after adding powdered limestone and reagent grade calcium carbonate to LKC brine and its dilutions

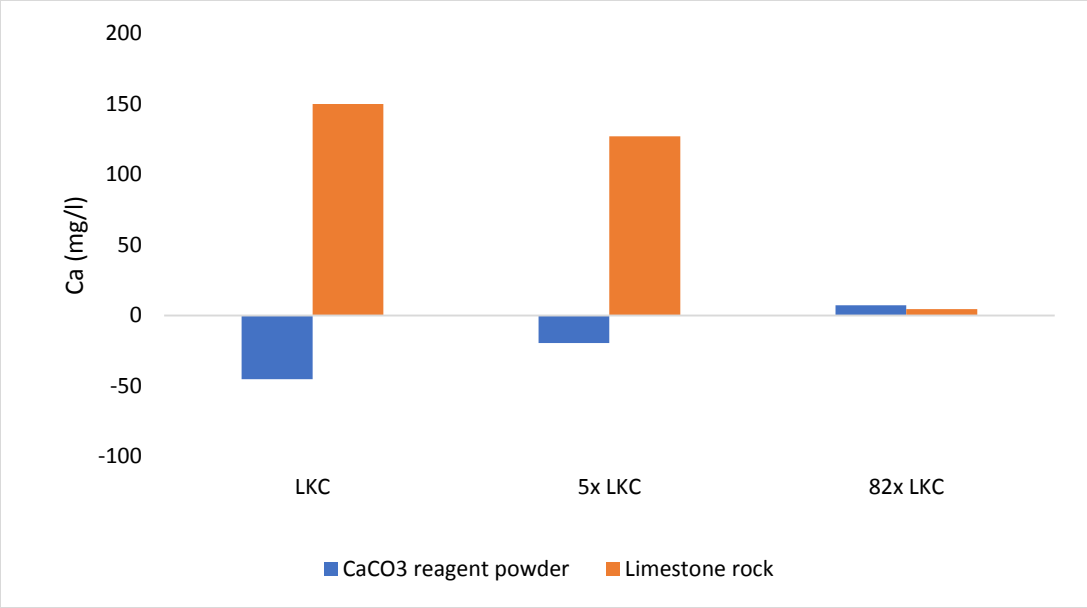

Figure 43: Change in Ca^{2+} concentration at 30 days using reagent-grade $CaCO_3$ vs powdered limestone

4.6 Scale formation predictions using PHREEQC.

The ability of PHREEQC to accurately predict scale formation in brines was assessed in a variety of ways using both the PHREEQC and Pitzer databases. Initially far from saturation, the LKC brine was equilibrated with both atmospheric CO_2 and humidified CO_2 and the experimental results were then compared to the modeling results. If the models indicated that the brines were supersaturated with respect to any of the precipitates of interest, as indicated by a positive SI, the models were made to predict the amount of precipitate formed. A few mixing scenarios involving the DC and RC brines were also used to compare model predictions with experimental results. Supersaturated conditions were created experimentally and then modeled to determine how closely the model predicted the observed precipitate formed.

4.6.1 SI values far below saturation (SI<−2)

4.6.1.2. Direct equilibration of LKC brine with the atmosphere

The modeling using both databases, as well as the results of the lab experiment, showed a decline in pH after the synthetic LKC brine was equilibrated with atmospheric CO_2. Using the PHREEQC database the model predicted a pH change from 6.6 to 5.6, with a similar change predicted by the Pitzer database. In comparison, the experimental pH measured in the lab changed from 6.6 to 6.14.

Equilibrating the synthetic LKC brine with CO2 caused part of the solution to evaporate. After accounting for 10 % evaporation of the samples in the model, the model and experiment agreed excellently with each other in terms of the concentrations of Ca^{2+} and Mg^{2+}, as shown in Figure 44. The standard deviations were 938 mg/l for the calcium ion and 183 mg/l for the magnesium ion as shown by the error bars in Figure 44. However, leaving the samples exposed to the atmosphere for longer periods (for about 10 more days after the initial three days equilibration) caused about 50 % evaporation of the samples, which greatly increased the Ca^{2+}, Mg^{2+}, Na^{+}, and Cl- concentrations, causing some mineral precipitation. The precipitate formed was white and formed around the sides of the beaker. Halite, gypsum, and anhydrite were predicted to be oversaturated with SIs of **+0.58, +0.14** and **+0.30**, respectively, when the PHREEQC database was used for modeling the reaction. These same minerals had SIs of **+0.65, +0.17** and **+0.27**, respectively, when the Pitzer database was used. The amount of Na^{+} that precipitated as a result of halite precipitation was 39.7 % and 39.2 % using the Pitzer and PHREEQC databases, respectively. Also, less than 0.5 % of Ca^{2+} was predicted to precipitate out of solution, for both databases, as a result of anhydrite precipitation. The model allowed anhydrite to preferentially precipitate over gypsum for the simple reason that in water-deficient systems, anhydrite is more

likely to form at ambient conditions. The precipitate formed from the experiment is more likely to be sodium chloride precipitate, as predicted by the model. The amount of CO_2 dissolved was too low to precipitate $CaCO_3$, based on the predicted SI values (of calcite and aragonite) for both databases. The model's prediction of no mineral precipitation when the LKC brine equilibrated with CO_2, without considerable water loss from the samples, agrees well with the experimental results.

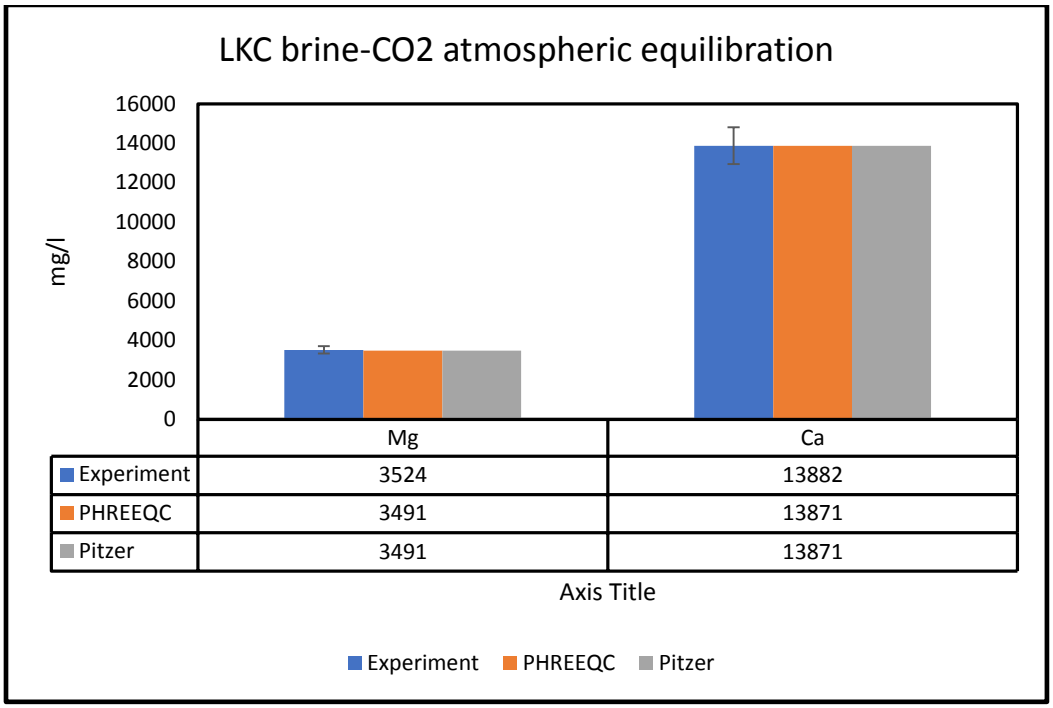

Figure 44: Concentrations of calcium and magnesium after equilibrating the LKC brine with atmospheric CO_2 and correcting for 10 % sample evaporation

4.6.1.3 Equilibrating the LKC brine with humidified CO_2

Bubbling humidified CO_2 through the LKC brine produced no precipitates as shown in Figure 45. The model and the experimental results complemented each other excellently, with both indicating no precipitation of any kind, similar to the results for direct equilibration with atmospheric CO_2, after 10 % sample evaporation. The standard deviations of the measured

concentrations, as indicated by the bars in Figure 41, were 70 and 352 mg/l for magnesium and calcium ions, respectively, before equilibration, and 50 and 402 mg/l, respectively, after equilibration. The SI values for all the carbonate phases were less than -2, representing extremely undersaturated conditions with respect to these minerals. It should also be noted that the starting bicarbonate concentration in this brine, prior to the introduction of CO_2, was zero. From the LKC brine CO2 equilibration experiment, it can be concluded that, far from saturation, the model provides an excellent prediction of whether a mineral phase would precipitate or not.

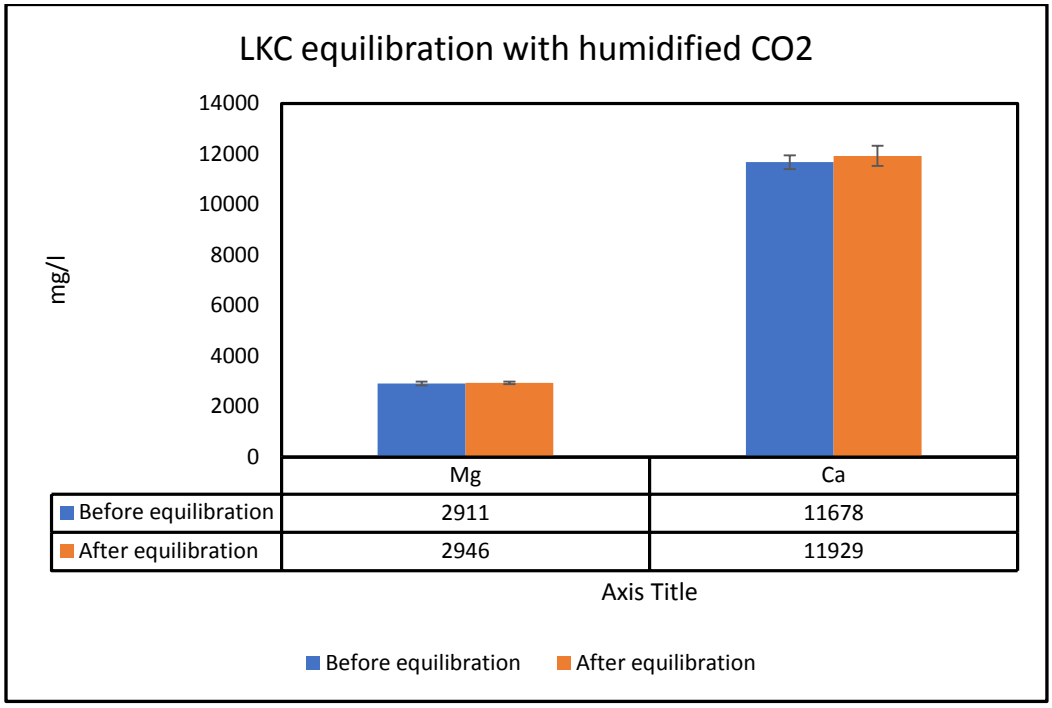

Figure 45: Concentrations of calcium and magnesium before and after equilibrating the LKC brine with humidified CO_2

4.6.2 SI values close to saturation (−0.5>SI>2)

As discussed in section 3.7, the initial cation concentrations (Ca^{2+}, Mg^{2+}, Sr^{2+}, and Ba^{2+}) for the mixing cases discussed here in section 4.5.2 were calculated from the compositions of the brines (RC and DC) prior to mixing because some precipitation reactions could proceed very rapidly

after mixing. As a result, the impact of background ions may have resulted in artificially low estimates of the final concentrations of cations in these experiments, which would result in overestimates of cation precipitation from these mixtures. When the effect of the ionic strength on the measured concentrations were estimated, it was surmised in section 3.7 that this effect could overpredict cation removal by 12 to 17 % for magnesium, 16 to 23 % for calcium, 8 to 16 % for strontium and 17 to 20 % for barium.

4.6.2.1 Mixing DC and RC brines in the ratio 80:20

No precipitate was visible when the two produced waters were mixed in an 80:20 ratio (DC:RC). However, both modeling approaches predicted oversaturation of some phases. Using the PHREEQC database, the model predicted SIs of **+1.65**, **+1.79**, **+1.75**, **+3.53** for the mineral phases aragonite, calcite, barite and dolomite, respectively. Using the Pitzer database on the other hand, the model predicted SI values of +**1.67, +1.95, +1.74** and **+3.74** for the same minerals respectively. Both databases predicted about the same amount of barite precipitate even though the SI associated with barite was slightly higher using the Pitzer database. Magnesium and strontium had no precipitation predicted using either database even though SIs of dolomite indicated supersaturation. In the models, calcite would preferentially precipitate over dolomite when both phases were allowed to precipitate at the same time, resulting in no loss of Mg.

The experimental results (Figure 46) showed dissolution of 2 % of the calcium, which is within the range of the calculated standard experimental error (±2 %) for all cations in this samples. (The error bars represent the standard deviation of the measured concentrations in Figure 46.) Since dissolution cannot occur when two solutions containing no solid phases are mixed together, these results indicate that no significant precipitation of a Ca-bearing phase occurred. The initial sulfate and barium concentrations were 20 and 400 mg/l, respectively, after mixing,

so some precipitation of barium sulfate was anticipated. However, barium ions would have had to compete with the other divalent cations to react with the sulfate ions, which could lead to the observed little or no significant precipitation of barium sulfate. Taking into consideration the effect of the background ions in the measurement of divalent cations, no significant precipitation of scale-forming cations was observed, because all precipitated values fall within the range mentioned in section 3.7.

A similar study conducted by He *et al.*[161], which investigated the kinetics and equilibrium of barium and strontium sulfate in the Marcellus shale flowback water, found that barite precipitation occurred after 30 min. However, they found barite precipitation to take longer in a high ionic strength solution (3.9 M) when the initial barium (236 mg/l) and sulfate (150 mg/l) concentrations were low and the strontium concentration was roughly 8 times the concentration of barium. Assuming all the available sulfate reacted with the barium in the solution, the removal of barium would have been 90 %; but only 55 % removal was found. Although the ionic strength of the solution in this study was less than 0.65 M (<<3.9 M), there could be secondary reactions occurring between sulfate and the other divalent cations (calcium, magnesium, and strontium), which could inhibit barite from forming altogether or on a time scale relevant to this study, which the model does not take into account. Another potential reason could be due to the fact there could be uncertainties in the reported Ksp values (close to saturation) of barite which makes it less soluble thermodynamically. Also, since the two databases are predicting the same amount of precipitate, with the PHREEQC database accounting for complexation and ion pairing, it is safe to assume that the PHREEQC database assumes these complexes are negligible, which may not be true for high strength brines.

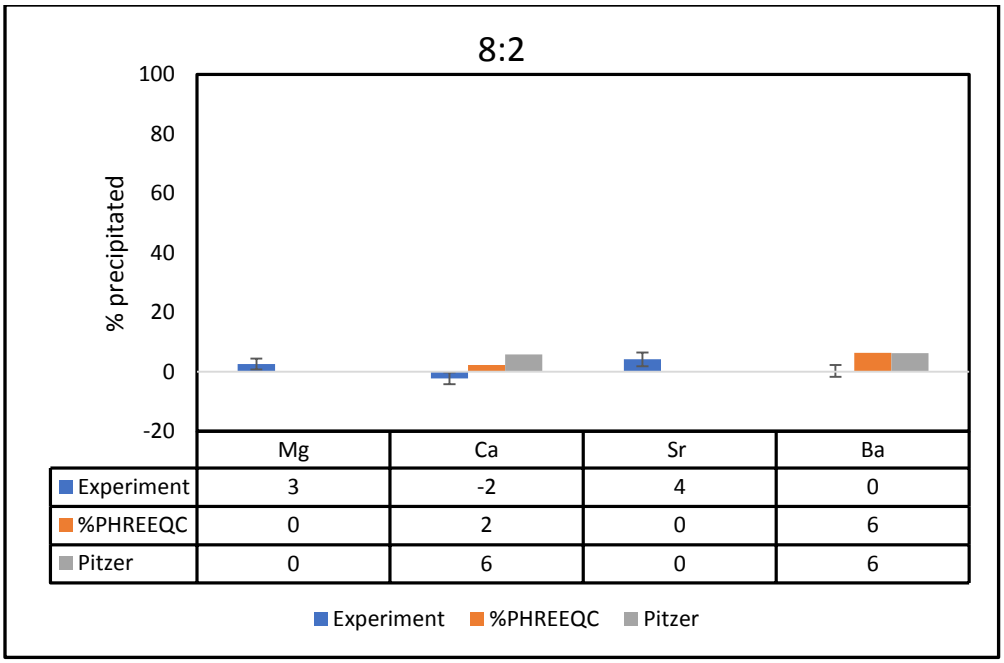

Figure 46: Percent precipitation of scale forming divalent cations from solution after mixing DC brine and RC brine in a 80:20 ratio.

4.6.2.2 Mixing DC and RC brines in a 50:50 ratio

Using the PHREEQC database, the model predicted **+1.57**, **+1.71**, **+1.73**, and **+3.34** for the mineral phases aragonite, calcite, barite and dolomite, respectively, when the two produced water brines were mixed in a 50:50 ratio. In contrast, using the Pitzer database, the model predicted SIs of **+1.62, +1.90, +1.81** and **+3.60** for the same minerals. The SI predictions associated with barite from both databases (+1.73 for PHREEQC and +1.81 for Pitzer) corresponded to 31 % and 26.7 % barium precipitation, respectively. Using the PHREEQC database the model predicted 1.4 % calcium precipitation while using the Pitzer database yielded a prediction of 2 % calcium precipitation. The experimental results from the ICP analysis indicated 2 % average barium and calcium precipitation, no precipitation of magnesium, and 7 % precipitation of strontium, as shown in Figure 47. The error bars represent the standard deviations of the measured concentrations and are approximately 2 % for all divalent cations. The effect of ionic strength on

the measurement of the divalent cation concentrations, due to the background NaCl concentration and ionic strength, indicates no significant change in the concentrations after mixing for all divalent cations, since the values reported for calcium, strontium and barium fall within the possible range of cation under-measurement discussed in section 3.7. Despite prediction of substantial barite precipitation, no significant loss of Ba from solution was observed. The initial concentrations of 250 and 50 mg/l for barium and sulfate, respectively, were evidently low enough that inhibition by other cations (especially strontium, which is more than 4 times the concentration of barium) could have prevented barium sulfate precipitation. Mineral solubility generally increases as the ionic strength of the solution increases. With a TDS of 80,000 mg/l, this is a reasonable explanation for the lack of barite precipitation under the circumstances of this study, as explained He *et al*.[161]. The model's failure to predict the amount of barite precipitation is presumably due to the same reasons mentioned in section 4.6.2.1.

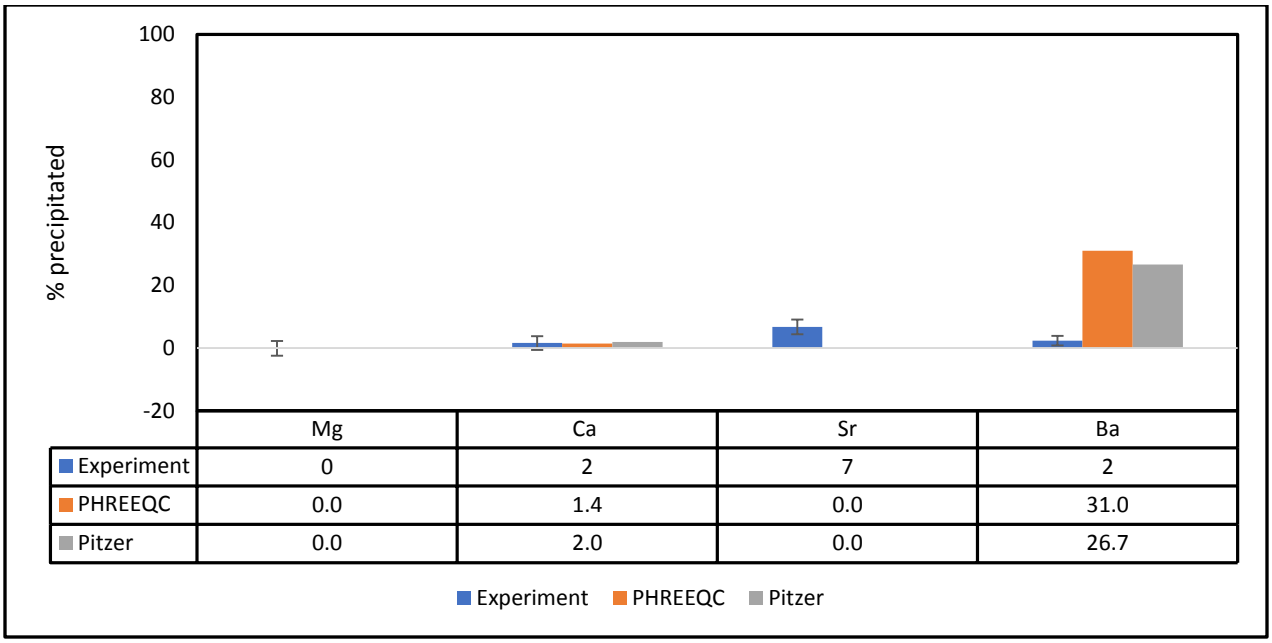

	Mg	Ca	Sr	Ba
Experiment	0	2	7	2
PHREEQC	0.0	1.4	0.0	31.0
Pitzer	0.0	2.0	0.0	26.7

Figure 47: Percent precipitation of scale forming divalent cations from solution after mixing DC and RC brines in a 50:50 ratio

4.6.2.3 Mixing DC and RC brines in the ratio 20:80

Barite, calcite, dolomite and aragonite were the only mineral phases for which PHREEQC predicted positive SI values for 20:80 mixtures of the DC and RC brines. Using the PHREEQC database the model predicted SIs of **+1.50, +1.36,** +**2.65** and **+1.21** for barite, calcite, dolomite and aragonite, respectively, and SIs of **+1.58, +1.62, +3.05,** and **+1.34**, respectively, when the Pitzer database was used. Once again, the SIs associated with the various cation saturation states were higher when the Pitzer database was used. The model predicted 87 % barium removal using the PHREEQC database, and 89 % using the Pitzer database, as shown in Figure 48, but only 6 % removal was observed experimentally. The experimental results showed no removal of magnesium or calcium, and strontium removal is not significant given the uncertainty in estimated cation removal discussed in section 3.7. The model predictions and experimental results diverge significantly for barium in this case. Barium and sulfate, after mixing, had initial concentrations of 103 and 80 mg/l, respectively, with a TDS of 110,000 mg/l, but the strontium

concentration in this case was about 16 times more than barium. As explained earlier, it is very plausible to conclude that the inhibitory effect of strontium might be pronounced if its relative ratio to barium is high, preventing or slowing down the formation of barium sulfate scale. If both barium and sulfate exist in equal amounts such that both reagents are not limiting, the model is more likely to predict a high removal percentage for barium as shown in Figure 48.

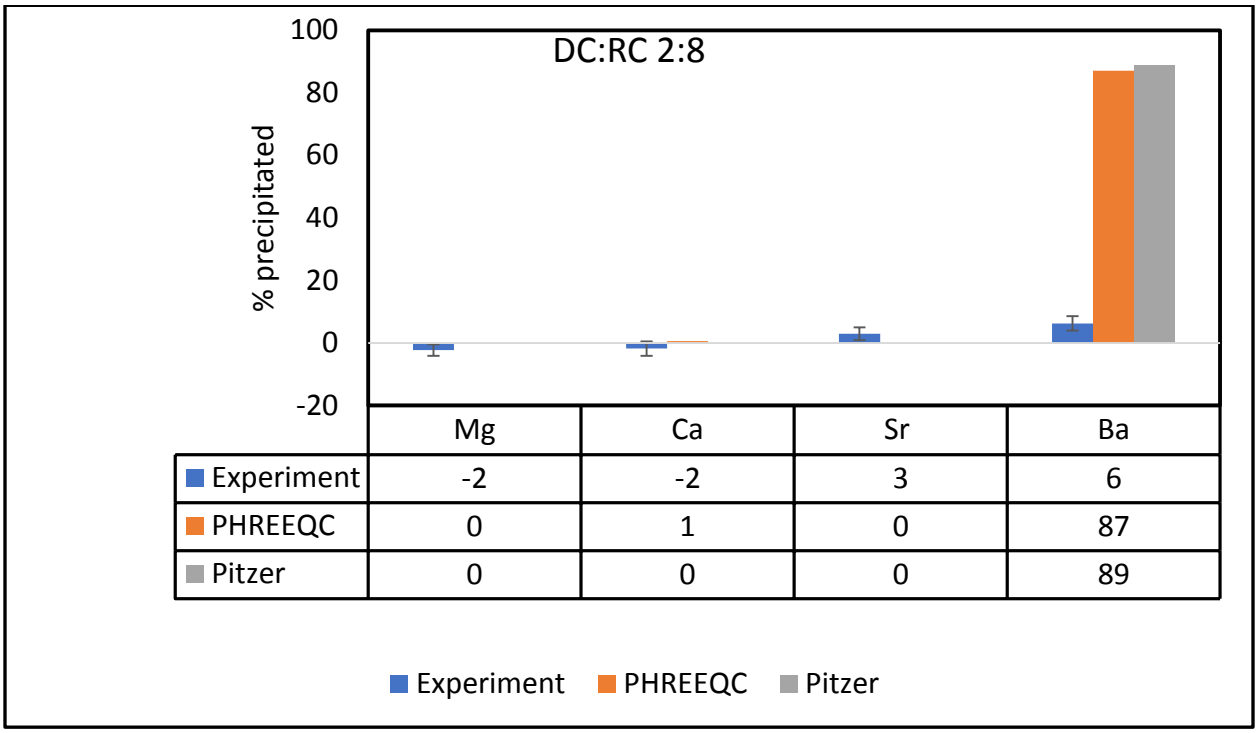

Figure 48*:* Percent precipitation of scale forming divalent cations from solution after mixing DC and RC brines in a 20:80 ratio

4.6.2.4. Arbuckle brine CO_2 equilibration experiment

Arbuckle synthetic brine was equilibrated with atmospheric CO_2. After exposure to the atmosphere for 3 days, the experimental results matched the predictions of both databases. The experimental results agreed with model predictions of approximately 20 % removal of Ca^{2+}. There was also excellent agreement between the experimentally observed final pH and the model-predicted final pH values, as shown in Figure 49.

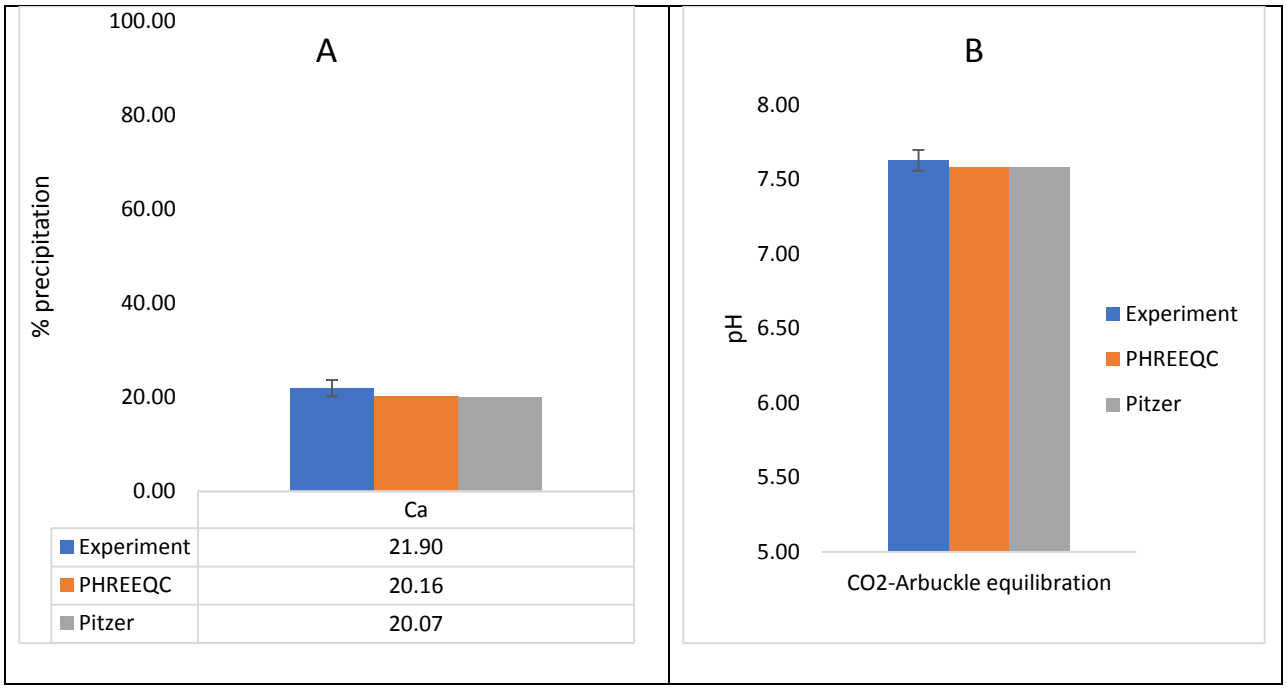

Figure 49: (A) Ca precipitated from solution during the CO_2-Arbuckle brine equilibration experiment. (B) Measured and model-predicted pH values after precipitation has taken place.

4.6.3 SI values far above saturation SI>2

4.6.3.1 Addition of 0.5M sodium sulfate to the DC brine

Aragonite, calcite, dolomite and magnesite ($MgCO_3$) were the only mineral phases with positive SIs, **+1.44, +1.73, +3.49, and +1.02**, respectively, when the Pitzer database was used to model the DC brine (without supplemental chemical addition). The model predicted 11 % and 12 % removal of calcium and magnesium ions, respectively, as a result of dolomite precipitation. On the other hand, the PHREEQC database predicted saturation indices of **+1.47, +1.61, +3.36, +1.21** and **+0.95** for aragonite, calcite, dolomite, strontianite and witherite, respectively, when the original DC brine was modeled. Estimated precipitate formation was similar to that predicted using the Pitzer database, i.e., 10 % and 12 % removal of calcium and magnesium, respectively. It should be noted that there was no measured loss of magnesium or calcium fom the solution when an ICP analysis was performed on the DC brine samples.

When 0.5 M sodium sulfate was added to the DC brine, the model identified celestite ($SrSO_4$), barite ($BaSO_4$), aragonite, calcite, dolomite and gypsum as phases that were oversaturated, with SIs of **+0.99, +4.40, +0.71, +0.99, +2.16** and **+0.09**, respectively, when the Pitzer database was used. The +0.09 gypsum SI corresponded to an estimated 80 % calcium precipitation. When the PHREEQC database was used, both anhydrite and gypsum were oversaturated, with SI values of **+0.10** and **+0.37**, respectively. The +0.37 gypsum SI corresponded to a prediction of 57 % calcium precipitation as calcium sulfate. Also identified with positive SI values were celestite, barite, aragonite, calcite, dolomite, strontianite and witherite, with SI values of **+1.25, +4.68, +1.03, +1.18, +2.41, +0.74,** and **+0.27**, respectively. After allowing precipitate formation to reach a target SI of 0.00 for all of the aforementioned solid phases, the model results, using both the Pitzer and PHREEQC databases, predicted the same amount of precipitation for barium, all associated with barite precipitation. Barite forms very quickly when there is enough barium and sulfate in the solution, even at high ionic strength.

The Pitzer and PHREEQC databases both overestimated the amount of strontium and calcium precipitated. The Pitzer database more closely predicted the amount of strontium sulfate precipitated. The models predicted that calcium would precipitate as a result of gypsum and dolomite formation, using both databases, with gypsum contributing over 90 % of the calcium precipitation. Also, the model predicted strontium removal as a result of celestite precipitation, using both databases. The Pitzer database model over predicted magnesium precipitation while the PHREEQC database model under predicted magnesium precipitation, due to oversaturation with respect to dolomite in both cases. Where there are complex reactions such as adsorption and coprecipitation, the model overestimates the concentrations of free ions available, hence the errors in estimating the amount of precipitation of related phases. The Pitzer model does not

account for complex formation as such, which increases the number of free ions available to form the mineral phases. On the other hand, the PHREEQC database may underestimate the concentrations of the complexes formed, making it more likely to over predict the amounts of precipitates formed. Also, another reason for the overestimation of precipitation might be the reaction time required to form precipitates. As the results in Figure 50 indicate, after 150 days strontium precipitation increased from 62 % to 81 % while magnesium and calcium precipitation decreased by 2 %. This brought the experimental strontium precipitate closer to the model predictions.

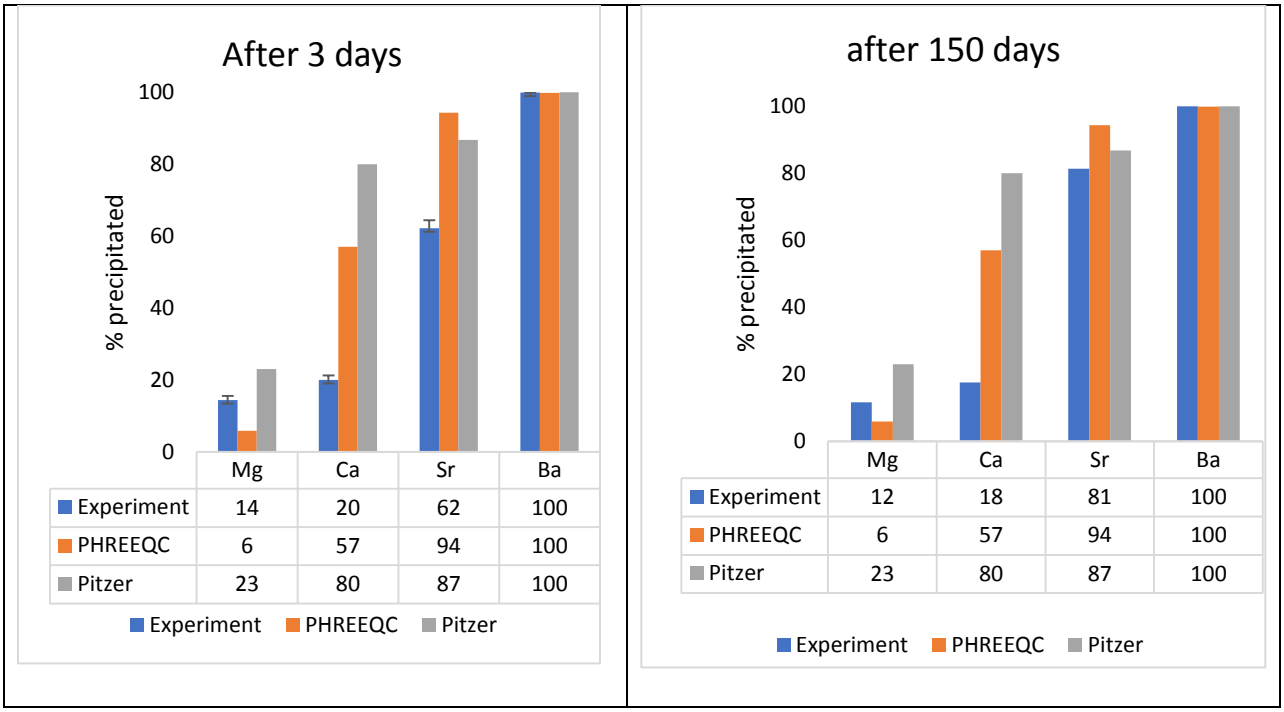

Figure 50: Experimental versus model-predicted removal of calcium, barium, strontium, and magnesium after 3 and 150 days when 0.5M sodium sulfate was added to the synthetic DC brine

4.6.3.2 Addition of 1M sodium carbonate to the RC brine

When the RC brine was modeled using both databases, aragonite, calcite, dolomite and barite were the only mineral phases that were predicted to be oversaturated, with SIs **of +0.58, +0.86, +1.54,** and **+0.19**, respectively, using the Pitzer database, while modeling using the PHREEQC

database predicted **+0.17, +0.31, +0.18** and **+0.57**, respectively for the same minerals. Allowing for precipitation caused the model to predict 35 % and 0.01 % removal of barium and calcium ions, respectively. This had a negligible bearing on the solution chemistry as the initial concentration of barium was only 3.8 mg/l. When the "precipitate function" was used in modeling the behavior of RC brine spiked with sodium carbonate, the model accurately predicted the experimentally determined brine composition, except for magnesium. The model predicted SI values of **+4.84, +5.12, +9.61,** and **+3.74** for aragonite, calcite, celestite ($SrSO_4$), and dolomite, respectively, when the Pitzer database was used. The PHREEQC database predicted SI values of **+4.83**, **+4.97**, **+9.94,** and **+5.01** for the minerals mentioned above in the same respective order. A consensus 99 % of calcium and strontium were precipitated out of solution based on model and experimental results after 3 and 150 days, respectively. It should be noted that the Pitzer database does not contain the strontianite mineral phase, so no comparison could be made between experimental and model-predicted results for the Pitzer database.

Magnesium removal improved from 79 % to 96 % (Figure 51) indicating the importance of kinetics to Mg removal. Assuming equilibrium is reached after 150 days, the model predicts the removal of magnesium fairly accurately. The mechanism underling experimentally measured magnesium removal could have been precipitation of magnesium substituted calcite, which would remove less magnesium that the dolomite precipitation incorporated into the model results for both databases. Magnesium removal might also have been caused by adsorption onto, or coprecipitation with, other solids, but probably not through magnesium sulfate precipitation, since magnesium sulfate is very soluble. Without SEM imaging, it is difficult to determine the mechanism responsible for Mg^{2+} removal. Nevertheless, in this experiment, the experimental results and the modeling results from both databases complemented each other well

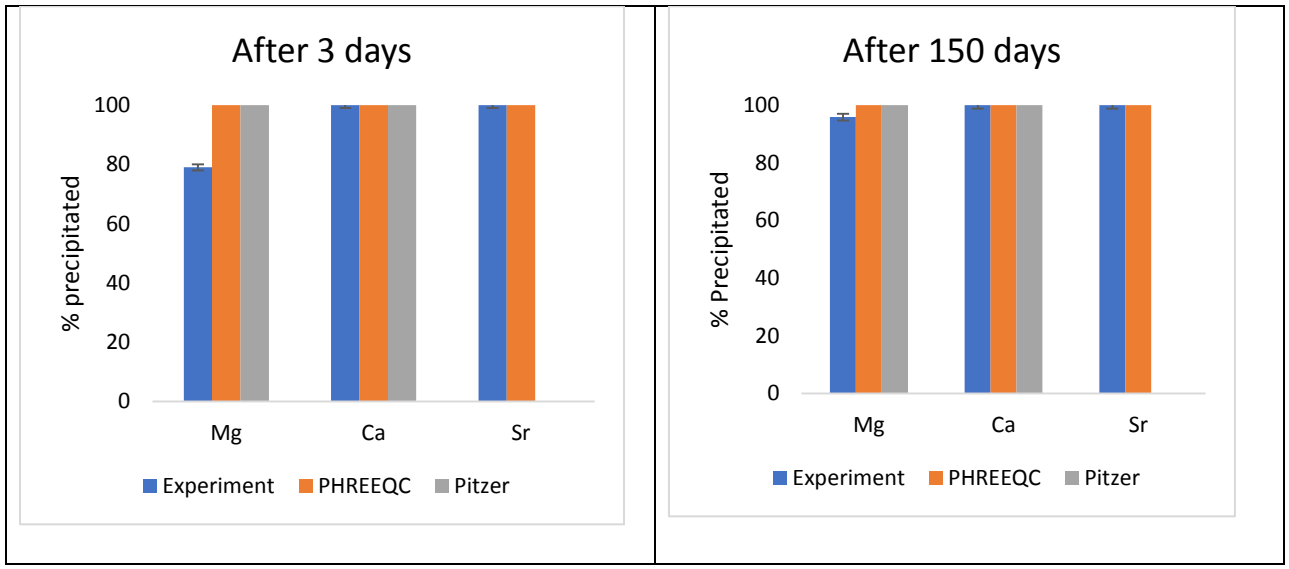

Figure 51: Comparison between model-predicted and experimental cation precipitation, after 3 and 150 days, when 1M sodium carbonate was added to the Reno County brine

4.7 Effect of Ionic strength on pH measurement.

To further understand the role of ionic strength on pH measurement, the pH 7 and 10 buffer solutions used for pH meter calibration were modified by adding sodium chloride salt in a stepwise manner to increase the TDS from 10,000 to 200,000 mg/l. As shown in Figures 52 and 53, the pH declined as the sodium concentration increased from 3,940 to 78,800 mg/l. The data points from the experimental results were fitted using both linear and polynomial equations. The R^2 values for the polynomial equations (plotted in Figures 52 and 53) were 0.9666 and 0.9829 for the pH 7 and 10 buffers, respectively. The linear equations had R^2 values of 0.8561 and 0.8681 for the pH buffer 7 and 10 buffers, respectively. From the R^2 values it is clear that the

polynomial equations provided a better fit, and the relationship is clearly non-linear as illustrated by

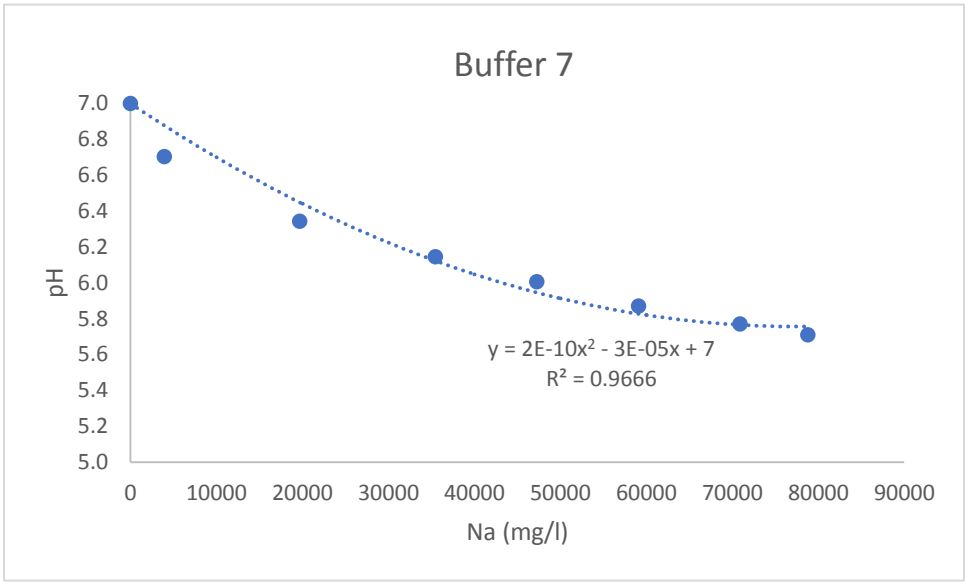

Figure 52 and 54.

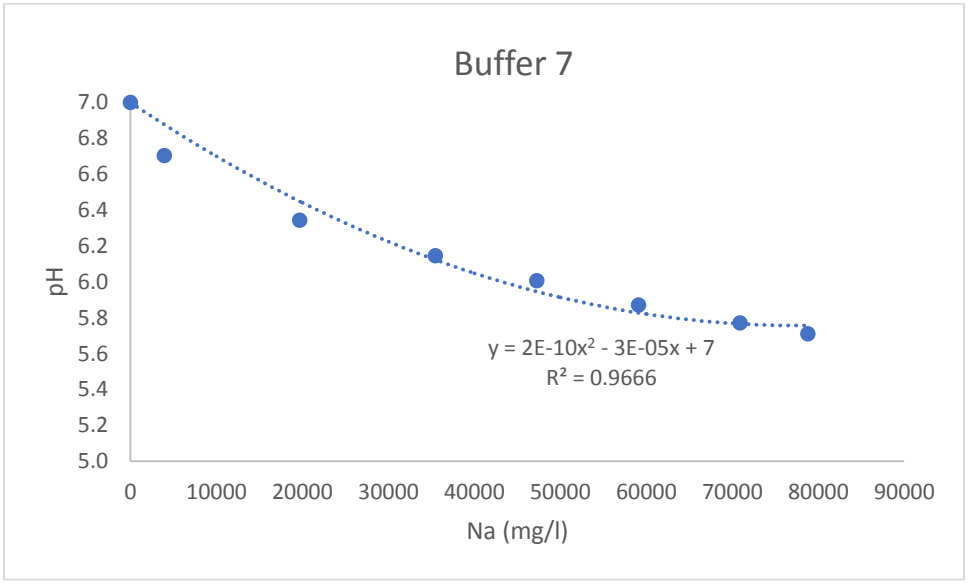

Figure 52: Effect of ionic strength on pH when a pH buffer solution with a pH of 7 is dosed with sodium chloride salt

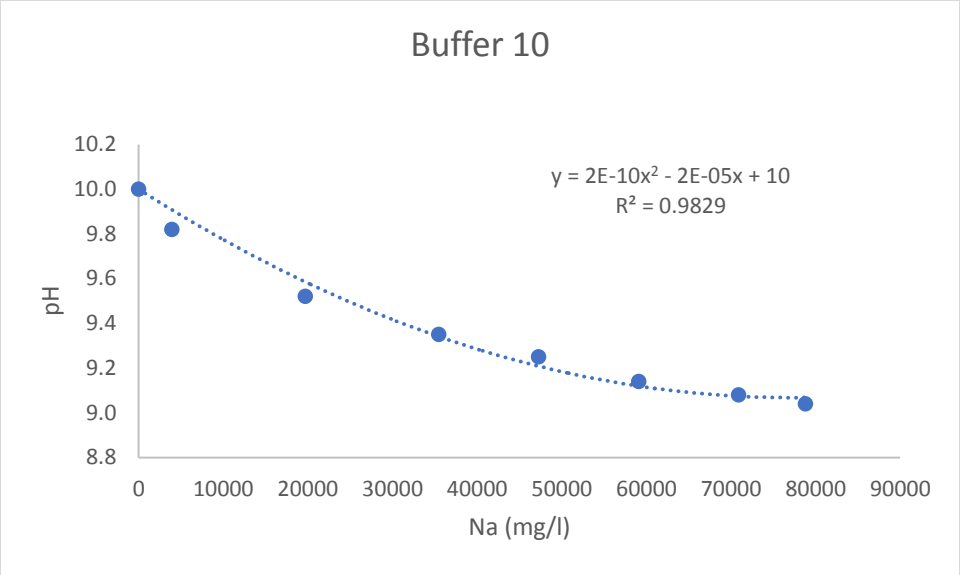

Figure 53: Effect of ionic strength on pH when a pH buffer solution with a pH of 10 is dosed with sodium chloride salt

The experiments were further modeled using the standard PHREEQC database only. This is because both borate (in the pH buffer 10 solution) and phosphate (in pH buffer 7 solution) are not included in the Pitzer database. The Na^+ ions in solution caused a decline in predicted pH, which is similar to what was observed experimentally. However, there was a steeper decline in pH in the experimental results relative to the model's prediction, as shown in Figure 54.

The decline in pH observed during the experiment with the pH buffer 7 solution was indicated by the model to be caused by the formation of the $NaHPO_4^-$ complex, which becomes very significant at high sodium chloride dosages. The experimental results, on the other hand, illustrated a steeper decline in pH, which is likely due to a combination of both $NaHPO_4^-$ complex formation and an interference of Na^+ with the electrode, commonly referred to as "sodium error", which is caused by high concentrations of Na^+ interacting with the electrode sufficiently to make the H^+ concentration appear higher than it actually is, resulting in a lower pH reading.

The model predicted the pH buffer 10 experiment to show little variation in pH. There were no significant sodium borate complexes predicted (for the borate-based pH buffer), so the pH was expected not to change much. The ~ 0.1 pH unit change observed can be explained by the effect of ionic strength on the activity of the H^+ ions. On the contrary, the actual experimental result illustrated a much steeper decline in the pH. This discrepancy might be due to the fact that at a higher pH, the H^+ concentration is lower, and the pH electrode would be more susceptible to sodium error.

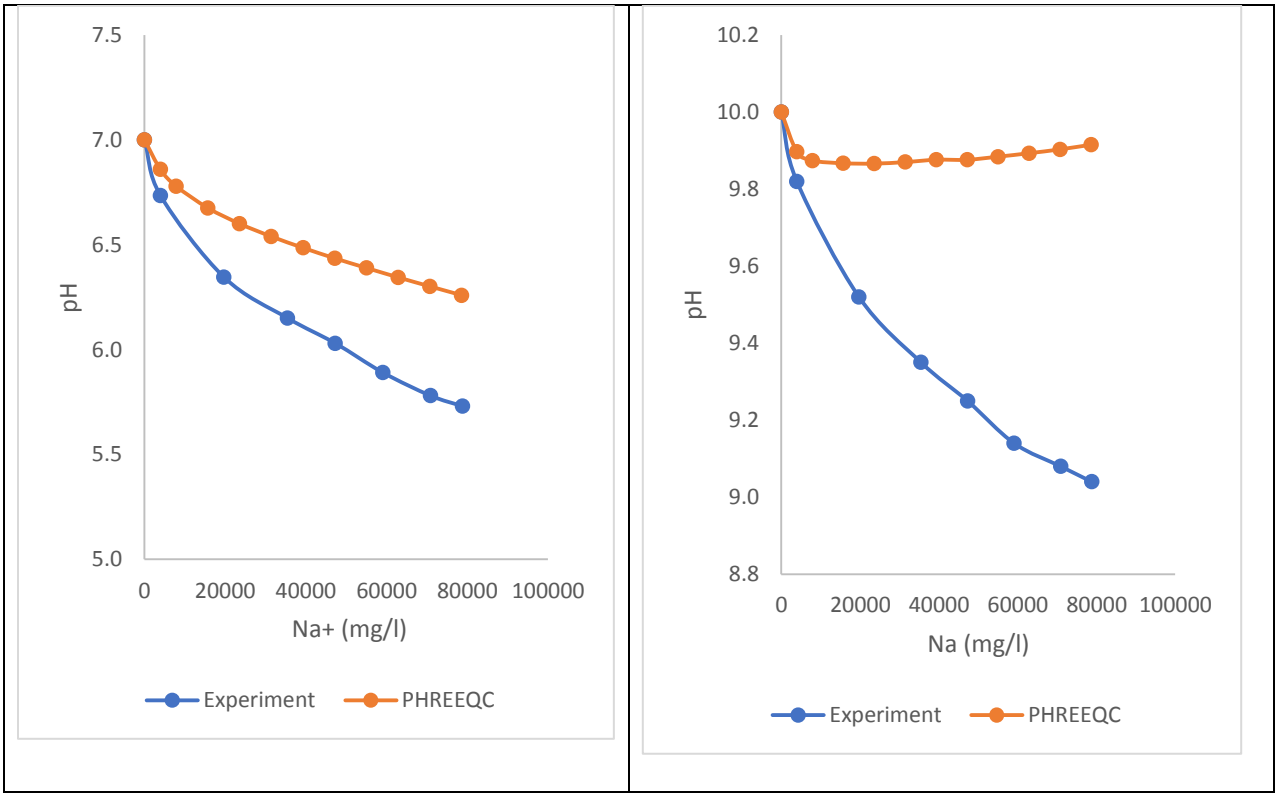

Figure 54: pH prediction of PHREEQC relative to experimental pH when buffer solutions with pH of values of 7 and 10 are dosed with sodium chloride.

A comparison of the experimentally measured pH values with those predicted by the model using both the PHREEQC and Pitzer databases, as shown in Figure 55 below, did not show any

particular trends. pH values from the modeling work were expected to be significantly higher than those found in the experiments, as shown in Figure 54. The only experiment that followed such trend involved the addition of 1 M sodium carbonate to the RC brine. The effect of Na^+ on pH electrodes is known to be more pronounced at elevated pH, so this is the most likely reason for the difference between the measured and predicted pH values. Also, a likely reason for this observation could be the diverse nature of the background salts in these solutions as compared to the buffer solutions used to determine the effect of sodium on pH. At this point, future experiments are planned to be performed to develop a means of making accurate adjustments to the measured pH of brine samples, or standardizing the pH meter to give accurate pH values in brine samples.

It is very vital to measure pH accurately especially when reactions that have a strong dependence on pH are involved. For the purpose of this study, key reaction parameters such as pH, temperature and individual ions would have to be inputted into the modeling software to give results that more accurately reflect the reactions occurring in the systems. If the pH used in modeling is significantly off, it will affect the speciation of the carbonate system; increase or decrease the concentration of carbonate, hydroxide, and other ions available to form various solid phases of interest; and render the associated SI values inaccurate. Furthermore, the concentrations of related cations remaining in solution will also differ significantly from their measured values.

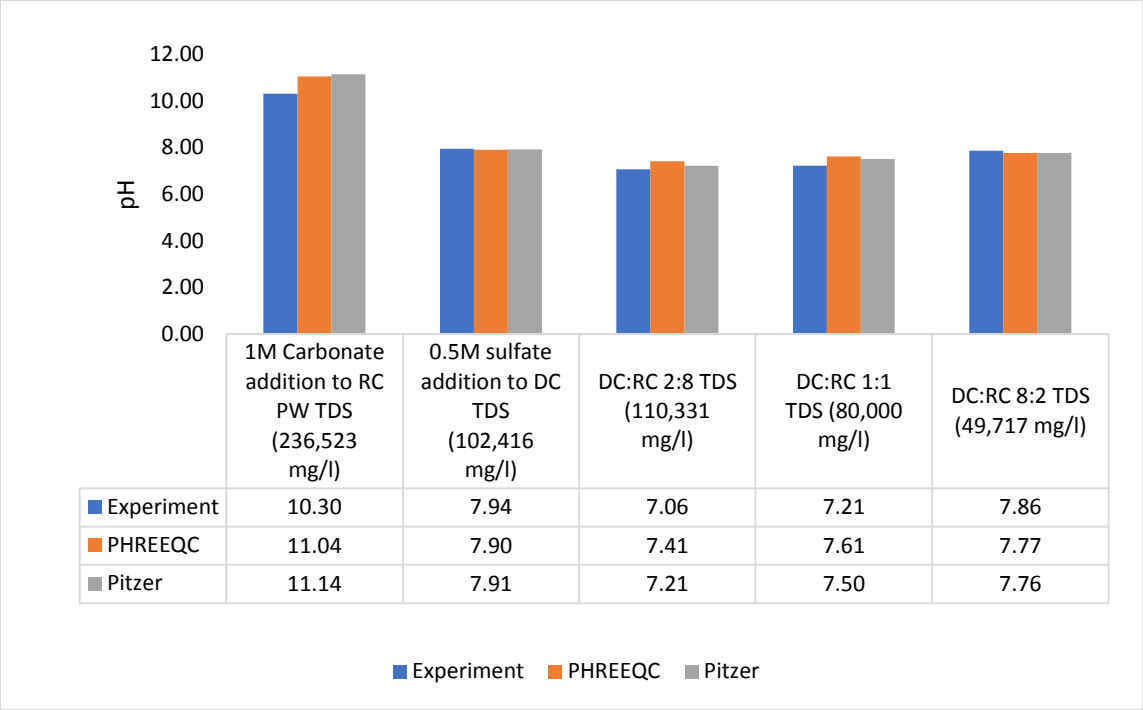

	1M Carbonate addition to RC PW TDS (236,523 mg/l)	0.5M sulfate addition to DC TDS (102,416 mg/l)	DC:RC 2:8 TDS (110,331 mg/l)	DC:RC 1:1 TDS (80,000 mg/l)	DC:RC 8:2 TDS (49,717 mg/l)
Experiment	10.30	7.94	7.06	7.21	7.86
PHREEQC	11.04	7.90	7.41	7.61	7.77
Pitzer	11.14	7.91	7.21	7.50	7.76

Figure 55: Predicted pH vs measured pH

Conclusions, Recommendations and Engineering Application

5.1 Conclusions

Modeling and laboratory experiments were conducted to evaluate the feasibility of exchanging Arbuckle PW with LKC PW in a scenario where the Arbuckle, which is lower in TDS, is used for water flooding the LKC formation to increase oil recovery and the Arbuckle is used for disposal of the more saline LKC PW. From the modeling results, it was found that if the mixture contains more than 20 % Arbuckle brine, the potential for scale formation is high. The pressure at the bottom of the formation might delay precipitation because calcite solubility increases slightly at high pressures.

Comparing the model predictions to experimental observations, it can be concluded that at a saturation index (SI) of >2 barium sulfate will be precipitated out of solution. The PHREEQC and Pitzer databases used for modeling in this study yield very similar results in terms of their predictions of the barite SI and amount of barium precipitated. However, the model is likely to overpredict the amount of barium precipitated when the SI for barite is <2. Also, the potential to precipitate gypsum, even at low SIs of +0.09 and +0.37 using the Pitzer and PHREEQC databases, respectively, is significant, although the model is expected to overestimate the amount of gypsum precipitated at this saturation state (i.e., SI <2). The activity corrections for the divalent cations at ionic strengths above 3 M are questionable for both the PHREEQC and Pitzer databases, so their used should be limited to solutions with an ionic strength less than or equal to 3 M.

An investigation carried out as part of this work showed a direct correlation between added NaCl and measured pH values. Sodium chloride addition drove down the measured pH values,

indicating that the solution was becoming more acidic. This trend was also found using PHREEQC, with the PHREEQC database, but the predicted decreases in pH were not as great as those observed in the experimental work.

5.2 Recommendations for future work

The following are recommended works that need to be completed to give a fuller understanding of the work described herein:

- PW samples from both the Arbuckle and LKC producing areas listed in Thompson's[5] study (2018) should be collected, analyzed, and remodeled using the PHREEQC software, as the produced water composition of a field may vary over time.
- The experiments should be repeated with actual produced water samples to more clearly understand the role of organic compounds on the scaling tendencies of some of the potential scale-forming minerals.
- The economics of brine exchange should be investigated and compared to other alternatives. This would serve as a guide to stakeholders in the water management sector on the financial feasibility and the scenarios in which this type of management scheme works best relative to the other alternatives available.
- The effect of background salts on pH measurement should be further investigated to shed more light on how individual ions collectively or singularly affect pH measurements, and how best to correctly measure pH in high strength brines.

5.3 Engineering applications

The results of this work can be applied to solve scaling problems that arise as a result of mixing of incompatible fluids for brine exchange, enhanced oil recovery applications (such as low salinity waterflooding), or discharges of PW to a saline environment (such as an ocean outfall). It can also be applied generally to predict if mixing brine solutions or altering their composition would cause scale formation. The PHREEQC modeling software is used by many to simulate geochemical reactions; understanding its capabilities to accurately model highly saline solutions are pertinent if PW is to be managed through brine exchange.

References

(1) Veil, J. A.; Puder, M. G.; Elcock, D.; Redweik Jr, R. J. *A white paper describing produced water from production of crude oil, natural gas, and coal bed methane*; Argonne National Lab, Illinois, U.S., 2004.

(2) Kansas Corporation Commission, Injection Wells: Frequently Asked Questions http://kcc.ks.gov/oil-gas/injection-wells-frequently-asked-questions (accessed Jun 5, 2019).

(3) Kansas Corporation Commission, Induced Seismicity http://kcc.ks.gov/oil-gas/induced-seismicity (accessed Jun 3, 2019).

(4) Xylem Incorporated. *Water use in oil and gas: trends in oil and gas production globally*; Charlotte, North Carolina, 2015.

(5) Thompson, S. L. Simulation of produced brine water exchange between Kansas Arbuckle and Lansing-Kansas City Formations, M.S. Thesis, Department of Chemical and Petroleum Engineering, University of Kansas, Lawrence Kansas, 2018.

(6) Kenny, J. F.; Barber, N. L.; Hutson, S. S.; Linsey, K. S.; Lovelace, J. K.; Maupin, M. A. Estimated use of water in the united states in 2005. Circular 1344, U.S Geological Survey, Reston, Virginia, 2009.

(7) Murray, K. E. State-scale perspective on water use and production associated with oil and gas operations, Oklahoma, U.S. *Environ. Sci. Technol.* **2013**, *47* (9), 4918–4925. https://doi.org/10.1021/es4000593.

(8) Boschee, P. Produced and flowback water recycling and reuse: economics, limitations, and technology. *Oil Gas Facil.* **2014**, *3* (01), 16–21. https://doi.org/10.2118/0214-0016-OGF.

(9) Vengosh, A.; Jackson, R. B.; Warner, N.; Darrah, T. H.; Kondash, A. A critical review of the risks to water resources from unconventional shale gas development and hydraulic fracturing in the United States. *Environ. Sci. Technol.* **2014**, *48* (15), 8334–8348. https://doi.org/10.1021/es405118y.

(10) Fakhru'l-Razi, A.; Pendashteh, A.; Abdullah, L. C.; Biak, D. R. A.; Madaeni, S. S.; Abidin, Z. Z. Review of technologies for oil and gas produced water treatment. *J. Hazard. Mater.* **2009**, *170* (2–3), 530–551. https://doi.org/10.1016/j.jhazmat.2009.05.044.

(11) Reynolds, R. R.; Kiker, R. D. *Produced water and associated issues*; Oklahoma Geological Survey, 2003.

(12) Dal, F.; Benoit; Michael, S. Global onshore and offshore water production. In *Oil and Gas Review, OTC edition*; 2007.

(13) Clark, C. E.; Veil, J. A. *Produced water volumes and management practices in the United States.*; Argonne, IL (United States), 2009. https://doi.org/10.2172/1007397.

(14) Azetsu-Scott, K.; Yeats, P.; Wohlgeschaffen, G.; Dalziel, J.; Niven, S.; Lee, K. Precipitation of heavy metals in produced water: influence on contaminant transport and

toxicity. *Mar. Environ. Res.* **2007**, *63* (2), 146–167. https://doi.org/10.1016/j.marenvres.2006.08.001.

(15) Kaur, G.; Mandal, A. K.; Nihlani, M. C.; Lal, B. Control of sulfidogenic bacteria in produced water from the kathloni oilfield in northeast india. *Int. Biodeterior. Biodegradation* **2009**, *63* (2), 151–155. https://doi.org/10.1016/j.ibiod.2008.07.008.

(16) Igunnu, E. T.; Chen, G. Z. Produced water treatment technologies. *Int. J. Low-Carbon Technol.* **2014**, *9* (3), 157–177. https://doi.org/10.1093/ijlct/cts049.

(17) Hansen, B. R.; Davies, S. R. Review of potential ,technologies for the removal of dissolved components from produced water. *Chem. Eng. Res. Des.* **1994**, *72* (A2), 176–188.

(18) Jacobs, R.; Grant, R.; Kwant, J.; Water, J. M. The composition of produced water from shell operated oil and gas production in the north sea. In *Produced Water*, Ray, J.P., Engelhardt, F.R., eds.; Springer, Boston, MA, 1992; pp 13–21.

(19) Neff, J. M. *Bioaccumulation in Marine Organisms: Effect of Contaminants from Oil Well Produced Water*; Elsevier, 2002.

(20) Zhang, T.; Gregory, K.; Hammack, R. W.; Vidic, R. D. Co-precipitation of radium with barium and strontium sulfate and its impact on the fate of radium during treatment of produced water from unconventional gas extraction. *Environ. Sci. Technol.* **2014**, *48* (8), 4596–4603. https://doi.org/10.1021/es405168b.

(21) Stephenson, M. T. A survey of produced water studies. In *Produced Water, Ray, J.P., Engelhardt, F.R., eds.*; Springer US: Boston, MA, 1992; pp 1–11. https://doi.org/10.1007/978-1-4615-2902-6_1.

(22) Vegueria, S. J.; Godoy, J. M.; Miekeley, N. Environmental impact studies of barium and radium discharges by produced waters from the “Bacia de Campos” oil-field offshore platforms, Brazil. *J. Environ. Radioact.* **2002**, *62* (1), 29–38. https://doi.org/10.1016/S0265-931X(01)00148-5.

(23) Ekins, P.; Vanner, R.; Firebrace, J. Zero emissions of oil in water from offshore oil and gas installations: economic and environmental implications. *J. Clean. Prod.* **2007**, *15* (13–14), 1302–1315. https://doi.org/10.1016/j.jclepro.2006.07.014.

(24) Bostick, D. T. *Characterization of soluble organics in produced water*; No. ORNL/TM-2001/78.Oak Ridge National Laboratory (ORNL): Oak Ridge, TN (United States), 2002; Vol. 27. https://doi.org/10.2172/814231.

(25) Stringfellow, W. T.; Domen, J. K.; Camarillo, M. K.; Sandelin, W. L.; Borglin, S. Physical, chemical, and biological characteristics of compounds used in hydraulic fracturing. *J. Hazard. Mater.* **2014**, *275*, 37–54. https://doi.org/10.1016/j.jhazmat.2014.04.040.

(26) Nagashio, D.; Tsuda, I.; Mayahashi, T.; Michishita, K.; Hanamoto, T. Development of sustainable operational technologies of the water treatment plant for stable water supply. *J. Water Supply Res. Technol.* **2010**, *59* (6–7), 392–399. https://doi.org/10.2166/aqua.2010.004.

(27) Boysen, D. B.; Boysen, J. E.; Boysen, J. A.; B.C Technologies, L. Creative strategies for produced water disposal in the rocky mountain region. *9th Annu. Integr. Environ. Pet. Consortium, Albuquerque* **2002**.

(28) Veil, J.; Clark, C. Produced water volume estimates and management practices. *SPE Prod. Oper.* **2011**, *26* (03), 234–239. https://doi.org/10.2118/125999-PA.

(29) Veil, J. A. US produced water volumes and management practices in 2012; Groundwater Protection Council, 2015.

(30) Jiménez, S.; Micó, M. M.; Arnaldos, M.; Medina, F.; Contreras, S. State of the art of produced water treatment. *Chemosphere*. 2018. https://doi.org/10.1016/j.chemosphere.2017.10.139.

(31) Asano, T.; Burton, F. L.; Leverenz, H.; Tsuchihashi, R.; Tchobanoglous, G. Metcalf & Eddy's *Water Reuse: Issues, Technologies, and Applications*; McGraw-Hill, New York, 2007.

(32) Fipps, G. Irrigation Water Quality Standards and Salinity Management Strategies. Texas AgriLife Extension Service, The Texas A&M System, 2003.

(33) Ayers, R. S.; Westcot, D. W. *Water quality for agriculture*; Vol. 29. Rome: Food and Agriculture Organization of the United Nations, 1985. https://doi.org/ISBN 92-5-102263-1.

(34) Carvalho, M. S.; Clarisse, M. D.; Lucas, E. F.; Barbosa, C. C. R.; Barbosa, L. C. F. Evaluation of the polymeric materials (dvb copolymers) for produced water treatment. In *Abu Dhabi International Petroleum Exhibition and Conference*; Society of Petroleum Engineers, 2002. https://doi.org/10.2118/78585-MS.

(35) Doyle, D.; Brown, A. Produced water treatment and hydrocarbon removal with organoclay. In *PE Annual Technical Conference and Exhibition*; Society of Petroleum Engineers, 2000.

(36) Al-Shalabi, E. W.; Sepehrnoori, K. A comprehensive review of low salinity/engineered water injections and their applications in sandstone and carbonate rocks. *J. Pet. Sci. Eng.* **2016**, *139*, 137–161. https://doi.org/10.1016/j.petrol.2015.11.027.

(37) Adewumi, M. A.; Erb, J. E.; Watson, R. W. Initial design considerations for a cost effective treatment of stripper oil well produced water. In *Produced Water*, Ray, J.P., Engelhardt, F.R., eds.; Springer US: Boston, MA, 1992; pp 511–522. https://doi.org/10.1007/978-1-4615-2902-6_40.

(38) Velmurugan, V.; Srithar, K. Prospects and scopes of solar pond: a detailed review. *Renew. Sustain. Energy Rev.* **2008**, *12* (8), 2253–2263. https://doi.org/10.1016/j.rser.2007.03.011.

(39) ALL Consulting, *Handbook on Coal Bed Methane Produced Water: Management and Beneficial Use Alternatives*; ALL Consulting, Tulsa, Oklahoma, 2003.

(40) Casaday, A. L. Advances in flotation unit design for produced water treatment. In *SPE Production Operations Symposium*; Society of Petroleum Engineers, 1993. https://doi.org/10.2118/25472-MS.

(41) Çakmakce, M.; Kayaalp, N.; Koyuncu, I. Desalination of produced water from oil production fields by membrane processes. *Desalination* **2008**, *222* (1–3), 176–186. https://doi.org/10.1016/j.desal.2007.01.147.

(42) Sirivedhin, T.; McCue, J.; Dallbauman, L. Reclaiming produced water for beneficial use: salt removal by electrodialysis. *J. Memb. Sci.* **2004**, *243* (1–2), 335–343. https://doi.org/10.1016/j.memsci.2004.06.038.

(43) Drewes, J.; Cath, T.; Xu, P.; Graydon, J. An integrated framework for treatment and management of produced water; 2009. *RPSEA Project, 07122-12*

(44) Li, Y. S.; Yan, L.; Xiang, C. B.; Hong, L. J. Treatment of oily wastewater by organic-inorganic composite tubular ultrafiltration (uf) membranes. *Desalination* **2006**. https://doi.org/10.1016/j.desal.2005.11.021.

(45) Bilstad, T.; Espedal, E. Membrane separation of produced water. *Water Sci. Technol.* **1996**, *34* (9), 239–246. https://doi.org/10.1016/S0273-1223(96)00810-4.

(46) Mitchell, R. W.; Grist, D. M.; Boyle, M. J. Chemical treatments associated with north sea projects. *J. Pet. Technol.* **2007**, *32* (05), 904–912. https://doi.org/10.2118/7880-pa.

(47) El-Hattab, M. I. GUPCO's experience in treating Gulf of Suez seawater for waterflooding the El Morgan oil field. *J. Pet. Technol.* **1982**, *34* (07), 1449–1460. https://doi.org/10.2118/10090-PA.

(48) Kan, A.; Tomson, M. Scale prediction for oil and gas production. *SPE J.* **2012**, *17* (02), 362–378. https://doi.org/10.2118/132237-PA.

(49) Kharaka, Y.; Gunter, W.; Aggarwal, P.K.; Perkins E. H.; DeBraal, J. D. *SOLMINEQ. 88:* A computer program for geochemical modeling of water-rock interactions. *Water-Resources Investigation Reports 88:* **1988***, (4227) 420.*

(50) Kharaka, Y. K., Gunter, W. D., Aggarwal, P. K., Perkins, E. H., & DeBraal, J. D. A computer program for geochemical modeling of water-rock reaction; *USGS Water Resources Investigation, Menlo Park, CA, USA* **1988***: 420-423.*

(51) Shen, D.; Fu, G.; Al-Saiari, H. A.; Kan, A. T.; Tomson, M. B. Barite dissolution/precipitation kinetics in porous media and in the presence and absence of a common scale inhibitor. *SPE J.* **2009**, *14* (03), 462–471. https://doi.org/10.2118/114062-pa.

(52) Yilmaz, I. Gypsum/anhydrite: some engineering problems. *Bull. Eng. Geol. Environ.* **2001**, *60* (3), 227–230. https://doi.org/10.1007/s100640000071.

(53) Klimchouk, A. The dissolution and conversion of gypsum and anhydrite. *Int. J. Speleol.* **1996**, *25* (3), 2

(54) Lu, H.; Kan, A. T.; Tomson, M. B. Effects of monoethylene glycol on carbonate equilibrium and calcite solubility in gas/monoethylene glycol/nacl/water mixed systems. *SPE J.* **2010**, *15* (03), 714–725. https://doi.org/10.2118/121562-PA.

(55) Kan, A. T.; Fu, G.; Tomson, M. B. Effect of methanol and ethylene glycol on sulfates and

halite scale formation. *Ind. Eng. Chem. Res.* **2003**, *42* (11), 2399–2408. https://doi.org/10.1021/ie020724e.

(56) Kan, A. T.; Fu, G.; Tomson, M. B. Effect of methanol on carbonate equilibrium and calcite solubility in a gas/methanol/water/salt mixed system. *Langmuir* **2002**, *18* (25), 9713–9725. https://doi.org/10.1021/la025620n.

(57) Siever, R. Silica solubility, 0°-200° C., and the diagenesis of siliceous sediments. *J. Geol.* **1962**, *70* (2), 127–150. https://doi.org/10.1086/626804.

(58) Kashpura VN; Potapov VV. Study of the amorphous silica scales formation at the mutnovskoe hydrothermal field. In *Proceedings of Twenty-Fifth Workshop on Geothermal Reservoir Engineering*; Stanford University, Stanford, California, 2000; pp 381–387.

(59) Zengler, D. H.; Dunham, J. D.; Ethington, R. L. (eds.). Concepts and models of dolomitization; Society of Economic Paleontologists and Mineralogists,Tulsa, OK, 1980.

(60) Deelman, J. Low-temperature nucleation of magnesite and dolomite. *Neues Jahrb. Fur Mineral. Monatshefte* **1999**, *289–302*.

(61) Lippman, F. *Sedimentary Carbonate Minerals*; New York, Springer Verlag, 1973.

(62) Van Lith, Y.; Warthmann, R.; Vasconcelos, C.; Mckenzie, J. A. Sulphate-reducing bacteria induce low-temperature Ca-dolomite and high Mg-calcite formation. *Geobiology* **2003**, *1* (1), 71–79. https://doi.org/10.1046/j.1472-4669.2003.00003.x.

(63) Vasconcelos, C.; McKenzie, J. A.; Bernasconi, S.; Grujic, D.; Tiens, A. J. Microbial mediation as a possible mechanism for natural dolomite formation at low temperatures. *Nature* **1995**, *377* (6546), 220–222. https://doi.org/10.1038/377220a0.

(64) Sánchez-Román, M.; McKenzie, J. A.; de Luca Rebello Wagener, A.; Rivadeneyra, M. A.; Vasconcelos, C. Presence of sulfate does not inhibit low-temperature dolomite precipitation. *Earth Planet. Sci. Lett.* **2009**, *285* (1–2), 131–139. https://doi.org/10.1016/j.epsl.2009.06.003.

(65) Kleinitz, W.; Dietzsch, G.; Köhler, M. Halite scale formation in gas-producing wells. *Chem. Eng. Res. Des.* **2003**, *81* (3), 352–358. https://doi.org/10.1205/02638760360596900.

(66) Pitzer, K. S.; Peiper, J. C.; Busey, R. H. Thermodynamic properties of aqueous sodium chloride solutions. *J. Phys. Chem. Ref. Data* **1984**, *13* (1), 1–102. https://doi.org/10.1063/1.555709.

(67) Andritsos, N.; Karabelas, A. J. Sulfide scale formation and control: the case of lead sulfide. *Geothermics* **1991**, *20* (5–6), 343–353. https://doi.org/10.1016/0375-6505(91)90025-Q.

(68) Oganov, A. R.; Glass, C. W.; Ono, S. High-pressure phases of $CaCO_3$: crystal structure prediction and experiment. *Earth Planet. Sci. Lett.* **2006**, *241* (1–2), 95–103. https://doi.org/10.1016/j.epsl.2005.10.014.

(69) Sawada, K. The mechanisms of crystallization and transformation of calcium carbonates.

Pure Appl. Chem. **1997**, *69* (5), 921–928. https://doi.org/10.1351/pac199769050921.

(70) Addadi, L.; Raz, S.; Weiner, S. Taking advantage of disorder: amorphous calcium carbonate and its roles in biomineralization. *Adv. Mater.* **2003**, *15* (12), 959–970. https://doi.org/10.1002/adma.200300381.

(71) de Leeuw, N. H.; Parker, S. C. Surface structure and morphology of calcium carbonate polymorphs calcite, aragonite, and vaterite: an atomistic approach. *J. Phys. Chem. B* **1998**, *102* (16), 2914–2922. https://doi.org/10.1021/jp973210f.

(72) Rodriguez-Blanco, J. D.; Shaw, S.; Benning, L. G. The kinetics and mechanisms of amorphous calcium carbonate (ACC) crystallization to calcite, via vaterite. *Nanoscale* **2011**, *3* (1), 265–271. https://doi.org/10.1039/C0NR00589D.

(73) Austad, T.; Shariatpanahi, S. F.; Strand, S.; Aksulu, H.; Puntervold, T. Low salinity EOR effects in limestone reservoir cores containing anhydrite: a discussion of the chemical mechanism. *Energy & Fuels* **2015**, *29* (11), 6903–6911. https://doi.org/10.1021/acs.energyfuels.5b01099.

(74) Alameri, W.; Teklu, T. W.; Graves, R. M.; Kazemi, H.; AlSumaiti, A. M. Experimental and numerical modeling of low-salinity waterflood in a low permeability carbonate reservoir. In *SPE Western Regional Meeting*; Society of Petroleum Engineers, 2015. https://doi.org/10.2118/174001-MS.

(75) Mohanty, K. K.; Chandrasekhar, S. Wettability alteration with brine composition in high temperature carbonate reservoirs. In *SPE Annual Technical Conference and Exhibition*; Society of Petroleum Engineers, 2016. https://doi.org/10.2118/166280-MS.

(76) Gomari, K. A. R.; Hamouda, A. A.; Denoyel, R. Influence of sulfate ions on the interaction between fatty acids and calcite surface. *Colloids Surfaces A Physicochem. Eng. Asp.* **2006**, *287* (1–3), 29–35. https://doi.org/10.1016/j.colsurfa.2006.03.018.

(77) Tetteh, J. T.; Rankey, E.; Barati, R. Low salinity waterflooding effect: crude oil/brine interactions as a recovery mechanism in carbonate rocks. *OTC Bras.* **2017**. https://doi.org/10.4043/28023-MS.

(78) Tetteh, J. T.; Barati, R. Crude-oil/brine interaction as a recovery mechanism for low-salinity waterflooding of carbonate reservoirs. *SPE Reserv. Eval. Eng.* **2018**. https://doi.org/10.2118/194006-PA.

(79) Tetteh, J.; Janjang, N. M.; Barati, R. Wettability alteration and enhanced oil recovery using low salinity waterflooding in limestone rocks: a mechanistic study. *SPE Kingdom Saudi Arab. Annu. Tech. Symp. Exhib.* **2018**. https://doi.org/10.2118/192425-MS.

(80) Gupta, R.; Mohanty, K. K. Wettability alteration mechanism for oil recovery from fractured carbonate rocks. *Transp. Porous Media* **2011**, *87* (2), 635–652. https://doi.org/10.1007/s11242-010-9706-5.

(81) Leslie Zhang, D.; Liu, S.; Puerto, M.; Miller, C. A.; Hirasaki, G. J. Wettability alteration and spontaneous imbibition in oil-wet carbonate formations. *J. Pet. Sci. Eng.* **2006**, *52* (1–4), 213–226. https://doi.org/10.1016/j.petrol.2006.03.009.

(82) Rezaei Gomari, K. A.; Denoyel, R.; Hamouda, A. A. Wettability of calcite and mica modified by different long-chain fatty acids (C18 acids). *J. Colloid Interface Sci.* **2006**, *297* (2), 470–479. https://doi.org/10.1016/j.jcis.2005.11.036.

(83) Zhang, P.; Tweheyo, M. T.; Austad, T. Wettability alteration and improved oil recovery in chalk: the effect of calcium in the presence of sulfate. *Energy and Fuels* **2006**, *20* (5), 2056–2062. https://doi.org/10.1021/ef0600816.

(84) Austad, T.; Strand, S.; Høgnesen, E. J.; Zhang, P. Seawater as IOR fluid in fractured chalk. In *SPE International Symposium on Oilfield Chemistry*; Society of Petroleum Engineers, 2005. https://doi.org/10.2118/93000-MS.

(85) Zhang, P.; Tweheyo, M. T.; Austad, T. Wettability alteration and improved oil recovery by spontaneous imbibition of seawater into chalk: impact of the potential determining ions Ca2+, Mg2+, and SO42-. *Colloids and Surfaces A: Physicochemical and Engineering Aspects*.. **2007**, *301* (1–3), 199–208. https://doi.org/10.1016/j.colsurfa.2006.12.058.

(86) Strand, S.; Høgnesen, E. J.; Austad, T. Wettability alteration of carbonates - effects of potential determining ions (ca2+and so42-) and temperature. *Colloids and Surfaces A: Physicochemical and Engineering Aspects*. 2006, pp 1–10. https://doi.org/10.1016/j.colsurfa.2005.10.061.

(87) Strand, S.; Høgnesen, E. J.; Austad, T. Wettability alteration of carbonates—effects of potential determining ions (Ca^{2+} and SO_4^{2-}) and temperature. *Colloids and Surfaces A: Physicochemical and Engineering Aspects*.. **2006**, *275* (1–3), 1–10. https://doi.org/10.1016/j.colsurfa.2005.10.061.

(88) Maitland, G. Oil and gas production. *Curr. Opin. Colloid Interface Sci.* **2000**, *5* (5–6), 301–311. https://doi.org/10.1016/S1359-0294(00)00069-8.

(89) Yousef, A. A.; Al-Saleh, S. H.; Al-Kaabi, A.; Al-Jawfi, M. S. Laboratory investigation of the impact of injection-water salinity and ionic content on oil recovery from carbonate reservoirs. *SPE Reserv. Eval. Eng.* **2011**, *14* (05), 578–593. https://doi.org/10.2118/137634-PA.

(90) Aladasani, a; Bai, B.; Wu, Y.-S. Investigating low salinity waterflooding recovery mechanisms in carbonate reservoirs. In *SPE EOR Conference at Oil and Gas West Asia 2012 - EOR: Building Towards Sustainable Growth, OGWA*; 2012; Vol. 2, pp 797–817. https://doi.org/10.2118/155560-MS.

(91) Hirasaki, G. J. Wettability: fundamentals and surface forces. *SPE Form. Eval.* **1991**, *6* (02), 217–226. https://doi.org/10.2118/17367-PA.

(92) Brady, P. V.; Krumhansl, J. L.; Mariner, P. E. Surface complexation modeling for improved oil recovery. In *SPE Improved Oil Recovery Symposium*; Society of Petroleum Engineers, 2012. https://doi.org/10.2118/153744-MS.

(93) Strand, S.; Standnes, D. C.; Austad, T. Spontaneous imbibition of aqueous surfactant solutions into neutral to oil-wet carbonate cores: effects of brine salinity and composition. *Energy & Fuels* **2003**, *17* (5), 1133–1144. https://doi.org/10.1021/ef030051s.

(94) Strand, S.; Standnes, D. C.; Austad, T. Spontaneous imbibition of aqueous surfactant

solutions into neutral to oil-wet carbonate cores: effects of brine salinity and composition. *Energy and Fuels* **2003**. https://doi.org/10.1021/ef030051s.

(95) Hognesen, E. J.; Strand, S.; Austad, T. Waterflooding of preferential oil-wet carbonates: oil recovery related to reservoir temperature and brine composition. In *SPE Europec/EAGE Annual Conference*; 2005. https://doi.org/10.2118/94166-MS.

(96) Shalabi, E. W. Al; Sepehrnoori, K.; Delshad, M. Mechanisms behind low salinity water injection in carbonate reservoirs. *Fuel* **2014**, *121*, 11–19. https://doi.org/10.1016/j.fuel.2013.12.045.

(97) Al-Shalabi, E. W.; Sepehrnoori, K.; Delshad, M.; Pope, G. A novel method to model low-salinity-water injection in carbonate oil reservoirs. *SPE J.* **2015**, *20* (05), 1154–1166. https://doi.org/10.2118/169674-PA.

(98) Al-Shalabi, E. W.; Sepehrnoori, K.; Delshad, M. Simulation of wettability alteration by low-salinity water injection in waterflooded carbonate cores. *Pet. Sci. Technol.* **2015**, *33* (5), 604–613. https://doi.org/10.1080/10916466.2014.919005.

(99) Mahani, H.; Keya, A. L.; Berg, S.; Bartels, W.-B.; Nasralla, R.; Rossen, W. Driving mechanism of low salinity flooding in carbonate rocks. *Eur. 2015* **2015**, 210–236. https://doi.org/10.2118/174300-MS.

(100) Plummer, L. N.; Wigley, T. M. L.; Parkhurst, D. L. The kinetics of calcite dissolution in CO2-water systems at 5 degrees to 60 degrees C and 0.0 to 1.0 atm CO2. *Am. J. Sci.* **1978**, *278* (2), 179–216. https://doi.org/10.2475/ajs.278.2.179.

(101) Unwin, P. R.; Compton, R. G. Effect of carboxylic acids on the dissolution of calcite in aqueous solution. Part 3. Polymaleic Acid. *J. Chem. Soc. Faraday Trans.* **1990**, *86* (9), 1517. https://doi.org/10.1039/ft9908601517.

(102) Rickard, D. T.; Sjoberg, E. L. Mixed kinetic control of calcite dissolution rates. *Am. J. Sci.* **1983**, *283* (8), 815–830. https://doi.org/10.2475/ajs.283.8.815.

(103) Morse, J. W. Dissolution kinetics of calcium carbonate in sea water; III, a new method for the study of carbonate reaction kinetics. *Am. J. Sci.* **1974**, *274* (2), 97–107. https://doi.org/10.2475/ajs.274.2.97.

(104) Morse, J. W.; de Kanel, J.; Harris, K. Dissolution kinetics of calcium carbonate in seawater - 7. The dissolution kinetics of synthetic aragonite and pteropod tests. *Am J Sci* **1979**, *279* (5), 488–502. https://doi.org/10.2475/ajs.279.5.488.

(105) Plummer, N. L.; Busenberg, E.; Glynn, P. D.; Blum, A. E. Dissolution of aragonite-strontianite soild solutions in nonstoichiometric $Sr(HCO_3)_2$-$Ca(HCO_3)_2$-CO_2-H_2O solutions. *Geochim. Cosmochim. Acta* **1992**, *56*, 3045–3072. https://doi.org/10.1016/0016-7037(92)90289-U.

(106) Reddy, M. M.; Plummer, L. N.; Busenberg, E. Crystal growth of calcite from calcium bicarbonate solutions at constant PCO_2 and 25°C: a test of a calcite dissolution model. *Geochim. Cosmochim. Acta* **1981**, *45* (8), 1281–1289. https://doi.org/10.1016/0016-7037(81)90222-2.

(107) Busenberg, E.; Plummer, L. N. The kinetics of dissolution of dolomite in CO_2-H_2O systems at 1.5 to 65 degrees C and 0 to 1 atm Pco_2. *American Journal of Science*. 1982, pp 45–78. https://doi.org/10.2475/ajs.282.1.45.

(108) Zhang, Y.; Dawe, R. The kinetics of calcite precipitation from a high salinity water. *Appl. Geochemistry* **1998**, *13* (2), 177–184. https://doi.org/10.1016/S0883-2927(97)00061-9.

(109) Appelo, C.; Postma, D. Hydrogeochemical modeling with PHREEQC. In *Geochemistry, Groundwater and Pollution, Second Edition*; CRC Press, 2010. https://doi.org/10.1201/9781439833544.axa.

(110) Talman, S. J.; Wiwchar, B.; Gunter, W. D. Dissolution kinetics of calcite in the H_2O-CO_2 system along the steam saturation curve to 210 °C. *Fluid-Mineral Interact. A Tribut. to H. P. Eugster* **1990**, No. 2, 41–55.

(111) Chou, L.; Garrels, R. M.; Wollast, R. Comparative study of the kinetics and mechanisms of dissolution of carbonate minerals. *Chem. Geol.* **1989**, *78* (3–4), 269–282. https://doi.org/10.1016/0009-2541(89)90063-6.

(112) de Kanel, J.; Morse, J. W. The chemistry of orthophosphate uptake from seawater on to calcite and aragonite. *Geochim. Cosmochim. Acta* **1978**, *42* (9), 1335–1340. https://doi.org/10.1016/0016-7037(78)90038-8.

(113) Morse, J. W.; Arvidson, R. S. The dissolution kinetics of major sedimentary carbonate minerals. *Earth-Science Rev.* **2002**, *58* (1–2), 51–84. https://doi.org/10.1016/S0012-8252(01)00083-6.

(114) Walter, L. M.; Morse, J. W. The dissolution kinetics of shallow marine carbonates in seawater: a laboratory study. *Geochim. Cosmochim. Acta* **1985**, *49* (7), 1503–1513. https://doi.org/10.1016/0016-7037(85)90255-8.

(115) Keir, R. S. The dissolution kinetics of biogenic calcium carbonates in seawater. *Geochim. Cosmochim. Acta* **1980**, *44* (2), 241–252. https://doi.org/10.1016/0016-7037(80)90135-0.

(116) Nancollas, G.; Reddy MM. The crystallization of calcium carbonate. II: calcite growth mechanism. *J. Colloid Interface Sci.* **1971**, *824–30* (37(4)).

(117) Davies, C. W.; Jones, A. L. The precipitation of silver chloride from aqueous solutions. Part 2.—kinetics of growth of seed crystals. *Trans. Faraday Soc.* **1955**, *51*, 812–817. https://doi.org/10.1039/TF9555100812.

(118) Kaufmann, G.; Dreybrodt, W. Calcite dissolution kinetics in the system $CaCO_3$–H_2O–CO_2 at high undersaturation. *Geochim. Cosmochim. Acta* **2007**, *71* (6), 1398–1410. https://doi.org/10.1016/j.gca.2006.10.024.

(119) Berner, R. A. Sulfate reduction and the rate of deposition of marine sediments. *Earth Planet. Sci. Lett.* **1978**, *37* (3), 492–498. https://doi.org/10.1016/0012-821X(78)90065-1.

(120) Baumann, J.; Buhmann, D.; Dreybrodt, W.; Schulz, H. D. Calcite dissolution kinetics in porous media. *Chem. Geol.* **1985**, *53* (3–4), 219–228. https://doi.org/10.1016/0009-2541(85)90071-3.

(121) Baxter, E. F. Field measurement of slow metamorphic reaction rates at temperatures of 500° to 600°C. *Science* **2000**, *288* (5470), 1411–1414. https://doi.org/10.1126/science.288.5470.1411.

(122) Malmström, M. E.; Destouni, G.; Banwart, S. A.; Strömberg, B. H. E. Resolving the scale-dependence of mineral weathering rates. *Environ. Sci. Technol.* **2000**, *34* (7), 1375–1378. https://doi.org/10.1021/es990682u.

(123) Zhu, C.; Lu, P. Alkali feldspar dissolution and secondary mineral precipitation in batch systems: 3. Saturation states of product minerals and reaction paths. *Geochim. Cosmochim. Acta* **2009**, *73* (11), 3171–3200. https://doi.org/10.1016/j.gca.2009.03.015.

(124) Buhmann, D.; Dreybrodt, W. The kinetics of calcite dissolution and precipitation in geologically relevant situations of karst areas. *Chem. Geol.* **1985**, *53* (1–2), 109–124. https://doi.org/10.1016/0009-2541(85)90024-5.

(125) Sulpis, O.; Lix, C.; Mucci, A.; Boudreau, B. P. Calcite dissolution kinetics at the sediment-water interface in natural seawater. *Mar. Chem.* **2017**, *195*, 70–83. https://doi.org/10.1016/j.marchem.2017.06.005.

(126) Sjöberg, E. L.; Rickard, D. T. Calcite dissolution kinetics: surface speciation and the origin of the variable pH dependence. *Chem. Geol.* **1984**, *42* (1–4), 119–136. https://doi.org/10.1016/0009-2541(84)90009-3.

(127) Plummer, L. N.; Wigley, T. M. L. The Dissolution of Calcite in CO_2-Saturated Solutions at 25°C and 1 Atmosphere Total Pressure. *Geochim. Cosmochim. Acta* **1976**, *40* (2), 191–202. https://doi.org/10.1016/0016-7037(76)90176-9.

(128) Lund, K.; Fogler, H. S.; McCune, C. C.; Ault, J. W. Acidization-II. The dissolution of calcite in hydrochloric acid. *Chem. Eng. Sci.* **1975**, *30* (8), 825–835. https://doi.org/10.1016/0009-2509(75)80047-9.

(129) Morse, J. W.; Arvidson, R. S. The Dissolution Kinetics of Major Sedimentary Carbonate Minerals. *Earth-Science Rev.* **2002**, *58* (1–2), 51–84. https://doi.org/10.1016/S0012-8252(01)00083-6.

(130) Sjöberg, E. L. A Fundamental Equation for Calcite Dissolution Kinetics. *Geochim. Cosmochim. Acta* **1976**, *40* (4), 441–447. https://doi.org/10.1016/0016-7037(76)90009-0.

(131) Gutjahr, A.; Dabringhaus, H.; Lacmann, R. Studies of the growth and dissolution kinetics of the caco3 polymorphs calcite and aragonite II. The influence of divalent cation additives on the growth and dissolution rates. *J. Cryst. Growth* **1996**, *158* (3), 310–315. https://doi.org/10.1016/0022-0248(95)00447-5.

(132) Gledhill, D. K.; Morse, J. W. Calcite dissolution kinetics in Na–Ca–Mg–Cl brines. *Geochim. Cosmochim. Acta* **2006**, *70* (23), 5802–5813. https://doi.org/10.1016/j.gca.2006.03.024.

(133) Sjöberg, E. L. Kinetics and mechanism of calcite dissolution in aqueous solutions at low temperatures, Doctoral dissertation, Stockholm University, Faculty of Science, Almqvist & Wiksell, 1978.

(134) Buhmann, D.; Dreybrodt, W. Calcite dissolution kinetics in the system H_2O– CO_2–$CaCO_3$ with Participation of Foreign Ions. *Chem. Geol.* **1987**, *64* (1–2), 89–102. https://doi.org/10.1016/0009-2541(87)90154-9.

(135) Compton, R. G.; Brown, C. A. The inhibition of calcite dissolution/precipitation: Mg^{2+} cations. *J. Colloid Interface Sci.* **1994**, *165* (2), 445–449. https://doi.org/10.1006/jcis.1994.1248.

(136) Alkattan, M.; Oelkers, E. H.; Dandurand, J.-L.; Schott, J. An experimental study of calcite dissolution rates at acidic conditions and 25 °C in the presence of $NaPO_3$ and $MgCl_2$. *Chem. Geol.* **2002**, *190* (1–4), 291–302. https://doi.org/10.1016/S0009-2541(02)00121-3.

(137) Van Cappellen, P.; Charlet, L.; Stumm, W.; Wersin, P. A surface complexation model of the carbonate mineral-aqueous solution interface. *Geochim. Cosmochim. Acta* **1993**, *57* (15), 3505–3518. https://doi.org/10.1016/0016-7037(93)90135-J.

(138) Pokrovsky, O. S.; Schott, J. Surface chemistry and dissolution kinetics of divalent metal carbonates. *Environ. Sci. Technol.* **2002**, *36* (3), 426–432. https://doi.org/10.1021/es010925u.

(139) Brezonik, P. L.; Arnold, W. A. *Water Chemistry*; Oxford University Press: New York, 2011.

(140) Finneran, D. W.; Morse, J. W. Calcite dissolution kinetics in saline waters. *Chem. Geol.* **2009**, *268* (1–2), 137–146. https://doi.org/10.1016/j.chemgeo.2009.08.006.

(141) Zuddas, P.; Mucci, A. Kinetics of calcite precipitation from seawater: ii. the influence of the ionic strength. *Geochim. Cosmochim. Acta* **1998**, *62* (5), 757–766. https://doi.org/10.1016/S0016-7037(98)00026-X.

(142) Pokrovsky, O. S.; Golubev, S. V.; Schott, J. Dissolution kinetics of calcite, dolomite and magnesite at 25 °C and 0 to 50 atm P_{CO2}. *Chem. Geol.* **2005**, *217* (3–4), 239–255. https://doi.org/10.1016/j.chemgeo.2004.12.012.

(143) Civan, F. *Reservoir Formation Damage*; Gulf Professional Publishing, 2015.

(144) Bishop, S. R. The experimental investigation of formation damage due to the induced flocculation of clays within a sandstone pore structure by a high salinity brine. In *SPE European Formation Damage Conference*; Society of Petroleum Engineers, 1997. https://doi.org/10.2118/38156-MS.

(145) The Geochemist's Workbench® Online Academy: High salinity fluids https://academy.gwb.com/high_salinity.php#REFERENCES (accessed May 8, 2019).

(146) Kim, H. T.; Frederick, W. J. Evaluation of Pitzer ion interaction parameters of aqueous mixed electrolyte solutions at 25 °C. 2. Ternary mixing parameters. *J. Chem. Eng. Data* **1988**, *33* (3), 278–283. https://doi.org/10.1021/je00053a017.

(147) Harvie, C. E.; Møller, N.; Weare, J. H. The prediction of mineral solubilities in natural waters: The Na-K-Mg–Ca–H–Cl–SO_4–OH–HCO_3–CO_3–CO_2–H_2O System to high ionic strengths at 25°C. *Geochim. Cosmochim. Acta* **1984**, *48* (4), 723–751. https://doi.org/10.1016/0016-7037(84)90098-X.

(148) Newell, K.; Watney, W.; Cheng, W.; Brownrigg, R. *Stratigraphic and spatial distribution of oil and gas production in Kansas*. Subsurface Geology Series 9, Kansas Geological Survey, Lawrence, Kansas, **1987**.

(149) Baars, D. L.; Watney, W. L. Paleotectonic control of reservoir facies. *Kansas Geol. Surv. Bull.* **1991**, *233*, 253–262.

(150) Mccool, S.; Walton, T.; Willhite, P.; Ahmed, S.; Liu, Z.; Zhang, W.; Senior, P. Oil & natural gas technology and independent oil producers; University of Kansas Center for Research, Inc., Lawrence, KS, 2012.

(151) Wilson, J. L; Fritz, R.D; Medlock, P. L. The Arbuckle Group—Relationship of core and outcrop analyses to cyclic stratigraphy and correlation. In *Arbuckle core workshop and field trip: Oklahoma Geological Survey Special Publication*; 1991; Vol. 3, pp 133–144.

(152) Ross Jr., R. J. Ordovician paleogeography of the western united states. In P*acific coast paleogeography symposium 1, Paleozoic paleogeography of the western United States*; 1977; pp 19–38.

(153) Franseen, E. K.; Byrnes, A. P.; Cansler, J. R.; Steinhauff, D. M.; Carr, T. R. The geology of Kansas - Arbuckle Group. *Kansas Geol. Surv. Earth Sci. Bull.* **2004**, *250* (part 2), 1–43.

(154) Watney, W. L. Cyclic Sedimentation of the Lansing-Kansas City Groups in Northwestern Kansas and Southwestern Nebraska. *Kansas Geol. Surv. Bull.* **1980**, No. 220, 70.

(155) McIntire, M. C. Rare earth elements (REE) in crude oil in the Lansing-Kansas City formations in central Kansas: potential indications about their sources, locally derived or long-distance derived. Doctoral dissertation, Department of Geology, Kansas State University, Manhattan, Kansas, 2014.

(156) Christiano, A. W.; Ali, H. A mineralogical and geochemical characterization of late Cambrian – Pennsylvanian carbonates in the central Kansas uplift, Kansas, with implications for diagenesis. In *GSA Annual Meeting in Denver, Implications for Diagenesis*; Geological Society of America: Denver, Colorado, 2016. https://doi.org/10.1130/abs/2016AM-282043.

(157) Parkhurst, D. L.; Appelo, C. A. J. Description of input and examples for PHREEQC (Version 3)-A computer program for speciation, batch-reaction, one-dimensional transport, and inverse geochemical calculations. US Geological Survey. 2013. https://doi.org/Rep. 99-4259.

(158) Pitzer, K. S. Thermodynamics of electrolytes. I. theoretical basis and general equations. *J. Phys. Chem.* **1973**, *77* (2), 268–277. https://doi.org/10.1021/j100621a026.

(159) Pabalan, R. T.; Pitzer, K. S. Thermodynamics of concentrated electrolyte mixtures and the prediction of mineral solubilities to high temperatures for mixtures in the system Na-K-Mg-Cl-SO_4-OH-H_2O. *Mol. Struct. Stat. Thermodyn. Sel. Pap. Kenneth S Pitzer* **1993**, 461–474. https://doi.org/10.1142/9789812795960_0065

(160) de Moel, P. J.; van der Helm, A. W. C.; van Rijn, M.; van Dijk, J. C.; van der Meer, W. G. J. Assessment of calculation methods for calcium carbonate saturation in drinking water for DIN 38404-10 Compliance. *Drink. Water Eng. Sci.* **2013**, *6* (2), 115–124.

https://doi.org/10.5194/dwes-6-115-2013.

(161) He, C.; Li, M.; Liu, W.; Barbot, E.; Vidic, R. D. Kinetics and equilibrium of barium and strontium sulfate formation in Marcellus shale flowback water. *J. Environ. Eng.* **2014**, *140* (5), B4014001. https://doi.org/10.1061/(ASCE)EE.1943-7870.0000807.

(162) van der Leeden, M. C.; van Rosmalen, G. M. Adsorption behavior of polyelectrolytes on barium sulfate crystals. *J. Colloid Interface Sci.* **1995**. https://doi.org/10.1006/jcis.1995.1160.

(163) Jones, F.; Piana, S.; Gale, J. D. Understanding the kinetics of barium sulfate precipitation from water and water–methanol solutions. *Cryst. Growth Des.* **2008**, *8* (3), 817–822. https://doi.org/10.1021/cg070110i.

(164) Hamdona, S. K.; Hamza, S. M.; Mangood, A. H. The influence of polyphosphonates on the precipitation of strontium sulfate (celestite) from aqueous solutions. *Desalin. Water Treat.* **2010**, *24* (1–3), 55–60. https://doi.org/10.5004/dwt.2010.1176.

(165) Den Ouden, L. Calcite dissolution behaviour during low salinity water flooding in carbonate rock, M.S. Thesis, Geoscience & Engineering, Delft University of Technology, The Netherlands, 2014.

(166) Dreybrodt, W.; Lauckner, J.; Zaihua, L.; Svensson, U.; Buhmann, D. The kinetics of the reaction $CO_2 + H_2O \rightarrow H^+ + HCO_3^-$ as one of the rate limiting steps for the dissolution of calcite in the system H_2O-CO_2-$CaCO_3$. *Geochim. Cosmochim. Acta* **1996**, *60* (18), 3375–3381. https://doi.org/10.1016/0016-7037(96)00181-0.

Appendix

Table 4: Recipe for synthetic brine preparation in 500 ml of deionized water

Salt	Molecular weight	Required amount of salt for LKC brine (mg)	Required amount of salt for Arbuckle brine (mg)	Required amount of salt for DC brine (mg)	Required amount of salt for RC brine (mg)
$CaCl_2 \cdot 2H_20$	147	20175	3852	1339	16874
$MgCl_2 \cdot 6H_20$	203	11710	3137	1297	10456
$BaCl_2 \cdot 2H_20$	244	0	0	418	3
$SrCl_2 \cdot 2H_20$	267	0	0	137	2891
NaCl	58	60852	28529	12048	45656
KCl	75	381	200	122	381
Na_2SO_4	142	192	339	0	74
$NaHCO_3$	84	0	136	586	58

Table 5: Recipe for salts added to 50 ml of 2 % nitric acid solution for preparing standards for calibrating the ICP instrument

Salts	Background Chloride 6000 mg/l	Background Chloride 26,000 mg/l	Background chloride 53,000 mg/l
$CaCl_2 \cdot 2H_20$	183.4	183.4	183.4
$MgCl_2 \cdot 6H_20$	418.2	418.2	418.2
$BaCl_2 \cdot 2H_20$	88.9	88.9	88.9
$SrCl_2 \cdot 2H_20$	152	152	152
NaCl	0	1678	3915

Table 6: Slopes of the measured ion concentrations as shown in Figure 23 to 26

Background chloride (mg/l)	Slope for magnesium	Slope for calcium	Slope for strontium	Slope for barium
6,000	11,815	64,569	2,626,601	2,554,393
26,000	12,598	68,347	2,724,330	2,724,330
53,000	12,110	71,263	2,971,400	1,464,308
Base standard	14,256	85,003	3,240,640	3,166,015

Table 7: Percentage of species in the carbonate system, estimated using the Pitzer database, when the RC brine is modified by changing the NaCl concentration to increase salinity

Species	1M	1.5M	2M	3M
HCO_3^-	82.3	84.4	86.2	88.7
CO_2	16.3	14.0	11.9	8.6
CO_3^{2-}	0.98	1.1	1.2	1.6
$MgCO_3^0$	0.5	0.5	0.6	1.2

Table 8: Percentage of species in the carbonate system, estimated using the PHREEQC database, when the RC brine is modified by changing the NaCl concentration to increase salinity

Species	1M	1.5M	2M	3M
HCO_3^-	41.4	37.58	33.0	23
$CaHCO_3^+$	30.4	30.7	31.8	35
$MgHCO_3^+$	17.1	18.61	20.7	27
CO_2	6.7	5.3	4.0	2
$NaHCO_3^+$	0	3.7	6.0	9
$SrHCO_3^+$	3.4%	3.2	3.2	3
CO_3^{2-}	<1%	<1%	<1%	<1%

Table 9: Percentage of species in the total sulfate system, estimated using the PHREEQC database, when the RC brine is modified by changing the NaCl concentration to increase salinity

Species	1M	1.5M	2M	3M
$CaSO_4^+$	37.6	30.5	25.4	18.0
SO_4^{2-}	31.3	31.0	29.0	23.4
$MgSO_4^0$	27.0	23.3	20.5	16.9
$SrSO_4^0$	3.7	28.5	2.2	1.4
$NaSO_4^-$	<1%	12%	22.9	40.1

Table 10: Change in Ca^{2+} concentration at 24 h and 30 d using reagent grade $CaCO_3$

Brine	Chane in calcium concentration after 24 h (mg/l)	Chane in calcium concentration after 30 d (mg/l)
82x LKC	8.03	7.15
5x LKC	-85.6	-19.5
LKC	-86	-45.33

Table 11: Activity coefficients estimated using the two databases when the RC brine is modified by changing the NaCl concentration

	PHREEQC	PITZER
% of free Ca2+ ion	99.62	100
activity coefficient	0.248	0.252
Ionic strength(M)	1	1
% of free Mg^{2+} ion	99.99	99.99
activity	0.3	0.28
Ionic strength	1	1
% of free Ba^{2+} ion	99.55	100
activity coefficient	0.18	0.23
Ionic strength	1	1
% of free Sr^{2+} ion	99.6	100
activity coefficient	0.23	0.25
Ionic strength	1	1
% of free Ca^{2+} ion	99.71	100
activity coefficient	0.45	0.68
Ionic strength(M)	3	3
% of free Mg^{2+} ion	99.51	100
activity	0.709	0.867
Ionic strength	3	3
% of free Ba^{2+} ion	99.81	100
activity coefficient	0.28	0.46
Ionic strength	3	3
% of free Sr^{2+} ion	99.73	100
activity coefficient	0.34	0.54
Ionic strength	3	3

Table 12*:* Change in concentration between the initial and final measurements for cations in the 80:20 DC:RC brine mixture

Ion	ICP measurement (mg/l)	Calculated concentration (mg/l)	Change in concentration (mg/l)	STD* (mg/l)
Mg	765	786	20	4.2
Ca	2454	2401	-53	37.1
Sr	445	464	20	0.4
Ba	369	370	1	2.1

* STD = standard measurement error (as determined by the ICP instrument software)

Note: A dilution factor of 500 was used to convert the concentration measured using ICP into the concentration reported in the table.

Table 13: Change in concentration between the initial and final measurements for cations in the 50:50 DC:RC brine mixture

Ion	ICP measurement (mg/l)	Calculated concentration (mg/l)	Change in concentration (mg/l)	STD (mg/l)
Mg	1463	1462	-1	34.2
Ca	4991	5074	83	108.9
Sr	958	1028	70	22.5
Ba	227	233	5	3.5

Note: A dilution factor of 500 was used to convert the concentration measured using ICP into the concentration reported in the table.

Table 14: Change in concentration between the initial and final measurements for cations in the 20:80 DC:RC brine mixture

Ion	ICP measurement (mg/l)	Calculated concentration (mg/l)	Change in concentration (mg/l)	STD (mg/l)
Mg	2187	2138	-49	39.5
Ca	7885	7747	-138	182.1
Sr	1545	1592	47	31.4
Ba	90	95	6	2.1

Note: A dilution factor of 500 was used to convert the concentration measured using ICP into the concentration reported in the table.